Calorimetric Studies on Molecular Ferromagnet [DMFc]TCNQ and Some Other Ferrocenium-Radical Salts at Very Low Temperatures

by

Microcalorimetry Research Center
Faculty of Science
Osaka University

1990

Calorimetric Studies on Molecular Ferromagnet [DMFc][TCNE] and Some Other Ferrocenium Radical Salts at Very Low Temperatures

by

Motohiro NAKANO

Microcalorimetry Research Center
Faculty of Science
Osaka University

1990

ACKNOWLEDGMENTS

This thesis owes very much to many persons, albeit the author is responsible for all descriptions. First of all, the author would like to express his most sincere gratitude to his mentor, Professor Michio Sorai, for many valuable instructions and patient encouragements to the author. Without them, this thesis would not be completed. The author is also grateful to Dr. Yatsuhisa Nagano for his technical advice and helpful discussions.

The author thanks very much Professor David N. Hendrickson, Drs. T.-Y. Dong and M. J. Cohn of University of California at San Diego for kindly providing the precious sample of biferrocenium triiodide. He also gratefully thanks Professor Hirotoshi Sano, Drs. Satoru Nakashima and Yuici Masuda of Tokyo Metropolitan University for allowing the author to use their sample of $1',1'''$-diethylbiferrocenium triiodide. The sample of ferrocenium hexafluorophosphate was prepared by Mr. Yutaka Shiomi, to whom the author is grateful. During the preparation of decamethylferrocenium tetracyanoethenide, the author could overcome some difficulties owing to helpful advice of Drs. Hitoshi Yamamoto and Atsushi Kajiwara.

The author is deeply indebted to Associate Professor Wasuke Mori for kindly showing his results on magnetic susceptibility of $1',1'''$-diethylbiferrocenium triiodide. The author wishes to thank sincerely Professor Kiichi Amaya and Dr. Mamoru Ishizuka for their guidance in magnetic susceptibility measurements of $1',1'''$-diethylbiferrocenium triiodide and stimulating discussions as well as their grant of copper powder, MD60.

Elemental analyses were performed by Mr. Masakazu Okumiya and Ms. Kazuyo Hayashi, infrared spectra were recorded by Mr. Shin-ichi Ishikawa, and X-ray powder diffraction was made by Mr. Tetsuo Yamamoto. The author expresses his sincere thanks to them.

The author gratefully acknowledges the construction of a very low temperature

calorimeter by Mr. Tomio Wakamatsu and Mr. Shigemi Murakawa.

The author is very happy to thank his obliging friend, Mr. Akihito Nishimori, who kindly helped the author to prepare this thesis. At last, the author wishes to express his sincere appreciation for warm supports and fruitful discussions from fellows of Microcalorimetry Research Center and Suga's Laboratory.

ABSTRACT

Correlation between magnetic and thermal properties was studied for five ferrocenium radical salts by means of heat-capacity measurements at very low temperatures. Of these five compounds, decamethylferrocenium tetracyanoethenide ([DMFc][TCNE]) and decamethylferrocenium tetracyanoquinodimethanide ([DMFc][TCNQ]) belong to a family of molecular charge-transfer complexes, while biferrocenium triiodide ([BFc]I_3) and $1',1'''$-diethylbiferrocenium triiodide ([DEBFc]I_3) are mixed-valence complexes. The last compound, ferrocenium hexafluorophosphate ([Fc]PF_6), is a simple radical salt. All these compounds contain anisotropic spins of ferrocenium moieties and hence their magnetic interactions in the solid state are very attractive subjects to study. The first two compounds contain both the $[DMFc]^+$ cation radicals and either the $[TCNE]^-$ or $[TCNQ]^-$ anion radicals. Consequently their magnetic interactions are of great interest.

A main part of the present doctoral thesis is part II, in which the so-called "molecular based ferromagnet" is mentioned. The first compound, [DMFc][TCNE], is known to show a bulk ferromagnetism below 4.8 K on the basis of magnetic measurements. In the present calorimetric study, the Curie temperature was precisely determined to be T_C = 4.74 K. The excess entropy associated with the observed heat-capacity anomaly was very close to the expected magnetic entropy, 2 R ln 2, so that it was concluded that the charge transfer from [DMFc] to [TCNE] is stoichiometrically complete. Detailed examination of the heat-capacity anomaly revealed a strong Ising character of the intrachain magnetic interaction. The strength of the Ising nature derived from the present study was consistent with that estimated from the magnetic susceptibility measurement for a single crystal. However, the present result conflicted with the result of ^{57}Fe Mössbauer spectroscopy which suggests the existence of a magnetic soliton excitation for interpretation of the line widths. The interchain interaction

was evaluated under a mean field approximation. The obtained value was as small as $\sim$0.02 per cent of the intrachain interaction. Hence the compound, [DMFc][TCNE], was proved to be a good one-dimensional (1D) Ising magnet.

For the related TCNQ complex with a homologous 1D crystal structure, an antiferromagnetic phase transition was observed at T_N = 2.54 K. This phase transition has been regarded as being accompanied by a structural transformation. In the present calorimetric study, however, the transition entropy roughly estimated suggested that significant part of the transition entropy can be accounted for solely in terms of the magnetic origin. Thus the structural change may be considered to play minor role in the phase transition of [DMFc][TCNQ], if any. In comparison with the TCNE salt, it was concluded that the magnetic lattice of the TCNQ salt has not so strong 1D character. The present study elucidated that there exists a considerable difference in the exchange-path structure between the TCNE and TCNQ salts in spite of their similar crystal structures.

In part III, the other three compounds are described. For all compounds, heat-capacity anomalies were found below 1 K. Unfortunately whole shapes of the anomalies could not be observed owing to the experimental limitation of the lowest attainable temperature. In order to interpret these anomalies, a new analytical method was introduced, which is an exponent "n" characterizing the temperature derivative of heat capacities, $n = -(\partial \ln C)/(\partial \ln T)$. This exponent, n, provided a useful criterion to judge whether an anomalous heat capacity would originate in a phase transition or a Schottky anomaly by use of only partial information about the anomaly. The magnetic behaviors of the three compounds, [BFc]I_3, [DEBFc]I_3, and [Fc]PF_6, were analyzed by this method and it was found that all the three compounds show a low dimensionality concerning magnetic lattice structure. Except for [BFc]I_3, apparent low dimensional structures are

hard to be found in their real crystal structures. Therefore, such a lattice anisotropy of the exchange path is considered to be a common feature inherent in molecular magnets.

CONTENTS

PART III. SOME OTHER FERROCENIUM RADICAL SALTS

PART I.

INTRODUCTION

Chapter 1. The Motive for the Present Study

1.1 Molecular Magnet, Exchange Path, and Lattice Dimensionality

Chemists are always longing for explanation of properties of materials in terms of their structural aspects. This attitude gives to the concept of *exchange path* a prominent position in magnetochemistry. The exchange path is a concept inherent in localized moment models. When magnetic moments are arranged in a crystal lattice, the exchange path corresponds to a tie-line between any two spins. The magnetic interaction, *i.e.* exchange of electrons, is considered to occur *via* this interaction path. For itinerant electrons described by band theories, however, such a path can not be defined.

A localized moment model is described by the so-called HDVV Hamiltonian (Heisenberg-Dirac-Van Vleck), $H_{ij} = -2J_{\parallel} S_i^Z S_j^Z - 2J_{\perp}(S_i^X S_j^X + S_i^Y S_j^Y)$, where H_{ij} denotes a Hamiltonian representing the interaction between two localized spins at i- and j-sites, S_i^{α} is the α-component of spin operator for i-site, and $J_{\parallel}$ and $J_{\perp}$ show the superexchange interaction parameters. By a positive J one can describe a ferromagnetic interaction in which the parallel spin configuration is preferred. Contrary to this, an antiferromagnetic interaction is described by a negative J. When the magnetic interaction is isotropic, *i.e.* $J_{\parallel} = J_{\perp}$, the interaction is called the *Heisenberg* type. Generally the magnetic interaction may have some anisotropy : the limiting case of $J_{\perp} = 0$ is called the *Ising* type, while another limiting case of $J_{\parallel} = 0$ is called the *XY* type. These three types of magnetic interaction reveal various characteristic features and a large field of statistical thermodynamics has been developed based on this HDVV Hamiltonian.

In simple ionic salts like transition metal oxides or halogenides, the

magnetic moments are localized on the transition metal cations. They interact magnetically with each other through superexchange interaction *via* intervening counter anions. In this case the exchange path is clearly recognizable and traced out as "d-orbital in a cation" ··· "p-orbital in monatomic anion" ··· "d-orbital in another cation". The magnetic interaction depends strongly on the exchange path. For example, the interaction is ferromagnetic when the bending angle of the exchange path is 90° , whereas it becomes antiferromagnetic when 180° for less than half filled transition metal cations. This effect can be semiquantitatively estimated by the theory of Kanamori and Goodenough[1].

On the other hand the situation is very different in rare earth metals. The magnetic interaction in rare earth metals is not superexchange interaction but RKKY interaction mediated by conduction electrons. The magnetic moment is spatially localized in f-orbitals of each rare earth ion but a particular direction in which the magnetic interaction occurs cannot be found because the conduction electrons are distributed isotropically around a rare earth ion. Hence the exchange path is considered to be isotropic. In addition, it should be remarkable that the interaction is not limited between neighboring rare earth ions. Since the conduction electron is in a delocalized state, the RKKY interaction exerts its effect on considerably separated ions. In this case the interaction depends strongly on the exchange path too, but only on the distance of the path. The intensity of the RKKY interaction shows oscillation with the distance, and consequently the ferromagnetic and antiferromagnetic interactions appear alternately. Thus the exchange path plays an important role also in rare earth metals.

In this paper we shall be concerned with another type of localized spin system called the *molecular magnet*. In the molecular magnet, magnetic moments are carried by molecules or molecular ions. This type of chemical modification,

in which a monatomic magnetic ion is replaced by a molecular species, is apparently minor change but yields plenty of new characteristics. One of the effects is that the molecular orbital which accommodates an unpaired electron has generally a complicated shape so that the overlapping of magnetic orbitals has preferred directions. It may cause the spatial anisotropy of superexchange interaction, eventually lead to a *low lattice dimensionality*. When the overlap is dominant in the direction parallel to a particular axis and negligible in the direction perpendicular to the axis, it is regarded as a one-dimensional (1D) magnet. Whilst, when the interaction in the parallel direction is negligible, a 2D magnet is provided. Although these low dimensional magnets had been studied only theoretically in the past because of their facility of mathematical treatments, they attract nowadays great attentions to their novel properties distinguished from ordinary 3D magnets, *e.g.* sine-Gordon soliton[2], low dimensional magnon[3], Kosterlitz-Thouless transition[4], Z_2-vortex transition[5], and the Haldane gap problem[6].

Although the molecular magnet is a good candidate of low dimensional magnet, it is sometimes difficult to identify the low dimensional exchange path explicitly. On the molecular surface of a magnetic species there are several contact points with its surrounding species, which are usually either the same kind molecules or polyatomic counter ions, and the most effective contact point is hard to be found. Thus identification of the exchange path in a molecular magnet is a challengeable problem. Moreover the type of magnetic interactions (Heisenberg, XY, or Ising type) is crucially affected by the exchange path and cannot be predicted easily. The character of magnetic interaction is dominated by a single ion anisotropy, *i.e.* the anisotropic g-factor of transition ions, in simple salt compounds. In the molecular magnet, however, the anisotropy of g-factor is not the only factor which determines the character of interaction. Although many molecular magnets involve radical species with isotropic g-factor,

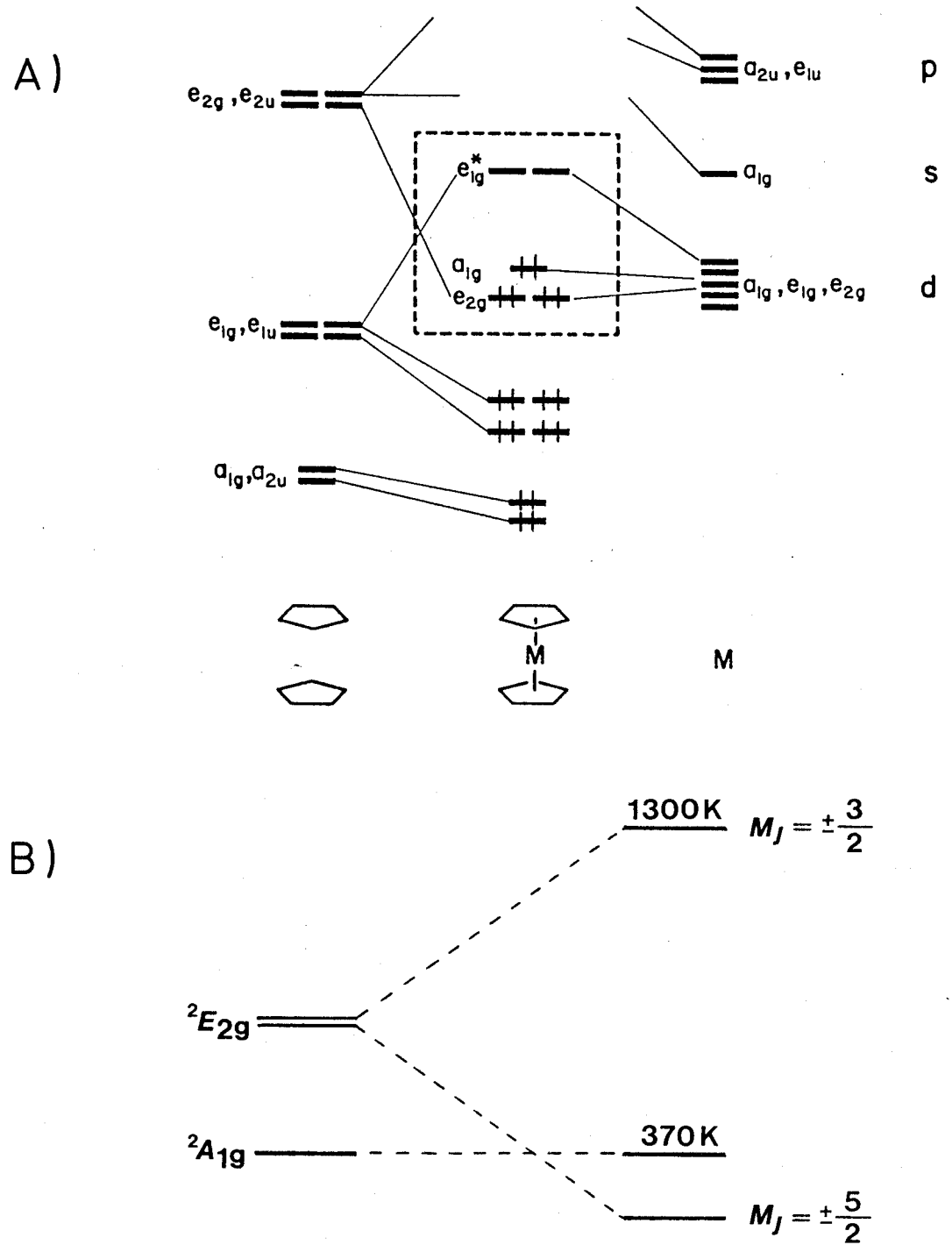

Fig. 1.1 Energy level schemes :
A) Molecular orbitals of a ferrocene [9],
B) ground multiplets of a ferrocenium cation.

the Heisenberg-type interaction is not necessarily a good approximation to describe such systems. This is because the exchange path contains intervening orbitals of nonmagnetic species (*e.g.* counter ions) and the symmetry of these orbitals reflects in the character of magnetic interaction[7]. Therefore, the molecular magnet is a very interesting system not only from its obscure exchange path but also from various unexpected characters such as anisotropic exchange interaction.

1.2 Ferrocenium Radical Cation

Ferrocene, bis(η^5-cycropentadienyl)iron(II), is a representative organometallic compound. It is a very stable molecule and the electronic structure has been intensively studied. In Fig. 1.1(a) drawn are one-electron energy levels of ferrocene. The HOMO and neighboring levels are mainly contributed from the iron d-orbitals and can be approximately regarded as pure d-orbitals under a uniaxial crystalline field. Because of the high axial-symmetry of a ferrocene molecule, the orbital angular momentum associated with them is not fully quenched. When a ferrocene molecule is subject to one-electron oxidation, an electron is removed from e_{2g} orbitals (effectively iron $3d_{\pm 2}$ orbitals) to produce a ferrocenium cation, $[Fe(C_5H_5)_2]^+$. The derivation of the ground multiplet of a ferrocenium cation is explained in Fig. 1.1(b). Although the $^2A_{1g}$ multiplet, where a hole is in a_{1g} orbital, has apparently the lowest energy, the true ground multiplet is split out from the $^2E_{2g}$ state by the spin-orbit interaction, orthorhombic field, and Jahn-Teller interaction[8]. If one takes into account only the spin-orbit interaction for simplicity, the ground Kramers doublet has the magnetic quantum number $M_J = \pm 5/2$ arising from coupling of the orbital angular momentum $M_L = \pm 2$ and the spin angular momentum $M_S = \pm 1/2$. In practice, the orbital angular momentum is weakly quenched by the

orthorhombic field and Jahn-Teller interaction with the same order of the spin-orbit interaction so that the magnetic moment of a ferrocenium cation is slightly reduced from that expected from the M_J value. As easily understood from these arguments, a characteristic feature of a ferrocenium ion is its anisotropic magnetic moment.

In the present work, five compounds related to the ferrocenium radical cation are studied by means of heat-capacity measurement at very low temperatures. They are decamethylferrocenium tetracyanoethenide ([DMFc][TCNE]), decamethylferrocenium tetracyanoquinodimethanide ([DMFc][TCNQ]), biferrocenium triiodide ([BFc]I_3), $1',1'''$-diethylbiferrocenium triiodide ([DEBFc]I_3), and ferrocenium hexafluorophosphate ([Fc]PF_6). All these compounds involve the anisotropic spins of ferrocenium moieties and their magnetism in the solid state is very attractive. Especially the first two compounds contain another magnetic species, $[TCNE]^-$ and $[TCNQ]^-$, and hence the character of their magnetic interaction is of great interest. Magnetic heat capacity is an useful probe to elucidate the interaction type and lattice dimensionality of magnetic systems. We attempted mainly to examine these two points for each compound.

Chapter 2. Improvement of a Very Low Temperature Calorimeter

2.1 ^{3}He/^{4}He Dilution Refrigerator

Nowadays ^{3}He/^{4}He dilution refrigerators have become a standard laboratory instrument for producing ultra-low temperatures below 1 K[10]. By means of this refrigerator one can easily obtain milli-kelvin temperatures over a long period of time. The advantage of this refrigerator is the capability of continuous running over several weeks without any interruption of refrigeration. This point is superior to any other one-shot type refrigerators in this temperature region, *i.e.* ^{3}He evaporation, adiabatic demagnetization, Pomeranchuk cooling, and so on.

Two properties of ^{3}He + ^{4}He mixture are utilized for the realization of ^{3}He/^{4}He dilution refrigerator : one is the finite solubility (6.4 %) of ^{3}He liquid into ^{4}He liquid even at 0 K and the other is the endothermic effect when ^{3}He liquid is dissolved into ^{4}He liquid. As seen from the phase diagram (Fig. 2.1), the liquid mixture of ^{3}He and ^{4}He undergoes a phase separation below the tricritical point, 0.86 K. The dilute phase is a superfluid with main component being ^{4}He, while the concentrated phase is a normal fluid which has smaller density. Since a superfluid does not contribute to the entropy, the dissolution of ^{3}He from the concentrated phase to the dilute phase may be described as being evaporation of ^{3}He into "mechanical vacuum" accompanied by absorption of heat from the environment. In a ^{3}He/^{4}He dilution refrigerator ^{3}He is circulated as follows : ^{3}He transferred from the concentrated phase through the phase boundary is distilled in a still controlled at $\sim$0.6 K and collected as pure vapor of ^{3}He, and then put back into the concentrated phase by re-liquefaction.

In our very low temperature calorimeter[11], commercially available refrigerator was used (Oxford Instruments, 300 μW economy type). The refrigeration down to $\sim$6 mK is possible when the refrigerator is operated without heat load. The lowest temperature attainable, however, becomes $\sim$20 mK

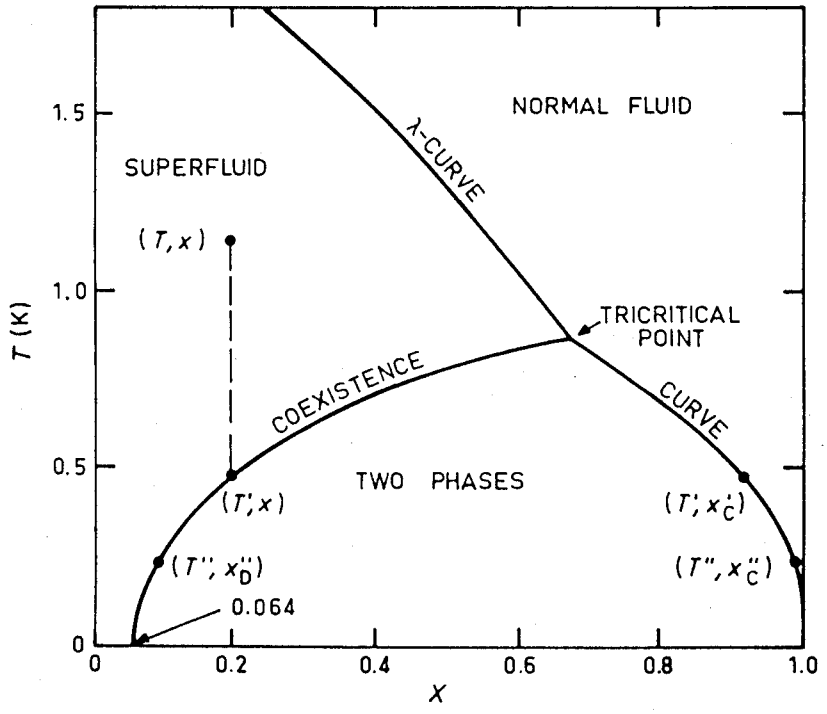

Fig. 2.1 Phase diagram of ^{3}He + ^{4}He mixture [10], where x denotes mole fraction of ^{3}He.

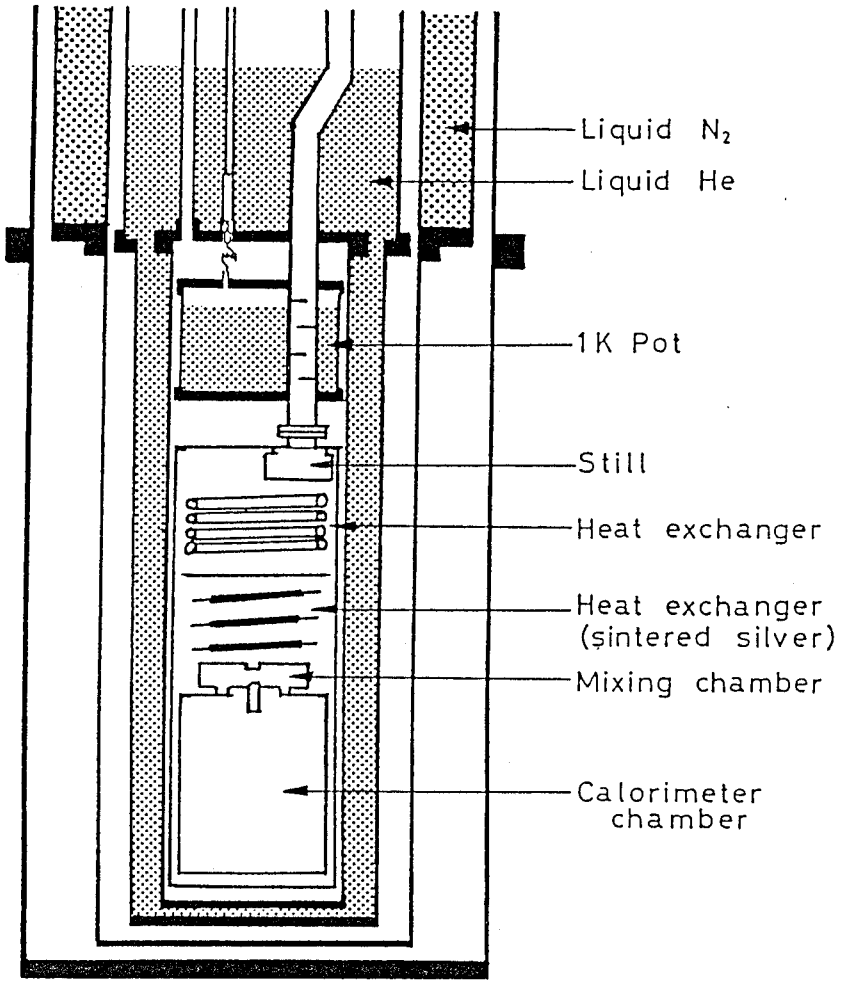

Fig. 2.2 Schematic diagram of the cryostat with a $^3He/^4He$ dilution refrigerator (Oxford Instruments Ltd.) [11].

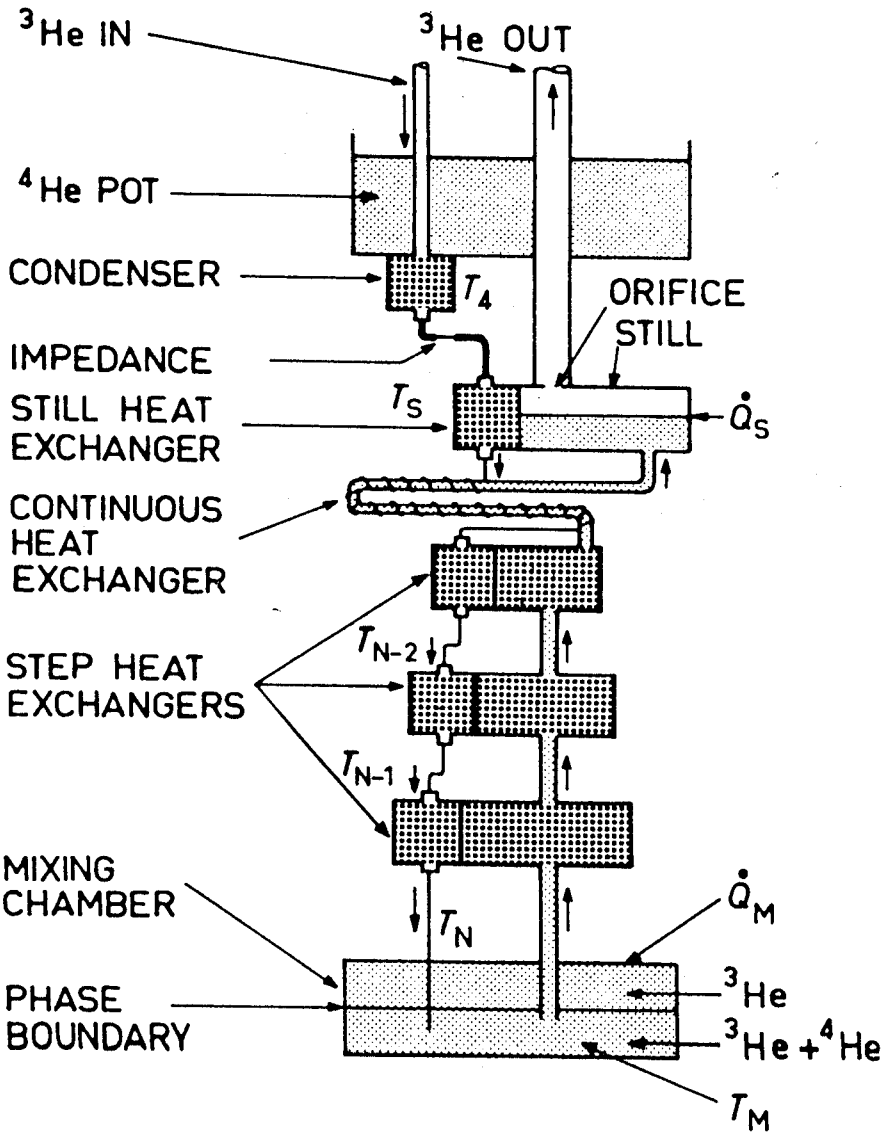

Fig. 2.3 Schematic diagram of the ^{3}He circulation line [10].

when the calorimeter unit is mounted. The schematic diagram structure of the cryostat is shown in Fig. 2.2. All the jackets are separable at the flanges located at the middle of the cryostat. From outer side there are successively an outer vacuum case (OVC) with rubber O-ring seal, a 77 K shield attached to liquid N_2 bath, a liquid ^{4}He-can, an inner vacuum case (IVC), and a 1 K shield. The liquid ^{4}He-can and the IVC are sealed with indium wires (1 mmϕ). The IVC and OVC can be independently evacuated or filled with some conduction gas. The evacuation tube for the IVC is equipped with a radiation baffle to prevent heat leaks as radiation in the tube. The innermost space used for accommodation of the calorimeter has the dimension of about 150 mm in diameter and 200 mm in height. All electrical lead wires from outside are introduced through three hermetic seals at the top of the cryostat.

The mixed gas consisting of 98 dm^3 of ^{4}He and 18 dm^3 of ^{3}He is charged in the ^{3}He circulation line of the refrigerator. A schematic drawing of the circulation line is given in Fig. 2.3. When a steady circulation is once established, pure ^{3}He gas ($\sim$5 kPa) is supplied to a condenser attached to a 1 K pot and liquefied there at $\sim$1 K (vapor pressure of ^{3}He being 1.2 kPa at 1 K). Then the concentrated phase (virtually pure liquid ^{3}He) flows through a flow impedance to heat exchangers. Two kind of heat exchanger are used for efficient thermal contact between the concentrated and dilute phases ; one is a tube-in-tube type and the other is a sintered-silver type. Both of them have large surface area and thin diameter to prevent convection of liquids. After heat exchangers, the concentrated phase enters a mixing chamber in which the phase separation occurs. Consequently the mixing chamber is the coldest part in the cryostat. ^{3}He moves from the concentrated phase to the superfluid dilute phase in this mixing chamber, to which a copper cold finger (a rod) is attached to connect with heat loads. ^{3}He in the dilute phase then moves into the still

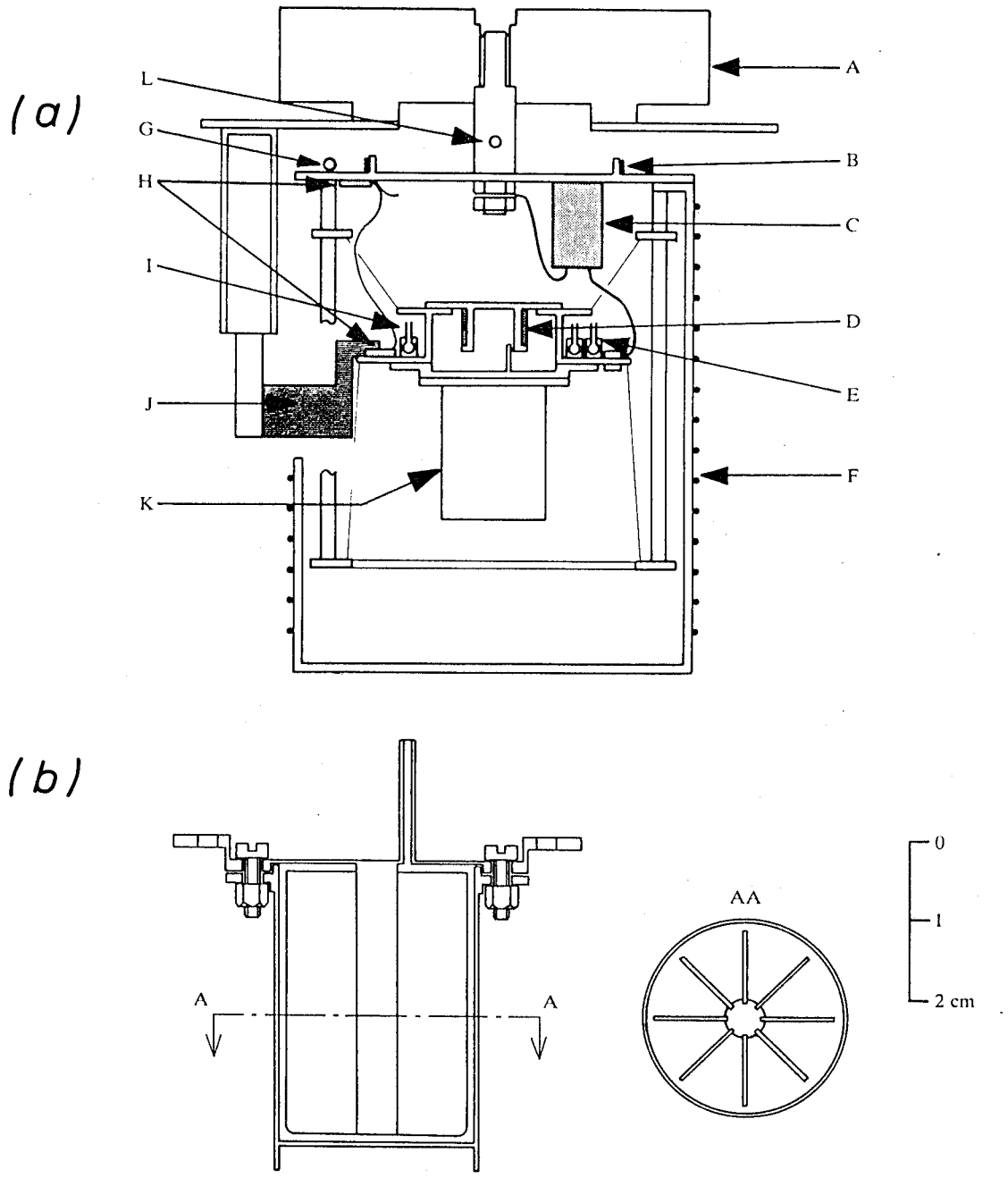

Fig. 2.4 (a), Calorimeter assembly [11].
A, mixing chamber; B, thermal anchor for lead wires; C, superconducting heat-switch; D, calorimeter heater; E, germanium resistance thermometer; F, adiabatic shield with a heater; G, carbon resistance thermometer; H, junctions of AuFe-chromel thermocouples; I, carbon resistance thermometer; J, clamping post for mechanical heat-switch; K, sample container; L, auxiliary heater.
(b), Sample container with inner volume of 14 cm^3 [11].

through heat exchangers. This still is maintained at ~0.6 K for efficient circulation rate of ^{3}He (for reference, at 0.6 K vapor pressures of pure ^{3}He and pure ^{4}He are ~70 Pa and ~40 mPa, respectively.). Just above the still there is a film burner to stop the film flow of superfluid phase. The ^{3}He vapor is evacuated from still with a large booster pump and purified in a liquid N_2 trap containing activated charcoal. Because the main trouble occurring during the operation of the refrigerator, if any, is the choking up with condensed impurity gas, this cold trap is very important for continuous drive. At last the pressurized ^{3}He gas is sent back to the condenser to complete the circulation.

2.2 Calorimeter

(1) Structure of calorimeter

The calorimeter assembly consists of a copper frame with an adiabatic shield and a calorimeter unit (Fig. 2.4). The copper frame is fixed to a copper cold finger attached to the mixing chamber of the refrigerator, which plays as a heat sink of the lowest temperature. The adiabatic shield screwed to the copper frame is equipped with a temperature control heater (75 Ω) of Manganin wire wound in inductionless fashion. These frame, shield, and calorimeter are all made of oxygen free copper and gold-plated to avoid heat conductions *via* radiation.

The calorimeter unit is demountable into two parts : a copper stage and a sample container. The copper stage is suspended from the copper frame by means of thin Nylon threads, while the sample container is screwed to the copper stage with small amount of Apiezon N grease.

On the copper stage an electrical heater and four resistance thermometers are placed. The heater used for energy supply to the calorimeter unit is made of Manganin wire (0.03 mmϕ) of 1200 Ω. Although Manganin is a commonly used material for heater-resistor, it exhibits heat capacity anomaly below ~0.2 K.

Two of the four thermometers are germanium resistors (CryoCal, CR100 and CR1000) and the other two are carbon resistors (Speer, 100 Ω 1/2 W). Their temperature scales have been calibrated against EPT-76 scale between 0.37 and 25 K, and against NBS cryogenic temperature scale-1 (traceable by the fixed-point device : NBS, SRM-768) down to 15 mK. Resistance of each thermometer is measured by four-terminal mode. Lead wires for electrical connections to the thermometers and the heater go out through a tag plate placed on the copper stage. Although oxygen free copper wires (0.06 mmϕ) with Formvar insulation are used for all the electric wires, short Constantan wires (0.1 mmϕ) are inserted to minimize heat leaks between the tag plate and a thermal anchor on the copper frame.

Two ways of heat paths, through which the calorimeter can be cooled, are prepared on the copper stage. One is a mechanical heat-switch and the other is a superconducting heat-switch. The mechanical heat-switch consists of a clamping post on the stage and gold-plated copper jaws thermally connected to the copper cold finger. At the junction between the jaws and the cold finger, small amount of silver solder is used. If possible, other solder should be used, for some silver solders are known to become a superconducting state with poor thermal conductivity. Although frictional heat evolved by the mechanical heat-switch operation has been minimized by use of Teflon lubricants, it is still difficult to obtain the temperatures lower than 50 mK by this heat-switch. In this regard, the superconducting heat-switch has the merit of less production of heat on its operation. However, as our superconducting heat-switch is made of indium, whose critical temperature is relatively low, rather large heat leak occurs unless heat-capacity measurements are made at extremely low temperatures. Hence this heat-switch was not used in this work in which the sample compounds with long thermal relaxation times were mainly dealt with.

The sample container has a bucket-like shape with 3.5 cm in height and 2.5 cm

in outer diameter : a lid with eight copper vanes and a bucket. This accommodates sample and heat conducting medium (silicone oil or ^{3}He gas) in vacuum-tight fashion using indium O-ring seal (0.5 mmϕ). The lid is equipped with a copper capillary to introduce ^{3}He gas. This capillary is usually sealed with soldering.

The present empty calorimeter shows two heat capacity anomalies. As already stated, one is located below 0.2 K which results from manganin heater wire[12]. The other is found at $\sim$13 K but its origin has been unidentified. Possible origin is a superconducting phase transition due to solders ($T_c \sim 7$ K in usual solders).

(2) Calorimetry

Adiabatic calorimetry is thought of as the method which provides the most confident values of heat capacity. This method is called the heat pulse method and based on the relation, $C = P \cdot \Delta t / \Delta T$, where C is the average heat capacity of a system, P is the power at which the joule heat is supplied to the system, Δt is the time interval of a heat pulse, and ΔT stands for the observed temperature increment of the system. Since the supplied joule heat, $P \cdot \Delta t$, is easily determined with high accuracy owing to recent development of electronics, precise measurements of accurate value for ΔT are the bottle-neck to obtain high quality data of heat capacities. For this purpose establishment of good adiabatic condition and complete thermal equilibration are important.

In our calorimeter the environment (inner vacuum case) is evacuated to $\sim$0.1 mPa to prevent the heat conduction through gas. Although the heat flux *via* radiation emitted from high temperature wall is serious at very low temperatures, this kind of heat leak is easily decreased to a negligible level by utilization of a radiation baffle, a few radiation shields, and some aluminium-foil coverings. Heat invasion through the electrical lead wires is usually large, so that all the wires are thermally anchored at many stages and,

moreover, short piece of constantan wires and superconducting wires intervene between a pair of copper wires. The most troublesome heat path is mechanical vibrations of the cryostat. The oil rotary pumps bring about violent vibrations. Many types of shock absorber are inserted and movable parts such as vacuum rubber tubes and bellows are fixed tightly to a heavy iron frame.

The adiabatic shield surrounding the calorimeter is utilized to reduce the heat leaks. Above 1 K the shield temperature is controlled to be equal to the calorimeter temperature by means of AuFe(0.07 %)-Chromel thermocouples. Under the optimal condition, the heat exchange is completely ceased, so that this setup is called the *adiabatic temperature control mode*. Another setup is used below 1 K because the electromotive force of the thermocouples and its derivative are too small to feed back to the shield heater current. In this mode the thermocouples are demounted from the calorimeter and the shield temperature is kept constant. This is the *isoperibol temperature control mode*. Even by this mode long thermal stability over 2 hours is possible.

To promote complete thermal equilibration in the calorimeter, some heat conducting medium is enclosed in the sample container. We use silicone oil (Toshiba Silicone, TSF-433) or ^{3}He gas for the medium. As ^{3}He has very low vapor pressure below 1 K, it is inevitable to use silicone oil when heat-capacity measurements of powdered or polycrystalline samples are made below 1 K. Except for its poor thermal conductivity, silicone oil has many favorable features as the conduction medium. For example, it is chemically inert for most substances and easily mixed with powder at room temperature. In addition it becomes a vitreous state on cooling, so that it brings about no cracks which prevent heat conduction in the sample container. Though superfluid helium is more desirable medium below 1 K, it is not used in this study because of difficult treatment.

The precision of ΔT values is mainly dominated by the reliability of the attained temperature after an energy input. To obtain this final temperature accurately, we must observe temperature drift of the calorimeter after a joule heat input. The drift observation provides information about progression of thermal relaxation. After fully relaxed, the final temperature is determined by extrapolation of temperature drift by assuming a straight line which corresponds to small amount of remanent steady heat leaks. When the calorimeter containing a sample has long thermal relaxation time, the extrapolation procedure may involve relatively large ambiguity. In such a case, one possible solution is to enlarge the absolute value of ΔT. In our calorimetry, typical temperature increment is chosen to be 3$\sim$10 per cent of the absolute temperature. For example, a temperature increment is 10 mK around 100 mK.

(3) Measuring systems

Three kinds of electronic systems are prepared for heat-capacity measurements : an energy supply system, a temperature measurement system, and an adiabatic control system. The first system is to supply the energy to the calorimeter and to measure the energy precisely. The main circuit of this system consists of an manganin heater fixed to the calorimeter, a standard resistor (Yokogawa Electric Works, Model 2792, 1000 Ω), a constant d.c. current generator (Yokogawa Electric Works, Model 2555), and a relay switch (OMRON, G2T-8424P), which are connected together in series. A digital voltmeter (Keithley, Model 195A) is used for the measurement of potential drops across the calorimeter heater and the standard resistor, and an universal counter (Advantest, TR5822) is used to measure the time interval of a heat pulse.

The temperature measurement system is composed of an a.c. resistance bridge (AΣA, Cryobridge Model 103) and a selector switch to choose an optimal resistor among the three resistance thermometers attached to the calorimeter. Owing to limited number of the lead wires, only three of the four thermometers

can be connected to the selector switch. The measurement of resistance is carried out by means of four-terminal method under minimized power dissipation of the order of 1 pW. Since the cryobridge is sensitive to the line noise, the power supply for the bridge is separated from those for other electronic devices by a noise cut transformer (Elgar, HIT-1.0-0.0005).

The adiabatic control system works in two distinct fashions according to the kind of input sensor. As already described, there are two different temperature control modes for the adiabatic shield : the *adiabatic* and *isoperibol* modes. In the adiabatic mode the input sensor is 2 pairs of AuFe(0.07 %)-Chromel thermocouples which detect the temperature difference between the calorimeter and the adiabatic shield. The signal voltage is amplified by a d.c. amplifier (Ohkura Electric, Model AM-1001) and applied into a home-made proportional controller which supplies a heater current to the shield heater (75 Ω). By this method, the shield temperature is controlled to be equal to the calorimeter temperature. In the isoperibol mode, the input sensor is a carbon resistor fixed on the adiabatic shield. This resistor is put in one arm of a simple Wheatstone bridge and the off-balance signal of the bridge is sent to the proportional controller. In this case the shield temperature is controlled at a preset value.

In addition to them some accessory electronics are necessary for actual drive of the refrigerator, which are a current supply for the film burner and the still heater, a liquid helium level meter, and an a.c. bridge to monitor the temperatures at various parts in the refrigerator.

2.3 Some Improvements of Calorimeter

(1) Pellet holder

As already stated in the last section we have used silicone oil in order to

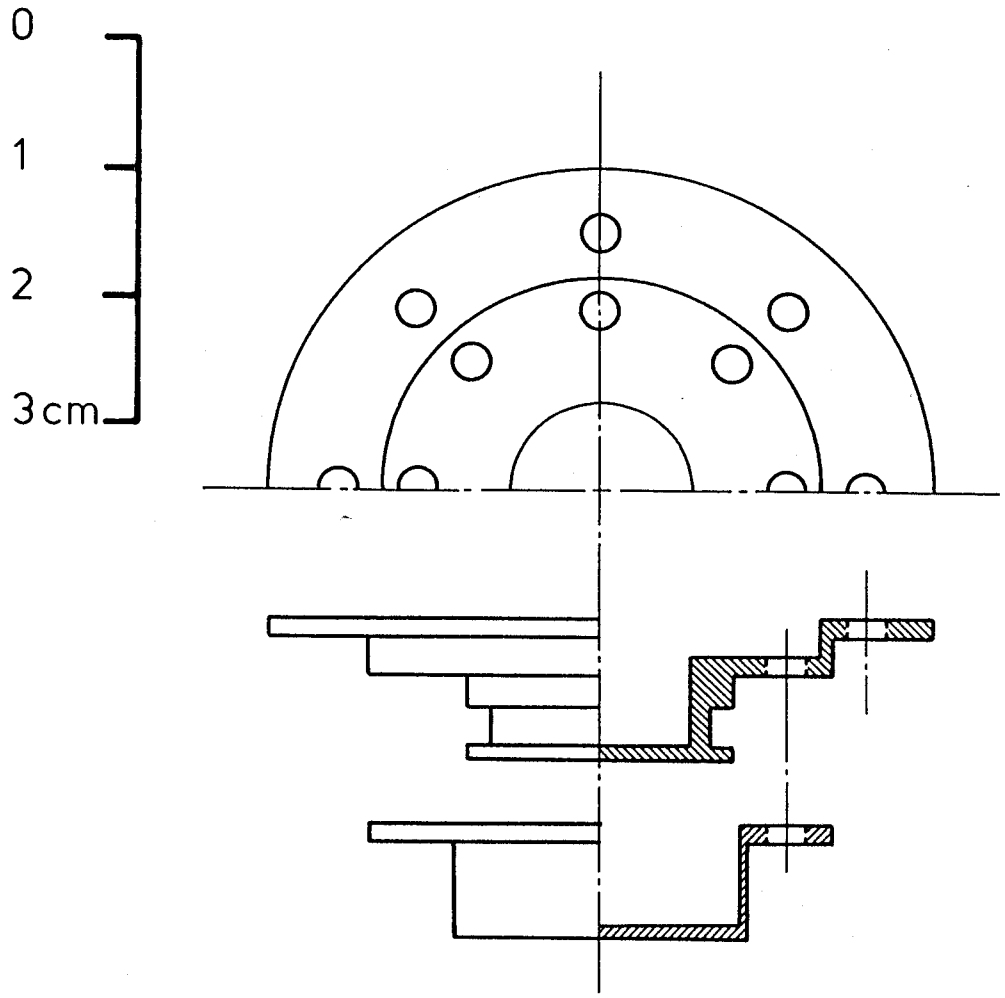

Fig. 2.5 Pellet holder.

promote the thermal equilibration in the sample container. In spite of its poor thermal conductivity which causes very long thermal relaxation time, utilization of silicone oil or any other heat conducting medium is inevitable as far as powdered or polycrystalline samples are concerned. Thus we attempted to make the samples a lump form to avoid the silicone oil.

An ordinary pellet maker for KBr disk in infrared spectroscopy was adopted with an oil press. The disk-shaped pellet, which has a dimension of 2 cm in diameter and 2 mm in thickness, was made in a vacuum under the condition of typically 300 MPa pressurizing for 300 s. Two types of pellets were examined. One is made of pure sample and the other is admixture of the sample and metal powder. The former method was attempted in the calorimetry of $[BFc]I_3$ described in chapter 7, while the latter method was adopted in $[Fc]PF_6$ in chapter 8. If metallic grains contact with each other, a network of high conductivity is established and, hence considerable diminution of thermal relaxation time can be expected. Although gold powder is a suitable material because of its high conductivity, low toxity, and chemical inertness, copper powder (Wolstenholme, MD60, 44 μm × 2 μm) was practically used in the amount which occupies about a half volume of the pellet.

A pellet holder was made of gold-plated oxygen free copper (Fig. 2.5). This holder is equipped with a rubber O-ring seal. At low temperatures this O-ring becomes ineffectual but it is no problem because vapor pressure of volatile components in the sample is low enough at low temperatures and decomposition of the sample is hard to occur.

In the case of $[BFc]I_3$, metal powder was not used because of high reactivity of iodine. To prevent the loss of iodine by evacuation, the O-ring seal was used. The residual air enclosed with the sample pellet served as relatively strong elastic resistance when the pellet was mounted in the holder. This problem may be avoided for small size pellets having enough room for air. In

the case of $[Fc]PF_6$ copper powder was used after washing with ether and vacuum desiccation. The sample pellet was slightly fragile. The O-ring seal was not used since the compound is stable in vacuum. The main problem in this case was relatively large uncertainty involved in determination of the sample mass. Uniform mixing of a sample and copper powder was assumed to estimate the sample amount. In both cases the thermal relaxation time was reduced, for example, from ~1 hour to 10~20 minutes. As a result, reliable measurements were able to be extended to lower temperatures.

(2) Automation by personal computer

By use of a microcomputer, the data collection and the control of energy input were automated. The temperature control of an adiabatic shield had been automated previously[13]. A microcomputer (NEC, PC-9801F) with a numerical coprocessor and memory area of 640 kB was adopted as main controller. Two types of interface were employed. One is a standard IEEE-488-1978 interface bus which connects to the digital voltmeter and an universal counter. The other is an interface board (Contec, PI-32 and PIO-16/16) which can accept the BCD signal of TTL level from the a.c. resistance bridge and send out the signal to a relay box for heater current.

Counterplan for electrical noise is important for the automation of experiments at very low temperatures. As stated in section 2.2 the noise from power supply was considerably reduced by utilization of the noise cut transformer. On the other hand, high frequency noise generated by the microcomputer arose another problem. For example, when the temperature of the calorimeter was about 40 mK, an apparent temperature rise of 5 mK due to self-heating of the thermometer was observed while the microcomputer was turned on. The greater part of the electrical noise had the frequency of 500 kHz and 25 kHz (~24.83 kHz of horizontal scanning frequency) and was generated from the

monitor display rather than the central unit of the microcomputer. These noises were almost eliminated by inserting an aluminum shield plate of 1 mm thick between the display and the a.c. resistance bridge.

Computer program was described by BASIC language because very fast calculation was not required in our calorimetry. This program controls the progression of a measurement and outputs all data on both a line printer and a floppy disk. In addition this program is capable of optimizing the heater current and the time interval of energy input. By virtue of the automation laborsome tasks have been considerably reduced.

(3) ^{3}He gas handling device

For chemically unstable samples, ^{3}He gas is more favorable heat conducting medium than silicone oil. Only the shortcoming of ^{3}He is its low vapor pressure below 1 K. Thus we used it for heat-capacity measurements of [DMFc][TCNE] and [DMFc][TCNQ] above 1 K.

A ^{3}He gas handling device was newly constructed. This device is equipped with two vacuum gauges, *i.e.* an ordinary Bourdon gauge and a Pirani gauge (ULVAC, GP-2A). To save expensive ^{3}He gas efficiently, a home-made cryopump was connected with the device. This pump was constructed with a needle valve (Hoke, 3752H4B) and a stainless steal tube filled with activated charcoal pellets.

Gas filling procedure is as follows. A sample container is connected with the device through a piece of copper capillary (1 mmϕ). After evacuation of the container, ^{3}He gas is introduced into it with a pressure of 10$\sim$20 kPa. Then a part of the capillary is pinched and covered with fused solder. While keeping the solder fused, the pinched part is cut by a miniature nipper. Residual ^{3}He in the line is collected in the cryopump cooled by liquid ^{4}He.

(4) Carbon resistor

One of the carbon resistor thermometers fixed on the copper stage of the calorimeter was processed in order to obtain quick response to a temperature

change. A part of outer insulating material and a part of core carbon of the resister (Speer, 100 Ω 1/2 W) was ground off and then the ground surface was sticked to a piece of oxygen free copper with epoxy resin (Emerson and Cumming, Stycast 1266). This modification brought about good thermal diffusivity and the temperature gap between the resistor and the calorimeter was reduced.

REFERENCES TO PART I

[1] J. B. Goodenough, "*Magnetism and the Chemical Bond*", John Wiley & Sons, New York (1963).

[2] H. J. Mikeska, *Physica* **120B**, 235 (1983); L. J. de Jongh, *J. Appl. Phys.* **53**, 8018 (1982).

[3] M. Takahashi, *Phys. Rev. Lett.* **54**, 168 (1987).

[4] J. M. Kosterlitz and D. J. Thouless, *J. Phys.* **C6**, 1181 (1973).

[5] H. Kawamura and S. Miyashita, *J. Phys. Soc. Jpn.* **53**, 4138 (1984).

[6] I. Affleck, *J. Phys.: Condens. Matter.* **1**, 3047 (1989).

[7] L. J. de Jongh and A. R. Miedema, *Adv. Phys.* **23**, 1 (1974).

[8] R. Rai, *Physica* **150B**, 414 (1988); R. Rai, *Can. J. Phys.* **60**, 329 (1982); J. H. Ammeter, *J. Magn. Res.* **30**, 299 (1978).

[9] J. W. Lauher and R. Hoffmann, *J. Am. Chem. Soc.* **98**, 1729 (1976).

[10] O. V. Lounasmaa, "*Experimental Principles and Methods Below 1 K*", Academic Press, London (1974).

[11] S. Murakawa, T. Wakamatsu, M. Nakano, M. Sorai, and H. Suga, *J. Chem. Thermodyn.* **19**, 1275 (1987).

[12] J. C. Ho, H. R. O'Neal, and N. E. Phillips, *Rev. Sci. Instrum.* **34**, 782 (1963).

[13] S. Murakawa, M. S. Thesis, Osaka University, Japan (1982); T. Wakamatsu, M. S. Thesis, Osaka University, Japan (1985).

PART II.

MOLECULAR FERROMAGNET, [DMFc][TCNE]

Chapter 3. Previous Works and Research Interests

3.1 Molecular Ferromagnet

In the era of ancient China, ferromagnetism was already recognized in magnetite and iron. Strictly speaking, magnetite is classified into ferrimagnet but these two materials are typical permanent magnets up to now. Magnetite is a kind of inorganic minerals with the formula Fe_3O_4, whilst iron is a metallic crystal. For a long time these two categories of materials, ionic salt and metal, have monopolized ferromagnets.

Nowadays the third category of ferromagnet, which is called "molecular based ferromagnetism" attracts our interests. Some theoretical models have been proposed for the potentiality of ferromagnetism in organic or polymeric materials, but actual substances which exhibit convincing ferromagnetism had not been obtained until 1986, when Miller *et al.*[1] made a breakthrough. They prepared, for the first time, a ferromagnetic molecular charge-transfer complex, decamethylferrocenium tetracyanoethenide, $[Fe(C_5Me_5)_2]^+[(NC)_2C{=}C(CN)_2]^-$, which is hereafter referred to [DMFc][TCNE]. Manganese(II)-phthalocyanine[2-3] and some inorganic coordination compounds[4-5] are so far only known as ferromagnets consisting of molecules or molecular ions. The impact of the report by Miller *et al.* is, however, based on its high Curie temperature (T_c) and on their proposal of a novel mechanism in which the mixing of an excited state with the ground state may lead to stabilization of bulk ferromagnetism.

Magnetic ordering in [DMFc][TCNE] has already been studied by means of magnetization and magnetic susceptibility measurements[1,6-8], ^{57}Fe Mössbauer spectroscopy[6,9], and neutron diffraction[8]. The results of these previous works will be summarized below.

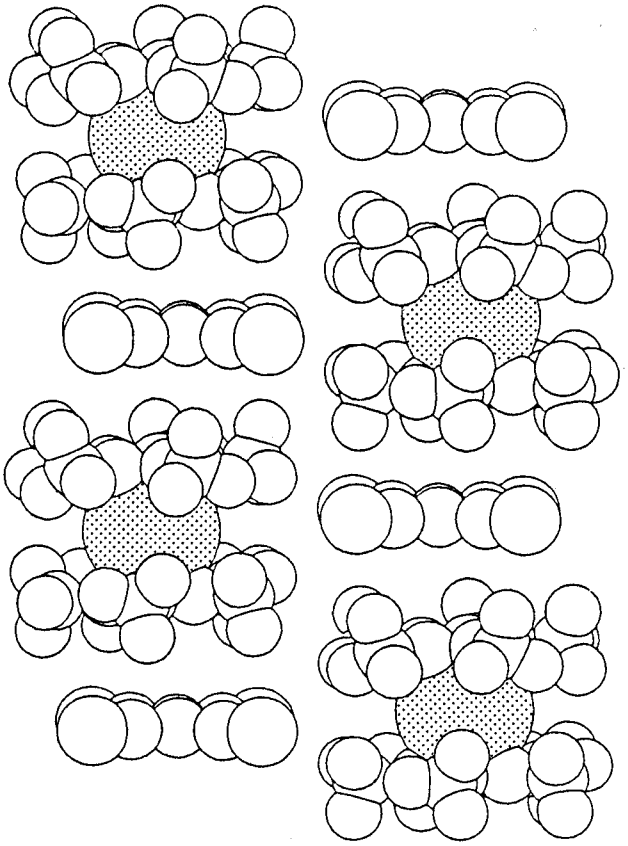

Fig. 3.1 Crystal structure of decamethylferrocenium tetracyanoethenide [10].

3.2 X-ray Structural Analysis

The crystal of [DMFc][TCNE] has a quasi-1D structure[6,10-11], whose linear chain is comprised of alternating s = 1/2 cations and s = 1/2 anions (see Fig. 3.1). The unit cell of [DMFc][TCNE] belongs to the orthorhombic $Cmc2_1$ space group with lattice constants of a = 1.0598 nm, b = 1.6091 nm, and c = 1.5566 nm at room temperatures. Although the $[DMFc]^+$ cation is completely ordered, the $[TCNE]^-$ anion is disordered. Details of this disorder have not been reported yet.

3.3 Magnetization and Magnetic Susceptibility Measurements

In their first paper[1], Miller *et al.* clearly proved the bulk ferromagnetism of [DMFc][TCNE] by showing spontaneous magnetization in zero applied field below 4.8 K. Since the spontaneous magnetization in zero applied field is smaller than the saturation moment in the presence of applied field, they thought ferromagnetic domain formation in a single crystal, which confirms the 3D ferromagnetism again. They also observed an well-defined hysteresis loop below 4.8 k and obtained a very high coercive field parallel to the stacking axis, H_C $\sim$ 0.1 T[7].

Magnetic susceptibility was measured for polycrystalline sample[1,6] and for single crystal[7-8]. Above 60 K the powder susceptibility obeys the Curie-Weiss law with a positive Weiss temperature of +30 K indicating that dominant interaction (*i.e.* intrachain interaction) is ferromagnetic. The deviation from the Curie-Weiss behavior below 60 K is well approximated by a s = 1/2 1D ferromagnetic Heisenberg model[12] down to 16 K. Below 16 K the 1D model cannot describe the powder susceptibility data and this fact suggests an effect of the bulk ferromagnetism.

Single crystal magnetic susceptibility revealed a magnetic anisotropy in the [DMFc][TCNE] crystal. The 1D Heisenberg model with ferromagnetic coupling, which was apparently adaptable to the analysis of powder susceptibility data, was again used to interpret independently the susceptibilities parallel and perpendicular to the stacking axis. Although the Heisenberg interaction is isotropic in the sense that $J_{\parallel} = J_{\perp}$, its use for an anisotropic system such as the present salt is justified by assuming the orthogonality between the fluctuation components parallel and perpendicular to the stacking axis. The analysis for each direction provided the exchange interactions of $J_{\parallel}/k_B \sim 27.4$ K and $J_{\perp}/k_B \sim 8.1$ K, which correspond to *z*- and *xy*-components of intrachain exchange interaction.

The ferromagnetic phase transition at 4.8 K has also been discussed, as a critical phenomenon, both for the magnetization and magnetic susceptibility. The critical exponent for magnetization, $M \propto (T_C - T)^{\beta'}$, was $\beta' \sim 0.5$. This value agrees well with the mean field approximation. Another exponent, δ, defined as $M \propto H^{1/\delta}$ was also obtained to be $\delta \sim 4.42$ from the magnetization parallel to the chain axis at T_C. Magnetic susceptibility provided the exponent $\gamma \sim 1.2$ for $\chi \propto (T - T_C)^{-\gamma}$ in both the cases parallel and perpendicular to the chain axis below 16 K. As the magnetic susceptibility could not be fitted to the Kosterlitz-Thouless scheme, $\chi \propto \exp(bt^{n})$, Chittipeddi *et al.* concluded that a dimensional crossover phenomenon occurs directly from 1D to 3D without intervening 2D scheme.

3.4 ^{57}Fe Mössbauer Spectroscopy

The most striking feature of ^{57}Fe Mössbauer spectra of [DMFc][TCNE] was zero-field Zeeman splitting observed even up to 20 K[6,9]. Below the Curie temperature spontaneous magnetization brings about six peaks in the Mössbauer spectra, corresponding to ^{57}Fe nuclear spin in a single internal hyperfine field

of 42.6 T. This split double-triplet does not vanish even above the Curie point 4.8 K and is clearly resolved up to 9 K. Owing to line broadening the spectra appear to be composed of two components, sharp and broad ones, above 9 K but the hyperfine splitting still persists.

This unusual behavior is partially due to slow paramagnetic relaxation of single ion and Miller *et al.* noted that the hyperfine splitting observed in zero field, *i.e.* slow relaxation, is a novel phenomenon because the transition between $M_S = \pm 1/2$ in a low spin Fe(III) is fully allowed and normally rapid under zero field in contrast to the relaxation in the ground Kramers doublet $M_S = \pm 5/2$ of a high spin Fe(III). The ground doublet $M_S = \pm 1/2$ of $[DMFc]^+$ cation is made up of low symmetry splitting of $^2E_{2g}$ state, so that rapid spin-lattice relaxation is presumably allowed through spin-orbital interaction in most cases. It is guessed that this novel slow relaxation has close connection to the strong spin correlation effect responsible for long wave length modes, known as the long time tail (LTT) behavior in ESR of low dimensional magnets.

In addition to the slow relaxation, there is another candidate to explain the Mössbauer line width. It is the line broadening by soliton excitation (*i.e.* moving domain wall). Miller *et al.*[13] insisted that the dipolar field arising from neighboring radical anions is not enough to explain the observed relaxational broadening and they tentatively attributed this broadening to the soliton effect. Excess line width due to soliton is known to obey $\Gamma \propto \exp[E_0/k_B T]$ for 1D antiferromagnet and $\Gamma \propto \exp[-E_0/k_B T]$ for 1D ferromagnet with XY-type exchange interaction, where E_0 denotes rest energy of a soliton[14]. Further investigation is necessary to obtain clear conclusion for this problem.

Mössbauer spectroscopy provides another information about the anisotropy of $[DMFc]^+$ cation which possesses a large contribution of orbital angular momentum.

As stated above, ^{57}Fe nuclei feel a strong hyperfine field of greater than 40 T. This value is much larger than 11 T expected for the Fermi contact term of an electron spin sitting on the iron nucleus. Thus a large orbital contribution is obvious. Such a large orbital contribution is attributable either to highly anisotropic single ion or to magnetically ordered state behavior. This question can be examined by means of high-field Mössbauer spectroscopy[9]. When an external field is applied longitudinally, an isotropic ion exhibits a large diminution of the second and fifth peaks of a typical six-line Zeeman pattern (*i.e.* $\Delta M_I = 0$ transitions). In contrast, anisotropic ion does not exhibit such behavior. In the case of [DMFc][TCNE], no observable polarization-diminution of the $\Delta M_I = 0$ transitions was detected up to $H_0 = 9$ T. This fact coincides with the large anisotropy of single crystal susceptibility.

3.5 Neutron Diffraction

Neutron diffraction study was done for deuterated polycrystalline sample using 14.7 meV neutrons[8]. Comparison between diffraction patterns recorded at 1.5 K and at 7.5 K demonstrates remarkable enhancement of the intensities at the scattering angles corresponding to *d*-spacings of 0.5235 nm and 0.3359 nm arising from the magnetic Bragg scattering. This observation again evidenced the appearance of ferromagnetic ordering.

The intensities of two magnetically enhanced peaks were tried to fit $I \propto (T_C - T)^{2\beta}$ with a critical exponent β. Although the observed values have not allowed to estimate accurate value of β, Chittipeddi *et al.* have thought that the variation of the intensities with temperature is not structural in origin.

3.6 Proposed Mechanism for Ferromagnetic Interaction

Magnetic interactions in [DMFc][TCNE] were compared with those of related complexes with the alternating anion-cation columnar structure in terms of

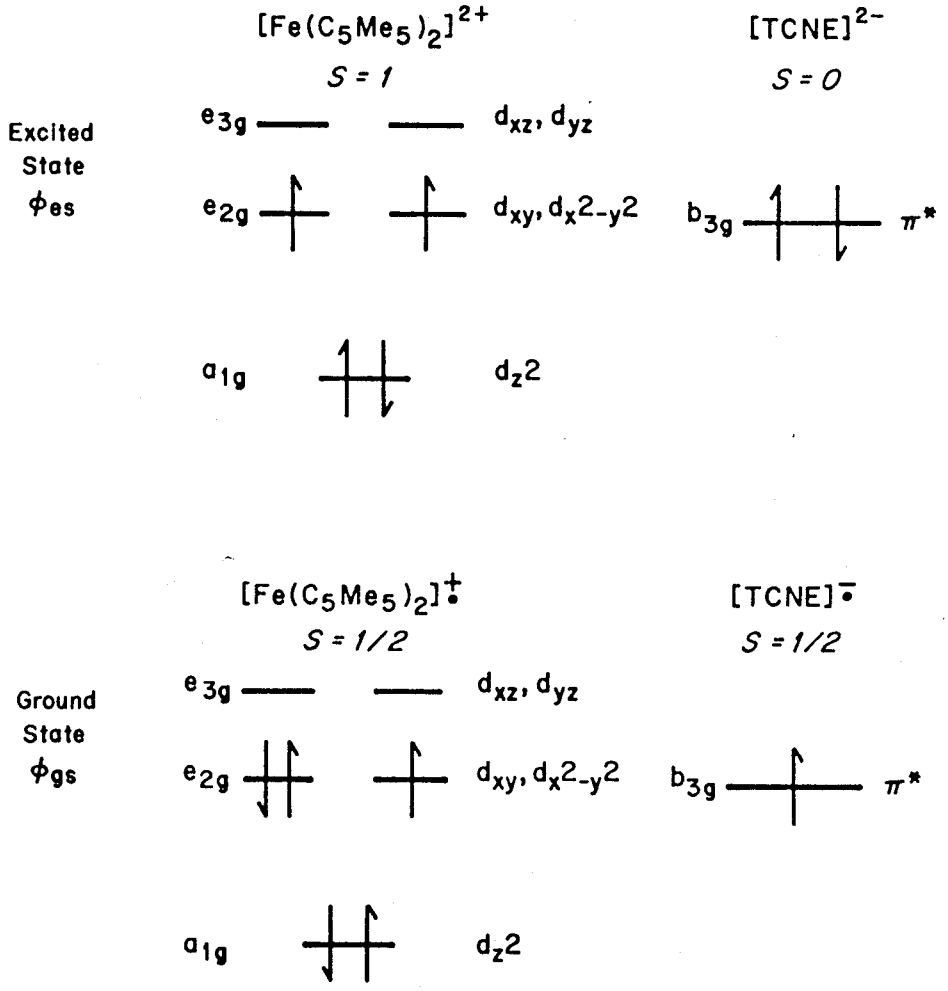

Fig. 3.2 Electron configurations of the ground and first excited states with the same spin multiplicity [6].

cation spin, anion spin, molecular symmetry, and electron configurations. As the result, it has been concluded that stabilization of the bulk ferromagnetism is due to admixing of the ground state with a virtual charge-transfer excited state (see Fig. 3.2)[15]. This mechanism is built up on the basis of McConnell's model[16] and contains an electron transfer process from the e_{2g}^3 configuration cation to non-half-filled partially occupied MO on the anion. This type of electron transfer produces the lowest excited state with the same spin multiplicity as the ground state, so that the excited state can stabilize the ground state by mixing. Generalized Hubbard model was used to examine the competition between various excited states arising from back and forth charge transfer. On the basis of this model, effective exchange interaction can be estimated as the sum of all possible excited states, $J \sim \Sigma\ \beta_n^2/\Delta E_n$, where β_n is a transfer integral and ΔE_n shows the energy necessary for the charge transfer. As this quantity, J, can in principle be evaluated, generalized Hubbard model provides a useful clue to the modification of molecular and crystal structures to enhance the ferromagnetic coupling.

3.7 The Objectives of the Present Study

Heat capacity is one of the macroscopic physical quantities obtained as a bulk property of a given system. In this sense, heat capacity measurement is a most suitable experimental method for the identification of "phase" and the detection of "phase transition" in thermal equilibrium states. As Miller *et al.*[6] pointed out, a more precise value for T_c should be decided because it is essential for the analysis of critical phenomena and for detailed examination of the reason for the unusual Mössbauer line width. One of the objectives of the present study is to determine precisely the phase transition temperature.

In addition, heat capacity is very sensitive to the nature of spin-spin

interaction, *i.e.* the type of exchange interaction and the dimensionality of exchange paths. These effects reflect on the shape of heat capacity against temperature curve. This study also aims at elucidation of the character of spin-spin interaction in this interesting molecular ferromagnet, [DMFc][TCNE].

Chapter 4. Experimental

4.1 Preparation

(1) Preparation of 1,2,3,4,5-pentamethylcyclopentadiene

1,2,3,4,5-pentamethylcyclopentadiene, the ligand moiety of decamethylferrocene, was prepared according to the method by Threlkel *et al.*[17]. As shown in Fig. 4.1, two step reactions are involved. First, 3,4,5-trimethyl-2,5-heptadien-4-ol was prepared by the reaction of ethylacetate with 2-butenyl-2-lithium in ether. Next step is dehydration of 3,4,5-trimethyl-2,5-heptadien-4-ol by acid catalyst.

The yield, 32 %, was considerably lower than the reported one (75 %). The product was identified by ^1H NMR and elemental analysis. *Anal.* Calcd for $C_{10}H_{16}$: C, 88.16; H, 11.84 %. Found : C, 85.04; H,11.65 %.

(2) Preparation of DMFc (decamethylferrocene)

At first, the preparation of DMFc was carried out by the method of King *et al.*[18]. This method is based on the reaction of iron(II) chloride and lithium pentamethylcyclopentadienide in THF. By this method the yield was only 10 %. The reason was thought of as the reductive elimination of excess butyllithium, $Fe(II) + 2BuLi \rightarrow Fe(0) + Bu_2 + 2Li^+$. Thus quantitative production of lithium pentamethylcyclopentadienide and complete elimination of excess butyllithium are essentially important. Butyllithium has high reactivity in THF solution since it exists as monomer form in polar solvent and sometimes gives rise to by-products based on over-deprotonated alkyllithium. More mild reaction in non-polar solvent, where butyllithium forms aggregates, is favorable for quantitative production of lithium pentamethylcyclopentadienide. We mixed pentamethylcyclopentadiene and butyllithium in hexane at 0 °C and warmed up to room temperatures to allow the deprotonation reaction. Then the reaction mixture was evaporated to dryness. A THF solution of this solid was used for reaction with iron(II) chloride. The yield of DMFc in this case was the same as

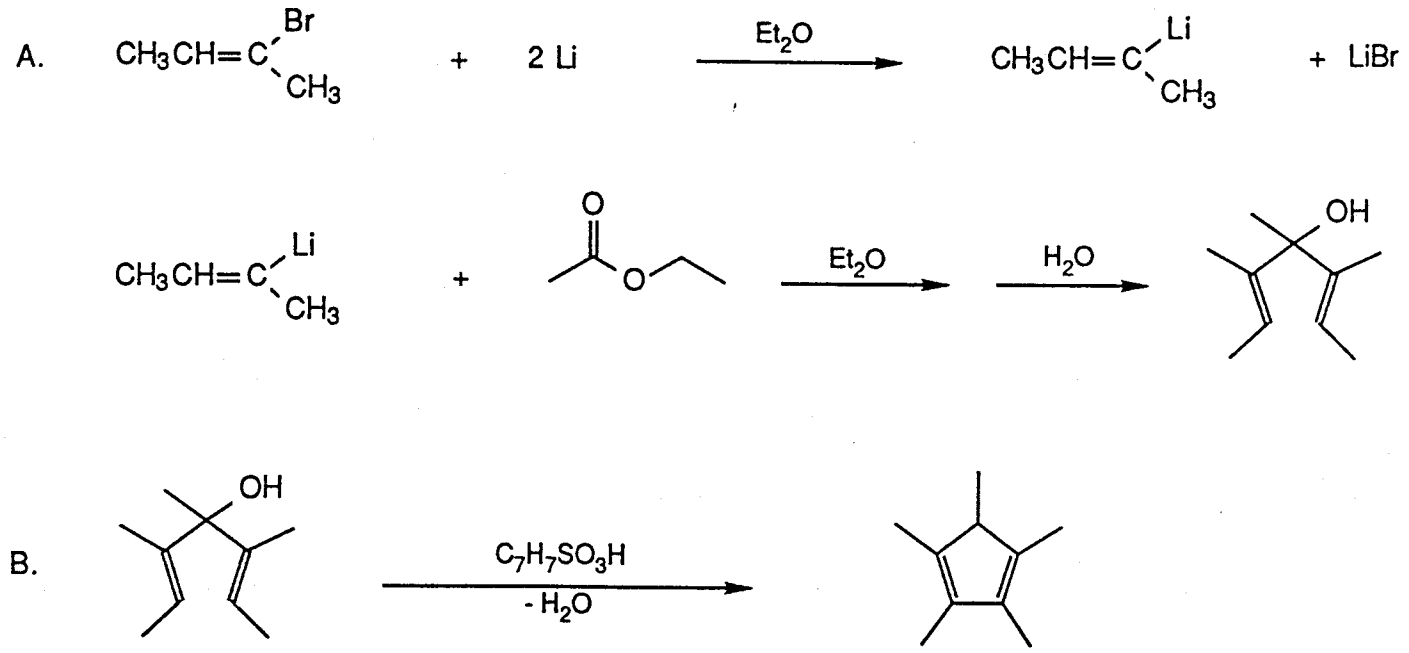

Fig. 4.1 Synthetic scheme for 1,2,3,4,5-pentamethylcyclopentadiene [17].

reported value, 57 %.

(3) Charge-transfer reaction of DMFc and TCNE (1,1,2,2-tetracyanoethene).

The last step of the preparation, CT reaction of DMFc, was carried out by Miller's method[6]. They proposed two methods in their paper : (a) low-temperature crystallization of the acetonitrile solution containing the neutral donor and acceptor, and (b) slow diffusion in a three-compartment cell filled with THF. The method (a) yields initially the solvated salts and it turns to the desolvated polycrystals *via* vacuum desiccation. On the other hand, the method (b) yields small amount of single crystals with good quality. Since heat capacity is a non-tensor quantity, polycrystalline sample is enough for the purpose of heat-capacity measurements. Therefore, we adopted the method (a) for the sake of of easiness for large scale preparation.

Prior to preparation, the solvent, acetonitrile, was refluxed with CaH_2 (4 g/l) for 4 hours. Hot acetonitrile solution of DMFc (typically, 2 g/200 ml) was added to acetonitrile solution of TCNE (0.79 g/5 ml) and then the mixture was evaporated to dryness. The crude product was recrystallized from acetonitrile solution with concentration of 2.5 g/100 ml at -25 °C. Obtained dark green crystals were evacuated for a few hours to give pseudomorphs with large needle shape. All procedures were carried out in a glove box and Schlenk apparatus filled with argon gas[19]. The yield of recrystallization was 66 %.

This compound is very sensitive to air. The reaction of TCNE anions with oxygen or water forms $[(NC)_2C{=}C(O)CN]^-$ or $[C_3(CN)_5]^-$. To check the admixture of such impurities, the product was identified by means of elemental analysis and IR spectrum measurement. The result of elemental analysis is given in Table 4.1, showing fairly well agreement with the calculated value for the TCNE salt. IR spectrum also supported the absence of oxidized anions because the absorption band for C≡N stretching was observed at a frequency nearer to the $[TCNE]^-$ anion

than to the $[C_3(CN)_5]^-$ anion (see Table 4.2).

4.2 Very Low Temperature Calorimetry

In usual cases polycrystalline samples are mixed with heat conducting medium, silicone oil, in the sample container as described in chapter 2. However, since the present compound is extremely sensitive to oxygen and water, it is incapable of mixing with silicone oil because complete removal of water from silicone oil is difficult. Hence we used ^{3}He gas as heat exchange medium in the sample container instead of silicone oil. A shortcoming of this medium is adsorption on the surface of powdered sample below about 1 K, which causes diminution of active carrier molecules. Fortunately, as the Curie temperature of [DMFc][TCNE] is about 4.8 K, heat capacities above 1 K are enough to examine thermodynamic properties of the magnetic anomaly.

Bleaney *et al.*[20] reported a heat capacity measurement using ^{3}He for heat exchanger between 0.45-20 K. They used about 20 kPa of ^{3}He at room temperature. The contribution of the ^{3}He to heat capacity becomes $\sim$1 mJ K^{-1} when the cell volume of 10 cm^3 and no adsorption are assumed. The heat capacity of this magnitude may be comparative to the lattice heat capacity of a few gram of sample at $\sim$1 K. We used the same order of ^{3}He gas as Bleaney *et al.*, *i.e.* 11.3 kPa of ^{3}He in 14 cm^3 sample container.

Sample mounting procedures were made in a glove box under argon atmosphere. As exact weighing of the sample cannot be done in the glove box, determination of the amount of sample was made again after heat capacity measurements by weighing the sample container with and without the sample. In this way the sample weight was finally estimated to be (4.4636$\pm$0.01) g (= 0.0098231 mol).

Table 4.1 Elemental analyses for [DMFc][TCNE].

		C	H	N
Calcd	$[TCNE]^-$ salt	68.72	6.65	12.33
	$[C_3(CN)_5]^-$salt	68.30	6.14	14.22
	$[(NC)_2C=C(O)CN]^-$ salt	67.57	6.80	9.46
Found	crude	68.66	6.72	12.25
	recrystallized	68.57	6.62	12.26

Table 4.2 Comparison of vibrational frequencies.

	$\nu(C\equiv N)$ / cm^{-1}		$\nu(CCC)$ / cm^{-1}
$[TCNQ]^-$	2153	2179	—
$[TCNE]^-$	2144	2183	—
$[C_3(CN)_5]^-$	—	2196	1500
Found	2157	2195	not observed

Chapter 5. Results and Discussion

5.1 Heat Capacity at Very Low Temperatures

Heat capacities of [DMFc][TCNE] in the temperature range 1-25 K are tabulated in Table 5.1 and shown in Fig. 5.1 on a logarithmic scale. A anomalous heat capacity peak was found at 4.74 K. This transition temperature is slightly lower than the Curie temperature already reported, T_c = 4.8 K[6]. The Curie temperature determined by the present calorimetry is more reliable because the temperature measurements were made by confirming thermal equilibration under precise temperature control. The small discrepancy may be attributable to the difference between polycrystalline and singly crystal samples.

The phase transition peak has a cusp-like shape and no indication of latent heat. The transition behavior bears a resemblance to an anomaly derived from a mean field approximation. Mean field behavior was also observed in temperature dependence of the magnetization[7]. Accordingly, the critical fluctuation is not so dominant in this higher-order phase transition. This aspect does not conflict with the fact that in the vicinity of phase transition the thermal relaxation time did not exhibit any remarkable elongation, which is expected from critical slowing down.

Since there are no reported evidences of strong spin-lattice coupling, one can regard the observed heat capacity as being a superposition of magnetic contribution and independent contribution from lattice vibrations. To examine the magnetic part closely, separation of these two contributions was attempted. A normal heat capacity curve was roughly estimated by a curve-fitting method in the range 10-25 K after subtraction of a guessed high-temperature tail of the magnetic contribution[21]. The estimated normal part, C_p(normal), has the following temperature dependence,

$$C_p(\text{normal}) = 7.05\ C_V(\text{Debye}, 49\ \text{cm}^{-1}) + 75.86\ C_V(\text{Debye}, 240\ \text{cm}^{-1}),$$

where C_V(Debye, $\tilde{\nu}$) stands for the Debye molar heat capacity having Debye's

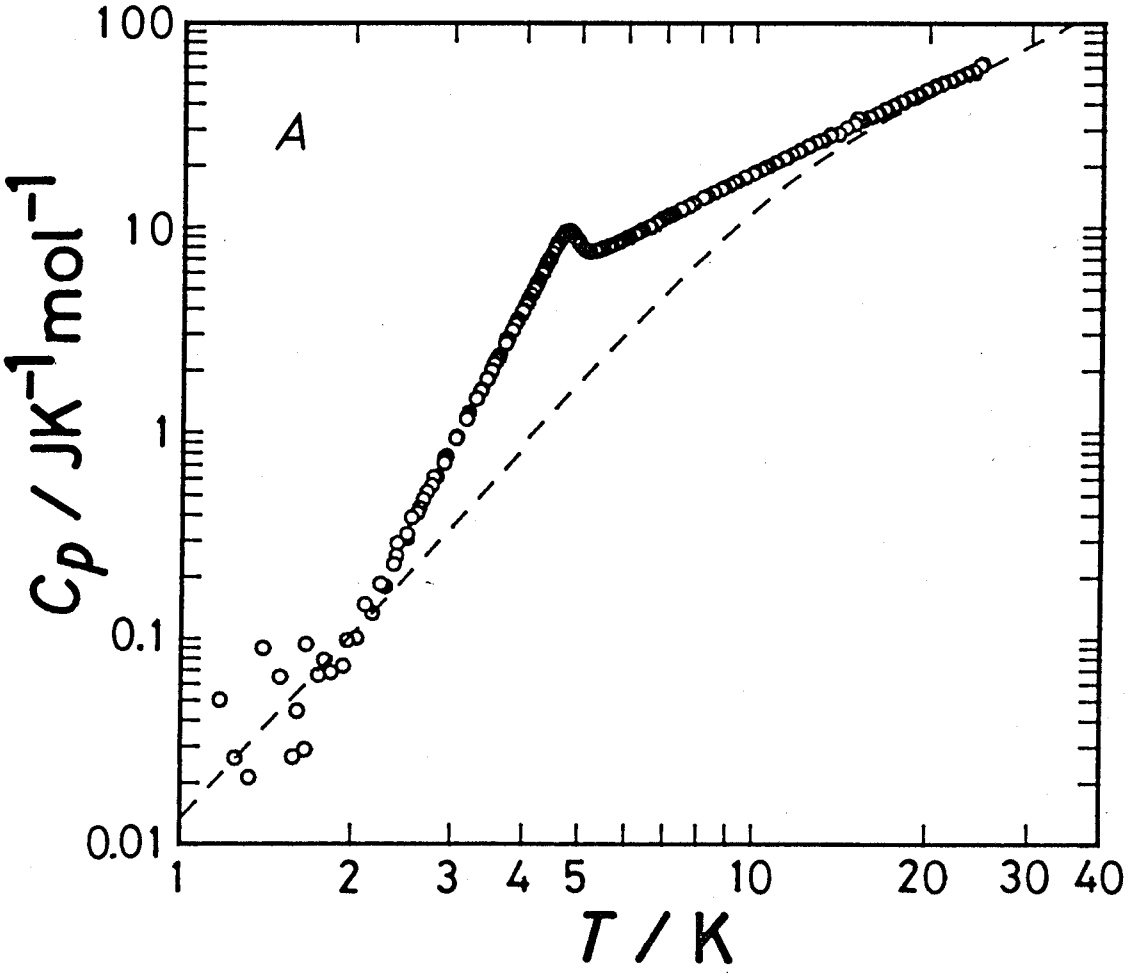

Fig. 5.1 Molar heat capacities of decamethylferrocenium tetracyanoethenide.
A, Log-log plot. The broken curve shows the estimated contribution from lattice vibration.

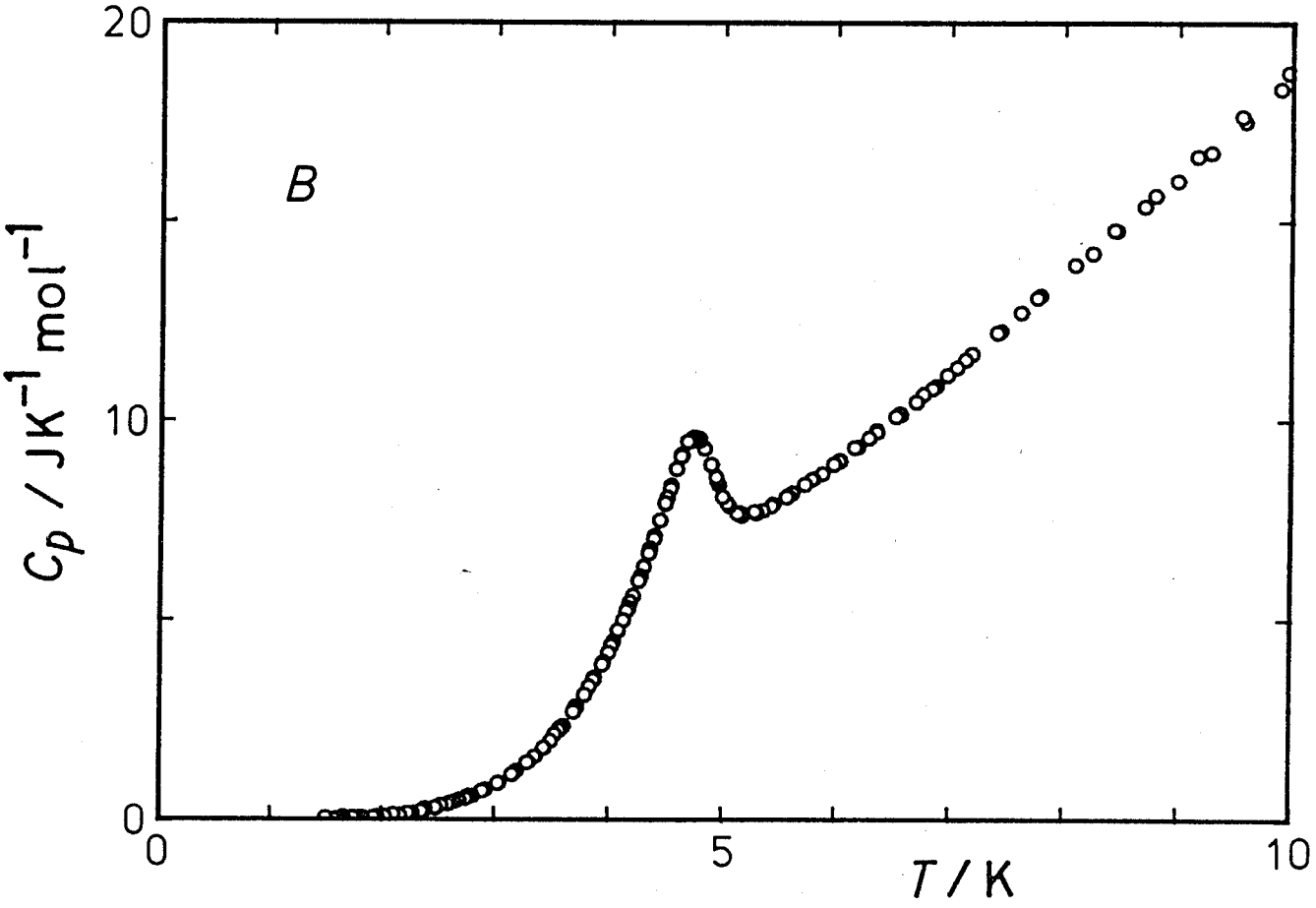

Fig. 5.1 Molar heat capacities of decamethylferrocenium tetracyanoethenide.
B, Heat capacities in the vicinity of the phase transition.

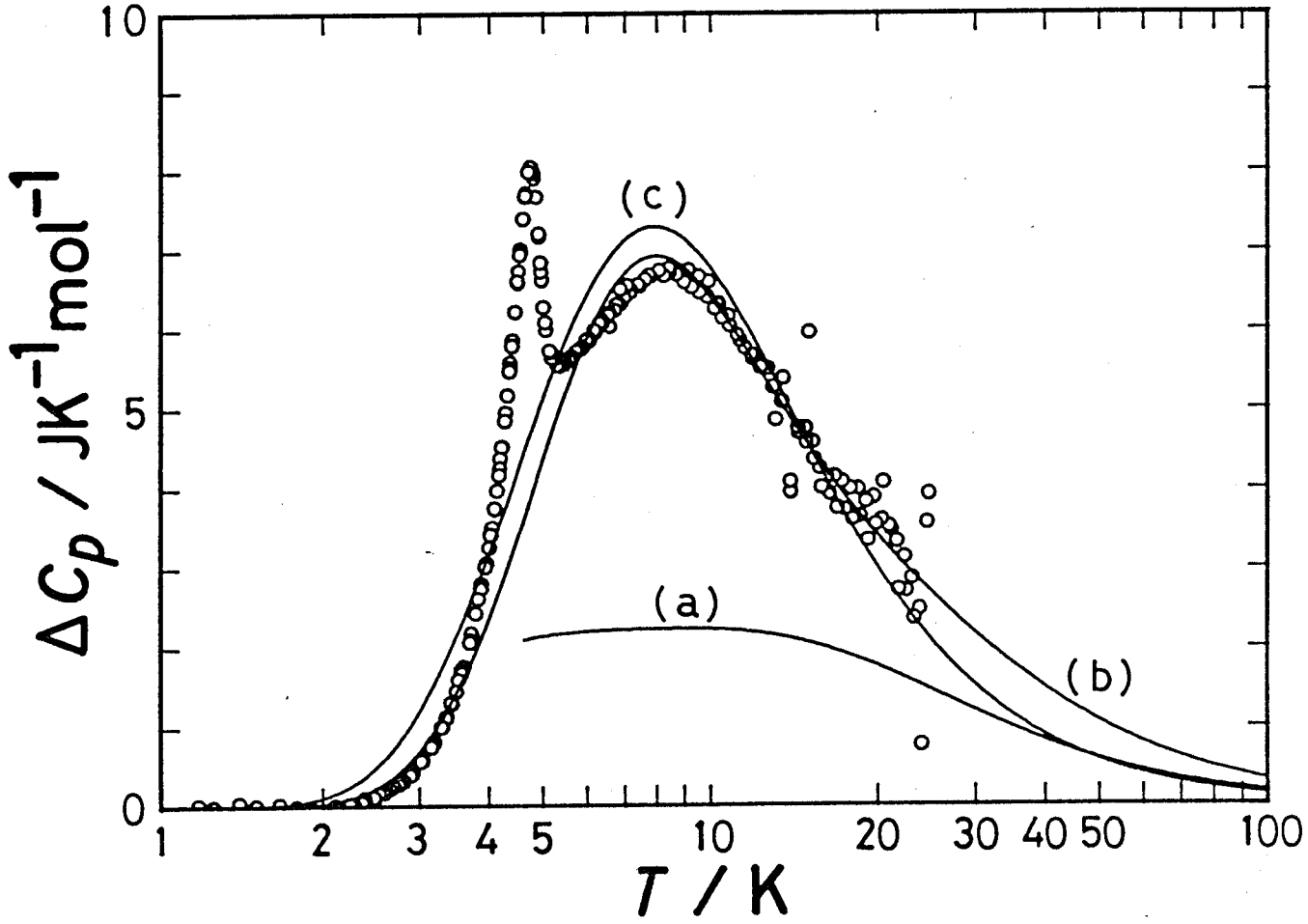

Fig. 5.2 Excess heat capacities of decamethylferrocenium tetracyanoethenide. Three theoretical curves are also shown :
(a), ferromagnetic Heisenberg chain [12];
(b), anisotropic Heisenberg chain with $J_{\perp}/J_{\parallel}$ = 0.5 [21];
(c), pure Ising chain.

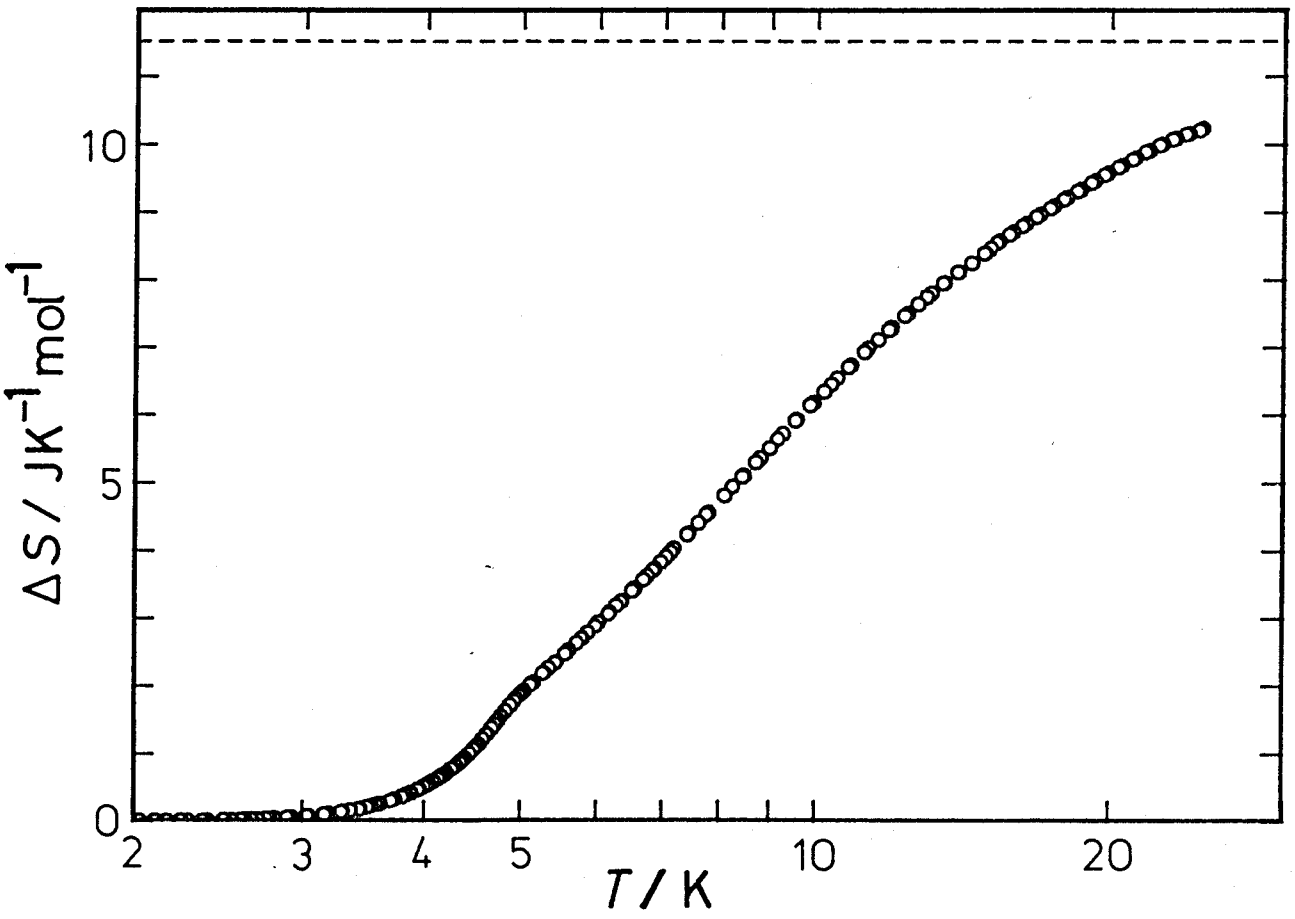

Fig. 5.3 Aquisition of excess entropy of decamethylferrocenium tetracyanoethenide. The broken line shows the theoretical magnetic entropy, 2 R ln 2.

characteristic temperature of $hc\tilde{\nu}/k_B$ (h, k_B and c being the Planck and Boltzmann constants and the speed of light in a vacuum, respectively). The normal heat capacity estimated tentatively is shown in Fig. 5.1 by a broken curve.

Generally more reasonable estimation can be made by use of vibrational spectroscopic data and heat-capacity data at higher temperatures where the magnetic part has a negligible contribution. For this purpose heat-capacity measurements were extended up to 320 K, whose results are given in Table 5.2. Curve-fitting procedures were again applied[22]. This lead to many normal heat-capacity curves which can excellently reproduce the observed heat capacities between 30-320 K. Many kinds of excess heat capacities at low temperatures were obtained by subtracting these normal heat-capacity curves. However, the excess heat capacity below 30 K depended strongly on the choice of normal heat-capacity curve. The unsuccessful extrapolation of normal heat capacities indicates that inclusion of data down to $\sim$10 K is necessary to obtain a conceivable fitting result, though such a procedure induces extra ambiguity because of large contribution of the magnetic part which must be estimated on a assumption, and degrades the reliability of resulting excess part. Therefore we decided to use the normal part described above, which are composed of two Debye heat capacities.

The excess heat-capacity curve is given in Fig. 5.2 against logarithmic temperature. A characteristic feature other than the phase transition at 4.74 K is a remarkable hump centered at 8.5 K. This large hump is hidden by the overwhelming lattice heat capacity and hence can hardly be seen in the observed heat capacity shown in Fig. 5.1. Obviously the hump corresponds to the strong short range order characteristic of the 1D stacking structure in the present compound.

To calculate the magnetic entropy, the excess heat capacity involving both the anomalies was integrated with respect to ln T. The entropy acquisition process is shown in Fig. 5.3. From this figure one can know the saturation value S_{excess} = (12±1) J K^{-1} mol^{-1} and the critical entropy S_c = 1.46 J K^{-1} mol^{-1}, which is defined as the entropy gain up to the critical temperature T_c = 4.74 K. The value of S_{excess} is well approximated by 2 R ln 2 (= 11.53 J K^{-1} mol^{-1}), so that we can conclude that the excess heat capacity arises solely from magnetic origin and contains no other degrees of freedom. In addition, this excellent agreement with 2 R ln 2 confirms that the charge transfer from the donor [DMFc] to the acceptor [TCNE] is complete and that the present compound consists of a spin 1/2 cation and a spin 1/2 anion. The fraction of S_c in S_{excess} is only ~0.12, which is very small in comparison to ordinary 3D Ising magnet 0.75-0.85 or Heisenberg magnet 0.6-0.7. This observation demonstrates the dominant short range order effect above the Curie temperature.

5.2 Anisotropic Character of Magnetic Interaction

The Hamiltonian describing exchange interaction between two spins i and j has the form,

$$H_{ij} = -2J_{\perp} (S_i^X S_j^X + S_i^Y S_j^Y) - 2J_{\parallel} S_i^Z S_j^Z,$$

where $J_{\perp}$ and $J_{\parallel}$ stand for exchange interaction parameters perpendicular and parallel to the molecular axis z, respectively, and S_i^{α} is the α-component of the spin operator for the i-th spin. This Hamiltonian accounts for magnetic properties of a material : positive J corresponds to a ferromagnetic interaction while negative J provides an antiferromagnetic interaction. Moreover, this Hamiltonian describes anisotropy of the magnetic interaction. Three types of interaction with different symmetries are discriminated : the Ising, Heisenberg, and XY types. For the Ising magnet spins interact only with their z-components and $J_{\perp}$ vanishes. The XY magnet is characterized by $J_{\parallel}$ = 0 and hence this may

be called a planer magnet. As an intermediate case between the Ising and XY magnets, the Heisenberg magnet has the so-called "isotropic" interaction $J_{\perp} = J_{\parallel}$. The terms "isotropy" or "anisotropy" do not stand for spatial symmetries but the symmetries with respect to interaction strengths along the spin component directions. In actual substances the Ising or XY type anisotropies are caused from anisotropic *g*-value and/or crystalline field anisotropy. In this section we shall focus on the Ising anisotropy which turns out to take an essential role for the magnetism of [DMFc][TCNE].

In order to interpret the heat capacity hump centered around 8.5 K, the high-temperature expansion of a 1D spin 1/2 isotropic Heisenberg ferromagnetic model [12] was first applied to the present complex, because Miller *et al.*[6-7] adopted this model for the analysis of their magnetic susceptibility data. It turned out, however, that agreement between the observed values and this model is poor (see the curve (a) in Fig. 5.2). More appropriate is rather Blöte's numerical treatment of an anisotropic Heisenberg chain[21]. The Ising type magnetic anisotropy inherent in this compound has already been suggested from magnetic susceptibility data for single crystals [8]. When the anisotropy of the magnetic interaction is relatively weak, the deviation of the heat capacity curve from the isotropic case, $J_{\perp}/J_{\parallel} = 1$, is obvious. However, if the magnetic interaction has a strong Ising character, say, $J_{\perp}/J_{\parallel} < 0.5$, it is practically difficult to discriminate its heat capacity curve from the case of the pure Ising chain, $J_{\perp}/J_{\parallel} = 0$. This is the case for the present complex (see curves (b) and (c) in Fig. 5.2). Taking into account the ambiguity involved in the estimated normal heat capacity, we can only conclude that there exists a really strong Ising type anisotropy of the order of $J_{\perp}/J_{\parallel} < 0.5$ in the present complex. This conclusion derived from the present calorimetric study coincides well with $J_{\perp}/J_{\parallel} \sim 0.30$ derived from the magnetic

susceptibility for single crystals [8].

In many cases the anisotropic exchange interaction is caused by the anisotropic g-value. This is easily understood according to the theoretical treatment by Abragam and Bleaney[23], in which isotropic J multiplet resulting from LS coupling is reduced into an anisotropic effective spin subspace *via* crystal field splitting. At first, isotropic exchange interaction is considered in the true spin space : $H = -2JS_i \cdot S_j$. Through spin-orbital coupling this isotropic spin angular momentum S is combined with an orbital angular momentum L to provide a resultant angular momentum J. As far as only the ground J manifold is concerned, the spin S can be projected onto J so that $S = (g_J-1)J$, where g_J is the Landé g-factor. This projection remains the symmetry of the interaction unchanged : $H = -2J(g_J-1)^2 J_i \cdot J_j$. Crystalline field anisotropy, however, acts on the ground J multiplet to give the ground state with effective spin s and with the degeneracy of $2s+1$. Generally speaking, this ground state is no longer isotropic and has an anisotropic g-factor, g, whose principal values are g_X, g_Y, and g_Z. Therefore, J can be replaced by $g \cdot s/g_J$, so that the exchange Hamiltonian can be rewritten as $H = -2J(1-1/g_J)^2 s_i \cdot g^2 \cdot s_j = -2s_i \cdot \tilde{J} \cdot s_j$. By this argument, it turns out that the anisotropy of the exchange interaction can be represented in terms of the anisotropy in the g-value as $J_\perp / J_\parallel \sim (g_\perp / g_\parallel)^2$.

The anisotropic nature of the exchange interaction in [DMFc][TCNE] is also understood by application of the above discussion. The magnetic interaction under consideration is the one between $[DMFc]^+$ cation radical and $[TCNE]^-$ anion radical in the direction of mixed-stack axis. This causes strong short range correlation as seen from the hump of heat capacity or the 1D magnetic behavior of magnetic susceptibility. As the interchain interaction is very weak, it is neglected at this stage. In the above discussion, the orbital angular momentum L has a finite value. It is this L that introduces anisotropy into the

isotropic exchange in the spin only case. In this respect, $[TCNE]^-$ radical cannot be responsible for an origin of the anisotropic exchange because of its $^2B_{3g}$ ground state. On the other hand, $[DMFc]^+$ radical has the ground state $^2E_{2g}$ and thus this may be responsible to the observed anisotropy. Even though this ground state is affected by the Jahn-Teller effect, the orbital angular momentum would be quenched only weakly, if any, and become an origin of the anisotropic g-factor. For the present complex, the relation between anisotropies in the interaction and g-value should be read as $J_\perp / J_\parallel \sim (g_\perp / g_\parallel)_{DMFc} \cdot (g_\perp / g_\parallel)_{TCNE}$. The $[DMFc]^+$ radical has extremely anisotropic g-value ($g_\perp$ = 1.35, $g_\parallel$ = 4.43)[24], while the $[TCNE]^-$ radical has isotropic g-value ($g_\perp = g_\parallel$ = 2.0)[25]. Consequently the magnitude of interaction anisotropy is expected to be $J_\perp / J_\parallel \sim 0.30$. This value exhibits excellent agreement with the value obtained from single crystal susceptibility and is consistent with the present calorimetric study. Therefore, we can conclude that the Ising character observed in the intrachain interaction arises mainly from the single ion anisotropy of $[DMFc]^+$ cation radical.

5.3 Magnetic Excitations in Ordered Phase

Close examination of the character of magnetic elementary excitations provides a useful information as to what kind of magnetic interaction is exerted between spins. For example, magnetic interaction with continuous symmetry (Heisenberg- or XY-type) causes a collective excitation mode called spin wave, while pure Ising-type interaction give no spin wave but static domain wall for lack of the terms like $S_i^+ S_j^-$ responsible for wave propagation.

Johnson and Bonner[26] studied the excitation spectrum and low temperature thermodynamics of the Ising-Heisenberg linear ferromagnet and found that the low temperature heat capacity behaves as if thermal excitation had a spin-wave

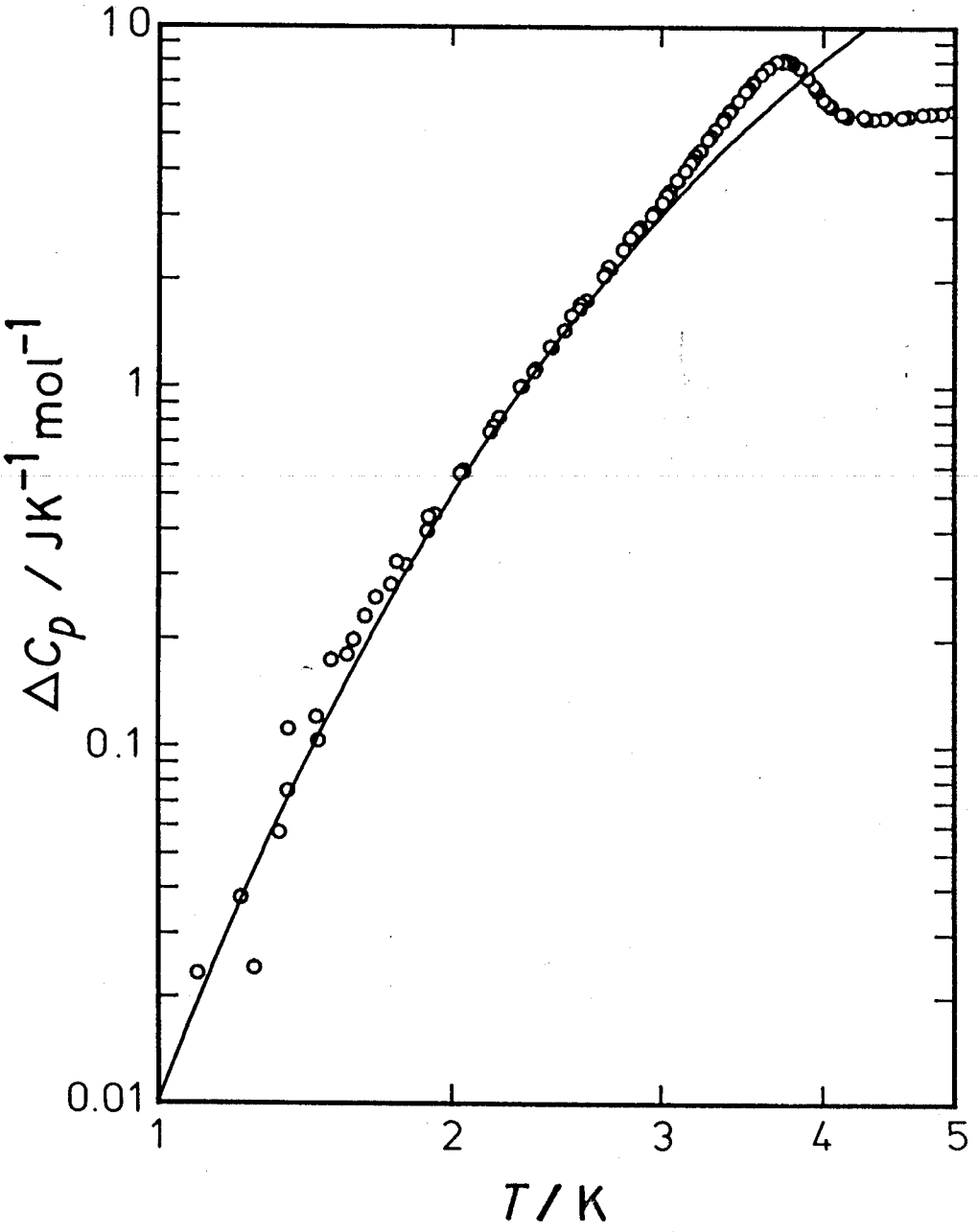

Fig. 5.4 Comparison between the observed and theoretical heat capacities for decamethylferrocenium tetracyanoethenide. The theoretical curve is calculated by 1D Heisenberg-Ising model with $J_{\parallel}/k_B$ = 32.5 K and $J_{\perp}/k_B$ = 16 K [26].

character for $J_\perp / J_\parallel > 3/5$ or a bound-state character for $J_\perp / J_\parallel < 3/5$ although there exists an energy gap for any value of $J_\perp / J_\parallel$ between 0 and 1. This is the reflection of the behavior of thermal excitation energy gap which obeys the following relations,

$\Delta E = (J_\parallel^2 - J_\perp^2)^{1/2}$ for $0 \leqq J_\perp / J_\parallel \leqq 0.6$

and

$\Delta E = 2(J_\parallel - J_\perp)$ for $0.6 \leqq J_\perp / J_\parallel < 1$.

In spite of such a crossover phenomenon, the symmetry of the interaction Hamiltonian remains unchanged with respect to a change in the linear parameter $J_\perp / J_\parallel$.

They also provided the expression for the low temperature heat capacity,

$C/R \sim (J_\parallel^2 - J_\perp^2)/(k_B T)^2 \cdot \exp[-(J_\parallel^2 - J_\perp^2)^{1/2} / k_B T]$.

Comparison between this expression and the excess heat capacity of [DMFc][TCNE] is made in Fig. 5.4, where $J_\parallel / k_B$ = 32.5 K and $J_\perp / k_B$ = 16 K are used. The observed heat capacity obviously exhibits characteristic behavior distinguishable from that of spin waves, which obeys a power law of temperature. Agreement between the observed heat capacity and the equation given above is very well over more than two decades of the temperature, so that we can conclude that the dominant thermal excitation in the present complex is obviously the bound-state type.

In their discussion, Johnson and Bonner are concerned mainly with the excitation spectrum and do not refer much to the dynamics of excitations. They only suggested a connection to the non-linear Schrödinger equation as the quantum soliton problem in the linear chain ferromagnet. Thus the "bound state" described above needs not be confined at a certain point on a chain but can propagate throughout a chain as the soliton. The bound-state character simply stands for the existence of an excitation gap. Solitons may be generally regarded as being a multi-magnon state because they involve many flopped spins.

Thus the bound-state character can be also interpreted as a bound-magnon state.

Soliton in 1D Ising ferromagnet is a subtle effect in contrast to the antiferromagnetic case, because introduction of $S_i^+S_j^-$ terms to an antiferromagnetic Ising chain makes a domain wall movable (Villain mode), while such terms can not provide transferability to a ferromagnetic domain wall of Ising chain[27]. Thus soliton in 1D ferromagnet must not be a simple moving domain wall but rather complicated excitation. Nevertheless, the existence of soliton excitation in a ferromagnetic chain is theoretically predicted for the Heisenberg model with local anisotropy[28], which relates closely to the present complex. ^{57}Fe Mössbauer spectroscopy has showed the possibility of soliton contribution to the line width for this compound[6,13]. The strong Ising character suggested by the present heat-capacity measurements, however, requires relatively thin thickness (close to the intermolecular separation) and low propagation velocity for soliton excitation, hence less contribution to spin relaxation. This discrepancy waits further investigations.

5.4 Estimation of Interchain Interaction

The ferromagnetic phase transition at 4.74 K is obviously a manifestation of the exchange interaction between columns consisting of alternating cation and anion arrays, because pure 1D system cannot bring about a long range order at finite temperatures. This interchain exchange interaction, J_{inter}, is much weaker than the exchange in a column, J_{intra}, which was already discussed and estimated in section 5.2. Note that $J_{\parallel}$ and $J_{\perp}$ in the last section stand for the *z*- and *xy*-components of the intrachain exchange interaction J_{intra}, respectively. In this section, a rough estimation of the interchain interaction is attempted by use of a mean field approximation. According to Scalapino *et al.*[29], the interchain coupling is replaced with a mean field. Then the

resulting 1D problem can be solved exactly for the Ising and Heisenberg cases.

The Hamiltonian of the system with weak coupling between the chains is given by the following equation :

$$H = - \Sigma \ (\ 2J_{\text{intra}} \ S_{m,n}S_{m,n+1} + 2J_{\text{inter}} \ S_{m,n}S_{m+1,n} + \ h \ S_{m,n} \ ),$$

where $S_{m,n}$ denotes the spin operator of the n-th spin on the m-th chain and h is an external field represented with dimension of energy. This Hamiltonian is then reduced to the mean field Hamiltonian for the m-th chain,

$$H_m = - \Sigma \ (\ 2J_{\text{intra}} \ S_n S_{n+1} + h' \ S_n \ ),$$

where the mean field $h' = h + 2zJ_{\text{inter}}\langle S\rangle$ is introduced with the coordination number z of a chain and the expectation value $\langle S\rangle$ of single spin operator S_n. The m-th chain is magnetized by the mean field h'. This relation is expressed as follows invoking the magnetic susceptibility χ_{1D} of a spin on an isolated chain :

$$\langle S\rangle = \chi_{1D} \cdot h' = \chi_{1D} \cdot \ \{ h + 2zJ_{\text{inter}}\langle S\rangle \} \ .$$

This expression gives the following linear response $\langle S\rangle$ with respect to the external field h :

$$\langle S\rangle = h \cdot \ \{ \chi_{1D} \ / \ (1 - 2zJ_{\text{inter}}\chi_{1D}) \} \ \equiv \ h \cdot \chi(T).$$

The divergence of $\chi(T)$ is expected for a ferromagnet at $T = T_C$. Hence the denominator of $\chi(T)$ must vanish at $T = T_C$, as $\chi_{1D}(T)$ has no singularities at finite temperatures. Thus the critical temperature T_C is given by

$$1 - 2zJ_{\text{inter}}\chi_{1D}(T_C) = 0.$$

From this equation one can estimate $J_{\text{inter}} = [2z\chi_{1D}(T_C)]^{-1}$.

The magnetic susceptibility χ_{1D} for an isolated chain can be solved exactly for several 1D magnetic systems. For the 1D Ising model with ferromagnetic coupling J, magnetic susceptibility is given by[30]

$$\chi_{1D}(T) = (S^2/k_B T) \ \exp[4JS^2/k_B T].$$

For the 1D Heisenberg model with ferromagnetic coupling J, the corresponding relation is expressed as follows[31] :

$$\chi_{1D}(T) = (S^2/3k_B T)\ (1+u)/(1-u),$$

where u means the Langevin function $u = \coth[2JS^2/k_B T] - k_B T/2JS^2$. In addition S^2 was put equal to 1/4 because above two expressions of χ_{1D} was provided for classical systems. Following above discussion the interchain interaction was estimated to be J_{inter}/k_B = 4.9 mK for the Ising case and J_{inter}/k_B = 0.97 K for the Heisenberg case by using T_C = 4.74 K, J_{intra}/k_B = 27.4 K[8], and assumed z = 6 (See Fig. 5.5). These two values are regarded as being extreme cases and the real value may be between the two. The interpolation formula for the Ising-Heisenberg 1D ferromagnet[26] is available to estimate more plausible value, which becomes

$$\chi_{1D}(T) \sim (S^2/k_B T)\ \exp[4S^2(J_{\parallel}{}^2 - J_{\perp}{}^2)^{1/2}/k_B T],$$

when the anisotropy of magnetic interaction $J_{\parallel}/J_{\perp}$ is large. If we adopt the anisotropic interactions determined from single crystal susceptibility, $J_{\parallel}/k_B$ = 27.4 K and $J_{\perp}/k_B$ = 8.1 K, we obtain J_{inter}/k_B = 6.3 mK. This value is the most realistic one in this mean field approach.

To examine the validity of this approach a comparison with exact solution was made for the 2D Ising quadratic model. Onsager's exact solution for 2D Ising model provides the value $J_{inter}/k_B \sim$ 29.3 mK by the equation,

$$\sinh(J_{inter}/k_B T_C)\ \sinh(J_{intra}/k_B T_C) = 1,$$

which can be reduced to $k_B T_C/J_{inter} = (1/2)\ \exp[J_{intra}/k_B T_C]$ under the condition of $J_{intra} \gg k_B T_C \gg J_{inter}$. For the same 2D model the mean field approximation provides J_{inter}/k_B = 14.7 mK when the coordination number is z = 2. Hence the mean field approach provides just a half value of the exact solution. This is a common behavior to mean field approximations. In many cases mean field approximations bring this tendency from their intrinsic character : neglection of fluctuations causes rather high estimate of critical temperature for a given system. That is, the overestimation of critical temperature is equivalent to

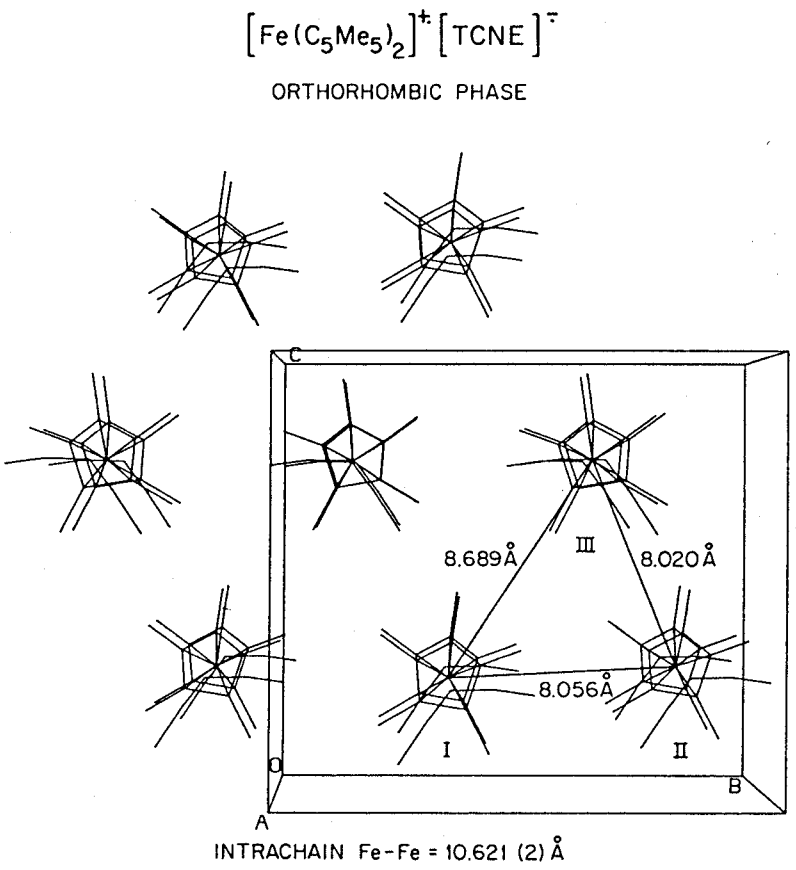

Fig. 5.5 Crystal structure of decamethylferrocenium tetracyanoethenide projected on *bc*-plane [11]. Each column is neighbored by six columns.

the underestimation of microscopic interaction strength. From the result of above test, the mean field estimation was confirmed within a factor of $\sim$2.

It can be concluded that [DMFc][TCNE] has strong anisotropy in its magnetic lattice structure, $J_{inter}/J_{intra} \sim 0.0002$, in addition to extreme Ising anisotropy of magnetic interaction, $J_{\parallel}/J_{\perp} \sim 3$.

5.5 Heat Capacity at Higher Temperatures

Heat capacities were also measured in the temperature region 25-320 K for the purpose of reliable estimation of the lattice heat capacity (Table 5.2). In this study two phase transitions were newly found at 248.7 K and at 281.8 K. To separate the anomalous heat capacities from the contribution of lattice vibrations, a normal heat capacity was estimated by invoking the effective frequency-distribution method[22]. Excess heat capacities around these phase transitions are shown in Fig. 5.6. The anomaly centered at 248.7 K exhibits rather sharp peak tailing to low temperatures, while the anomaly around 281.8 K seems to be a broad cusp. Heat capacity near 295 K has small waving caused by incomplete cancellation of the contribution from Apiezon L grease used in cell sealing.

The excess enthalpy and entropy arising from these two anomalies were calculated to be ΔH = 3320 J mol^{-1} and ΔS = 12.8 J K^{-1}mol^{-1}, respectively. These values are too large to attribute the anomalies to impurity effect, if any. As shown in Fig. 5.6 the two anomalies were tentatively separated by a straight line and the respective transition entropies were obtained as follows : $\Delta S \sim$ 5.9 J K^{-1} mol^{-1} for the low temperature anomaly and $\Delta S \sim$ 7.0 J K^{-1} mol^{-1} for the high temperature one. Both values are close to R ln 2 (= 5.76 J K^{-1} mol^{-1}), suggesting these phase transitions are of order-disorder type in nature.

Several candidates responsible for these phase transitions are easily listed

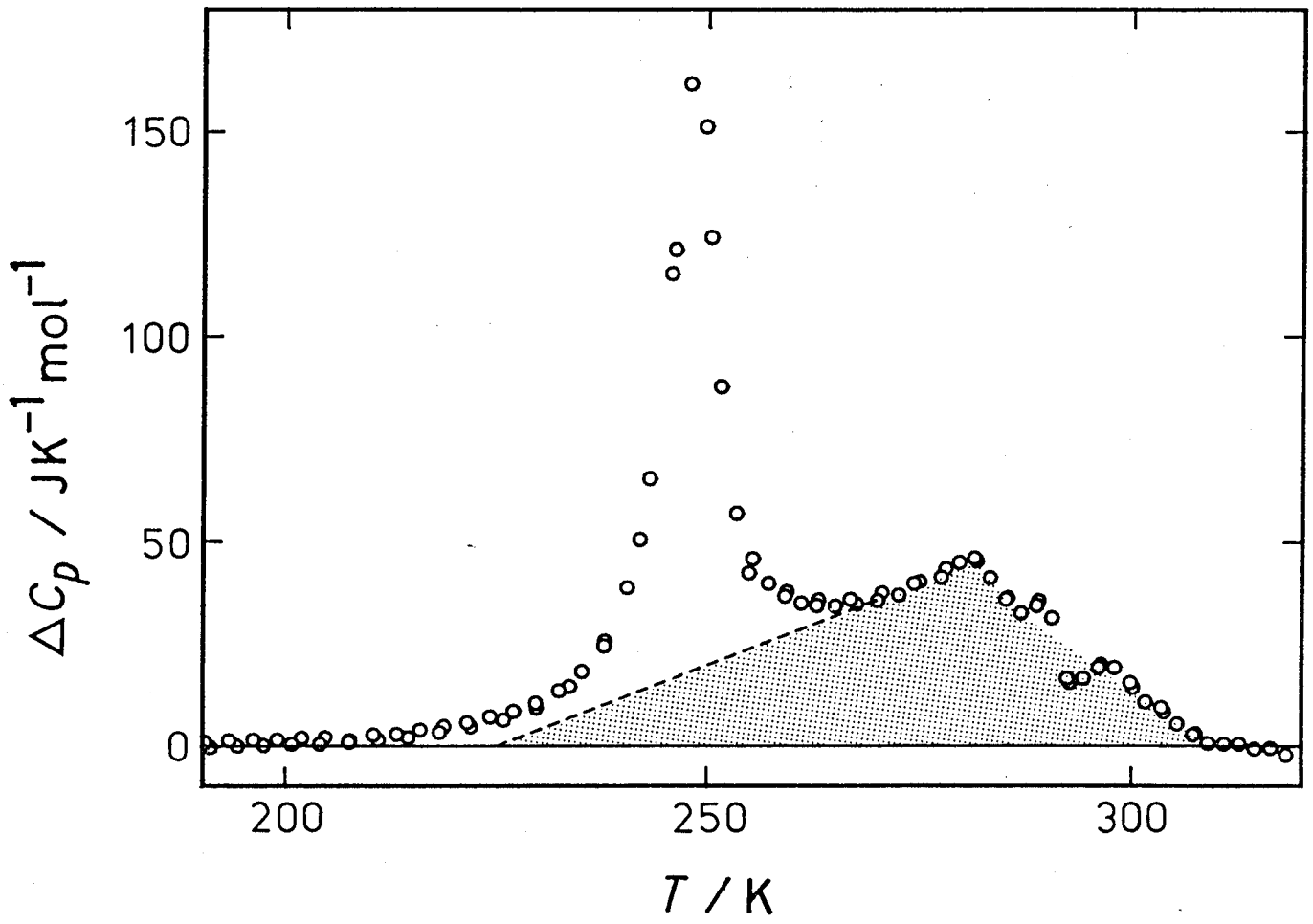

Fig. 5.6 Anomalous heat capacities of decamethylferrocenium tetracyanoethenide. Two anomalies are tentatively separated by a broken line.

up, for example, cooperative Jahn-Teller phenomenon, neutral-to-ionic phase transition, and orientational order-disorder phenomenon. Cooperative Jahn-Teller phenomenon likely occurs in $[DMFc]^+$ cations, which have the electronically degenerate ground state $^2E_{2g}$ and must have a vibronic coupling leading the $e \times E$ Jahn-Teller effect. It is pointed out that Jahn-Teller species on a quasi-1D lattice may have a partially disordered phase[32] or undergo a commensurate-incommensurate phase transition[33], so that it may provides a explanation of successive phase transitions. Neutral-to-ionic phase transitions are sometimes induced in charge-transfer complexes by varying temperature or pressure[34]. Orientational order-disorder transition is most plausible candidate because a disorder in $[TCNE]^-$ anion was reported from X-ray structural analysis at room temperature and at -40 °C[6]. Such a disorder has a potential to cause a phase transition within its ordering process. It is, however, incomprehensible that the disorder of $[TCNE]^-$ anion was observed not only at room temperature but also at -40 °C in spite that the both transition temperatures, 248.7 K and 281.8 K, are higher than -40 °C. Further investigations, especially structural analysis below 200 K, are necessary.

Table 5.1 Molar heat capacities of decamethylferrocenium tetracyanoethenide.

$\frac{T}{K}$	$\frac{Cp}{JK^{-1}mol^{-1}}$	$\frac{T}{K}$	$\frac{Cp}{JK^{-1}mol^{-1}}$	$\frac{T}{K}$	$\frac{Cp}{JK^{-1}mol^{-1}}$	$\frac{T}{K}$	$\frac{Cp}{JK^{-1}mol^{-1}}$	$\frac{T}{K}$	$\frac{Cp}{JK^{-1}mol^{-1}}$	$\frac{T}{K}$	$\frac{Cp}{JK^{-1}mol^{-1}}$
2.3947	0.2913	12.9852	27.1804	3.9610	3.9620	13.9681	28.5594	3.8840	3.5713	4.4029	7.1042
2.5401	0.3888	13.4965	28.1839	4.0873	4.7400	14.4086	30.7688	4.0307	4.3657	4.4491	7.5027
2.6611	0.4781	13.9658	28.6830	4.2181	5.6121	14.8594	32.1945	4.1641	5.2176	4.4960	7.9119
2.7790	0.6087	14.4253	30.7596	4.3535	6.6702	15.2921	33.3986	4.2819	6.0888	4.5431	8.3712
2.9056	0.7574	14.8982	32.1402	4.4916	7.9231	15.7437	34.4911	4.3951	7.0246	4.5908	8.7946
3.0343	0.9412	15.3841	33.4705	4.6366	9.1201	16.2502	35.9786	4.5114	8.0685	4.6393	9.1561
3.1630	1.1630	15.8845	34.6825	4.7921	9.4939	16.7799	37.6426	4.6321	9.1173	4.6883	9.4798
3.2962	1.4675	16.4015	36.2346	4.9614	8.3974	17.3269	39.2887	4.7593	9.5724	4.7382	9.5863
3.4355	1.8281	16.9354	37.7358	5.1287	7.6799	17.8915	41.0155	4.8960	8.8706	4.7887	9.5606
3.5770	2.2663	17.4849	39.4252	5.2851	7.7146	18.4731	42.7857	5.0344	7.9347	4.8398	9.3114
3.7219	2.8599	18.0522	41.0684	5.4483	7.9106	19.0731	44.6154	5.1667	7.6292	4.8927	8.9021
3.8728	3.5065	18.6381	42.9284	5.6222	8.2063	19.6929	46.5602	5.2984	7.6896	4.9459	8.4826
4.0308	4.3766	19.2432	44.5823	5.8004	8.5467	20.3318	48.1825	5.4366	7.8715	4.9995	8.0866
4.1929	5.4492	19.8658	46.6667	5.9830	8.9246	20.9894	50.1567	5.5803	8.1235	5.0548	7.8626
4.3618	6.7856	20.5069	49.1422	6.1705	9.3292	21.6682	52.0531	5.7282	8.4138		
4.5379	8.3007	21.1690	50.5789	6.3639	9.7732	22.3633	54.0181	5.8804	8.6865		
4.7254	9.4970	21.8458	51.9350	6.5640	10.2046	23.0754	56.0181	6.0364	9.0232		
4.9383	8.5869	22.5401	54.4163	6.7696	10.6847	23.8077	58.0946	6.1965	9.3557		
5.1573	7.6941	23.2543	56.5040	6.9808	11.1669	24.5575	61.6269	6.3611	9.7262		
5.3595	7.7559	23.9898	57.7496	7.1986	11.6861			6.5300	10.1202		
5.5684	8.0942	24.7381	62.8030	7.4228	12.2221	1.5848	0.0270	6.7041	10.4926		
5.7938	8.5338			7.6268	12.7258	1.6620	0.0293	6.8822	10.8801		
6.0362	8.9965	1.5043	0.0650	7.8000	13.1556	1.7487	0.0663	7.0657	11.3586		
6.2952	9.5690	1.6634	0.0940	8.2529	14.2238	1.8398	0.0686				
6.5704	10.1735	1.6098	0.0448	8.4641	14.7736	1.9348	0.0737	3.3588	1.6009		
6.8501	10.8273	1.7934	0.0789	8.7063	15.3795	2.0373	0.1008	3.5019	2.0086		
7.1415	11.5391	1.9673	0.0981	8.9894	16.0184	2.1724	0.1334	3.6120	2.3772		
7.4484	12.2606	2.1132	0.1467	9.2803	16.7471	2.2850	0.1801	3.7087	2.7616		
7.7672	13.0940	2.2435	0.1855	9.5799	17.5116	2.3910	0.2538	3.7957	3.1474		
8.0991	13.9220	2.3651	0.2305	9.8888	18.3354	2.4950	0.3068	3.8753	3.5115		
8.4429	14.7866	2.4887	0.3225	10.2079	19.1152	2.5958	0.4096	3.9489	3.9032		
8.7982	15.6521	2.6185	0.4336	10.5363	19.9703	2.7006	0.5181	4.0055	4.1884		
9.1653	16.6441	2.7566	0.5569	10.8747	20.8986	2.8147	0.6126	4.0477	4.4748		
9.5528	17.6371	2.8982	0.7373	11.2244	21.8528	2.9290	0.7723	4.0906	4.7328		
9.9573	18.7239	3.0479	0.9569	11.5849	22.8117	3.0487	0.9529	4.1338	5.0036		
10.3784	19.6842	3.2026	1.2544	11.9565	23.8384	3.1760	1.1995	4.1775	5.3114		
10.8153	20.8428	3.3660	1.6268	12.3366	24.9244	3.3061	1.4788	4.2217	5.6084		
11.3303	22.1164	3.5363	2.1706	12.7261	26.1506	3.4413	1.8284	4.2659	5.9725		
11.8753	23.6299	3.6992	2.7259	13.1277	26.7895	3.5810	2.3177	4.3109	6.3346		
12.4272	25.2394	3.8350	3.3545	13.5407	28.6228	3.7314	2.8415	4.3569	6.7100		

Table 5.2 Molar heat capacities of decamethylferrocenium tetracyanoethenide.

$\frac{T}{K}$	$\frac{Cp}{JK^{-1}mol^{-1}}$	$\frac{T}{K}$	$\frac{Cp}{JK^{-1}mol^{-1}}$	$\frac{T}{K}$	$\frac{Cp}{JK^{-1}mol^{-1}}$	$\frac{T}{K}$	$\frac{Cp}{JK^{-1}mol^{-1}}$	$\frac{T}{K}$	$\frac{Cp}{JK^{-1}mol^{-1}}$
79.911	236.892	179.007	456.729	199.120	495.201	292.493	661.408	27.464	69.513
82.397	244.115	181.937	461.927	201.996	500.651	294.316	664.192	28.318	74.054
84.807	250.859	184.916	467.723	204.855	505.779	296.148	669.623	28.863	76.638
87.153	257.282	187.945	473.518	207.698	509.939	297.980	672.419	29.394	80.136
89.441	263.482	191.059	479.192	210.526	516.039	299.811	671.508	29.917	83.663
91.678	269.508	194.255	485.052	213.337	521.087	301.644	669.557	30.431	86.533
93.866	275.275	197.499	490.984	216.132	526.738	303.477	671.065	30.431	86.533
96.012	280.861	200.789	496.987	218.910	532.436	305.313	669.831	32.208	85.190
98.117	286.197	204.159	502.882	221.673	537.976	307.149	669.920	34.059	90.120
100.186	291.709	207.608	509.209	224.421	543.912	308.984	670.454	35.725	96.707
102.222	296.523	211.135	515.921	227.154	549.759	310.815	673.053	36.855	99.872
104.226	301.406	214.736	522.590	229.872	556.258	312.645	675.748	37.904	103.090
106.201	306.348	218.411	529.992	232.573	563.679	314.471	677.319	39.289	107.389
108.627	312.388	222.159	537.616	235.256	572.851	316.295	680.122	40.586	111.955
111.489	319.147	225.978	545.666	237.918	584.597	318.119	681.280	41.559	116.607
114.300	325.785	229.897	555.059	240.554	601.955			42.235	117.834
117.065	332.133	233.877	566.839	243.150	632.684	15.099	26.435	42.887	120.003
119.787	338.340	237.910	583.381	245.683	686.831	15.786	29.321	44.129	122.710
122.469	344.273	242.001	616.223	247.842	736.718	16.432	39.574	45.904	128.623
125.115	350.126	246.110	693.513	249.663	729.103	17.217	38.910	47.571	134.202
127.726	355.851	250.347	703.286	251.517	668.855	18.073	46.025	48.997	139.057
130.306	361.223	254.863	628.757	253.408	641.040	18.916	44.036	50.255	143.393
132.855	366.491	259.323	631.155	255.313	632.869	19.759	46.000	51.560	147.807
135.377	371.562	263.129	635.122	257.222	629.869	20.965	46.250	52.906	152.390
137.872	377.029	266.908	641.177	259.129	629.737	22.473	49.078	54.331	157.300
140.343	381.478	270.663	648.710	261.031	631.011	23.929	56.624	55.830	162.410
142.791	386.585	274.401	656.824	262.929	633.500	25.290	62.598	57.391	167.628
145.217	391.485	278.122	666.267	265.135	636.774	26.526	66.320	59.049	173.173
147.621	396.012	281.826	673.839	267.643	641.180	27.666	69.781	60.794	178.959
150.003	401.315	285.513	670.525	270.141	645.927	28.839	73.996	62.651	184.904
152.363	405.808	289.164	675.379	272.631	651.247	30.284	79.359	64.610	191.179
154.705	410.554	292.795	660.806	275.114	658.394	31.986	83.697	66.659	197.576
157.030	414.967	296.448	670.794	277.589	663.368	33.654	88.444	68.823	204.087
159.337	419.639	300.117	670.740	279.744	670.324	35.181	93.247	71.120	210.942
161.628	424.126	303.787	670.448	281.583	674.224	36.592	98.293	73.569	218.227
164.279	429.071	307.459	670.597	283.420	672.194			76.153	225.908
167.285	434.809			285.253	669.650	20.629	48.915	78.889	233.532
170.269	440.684	190.382	479.123	287.081	669.100	23.437	55.394	81.819	241.635
173.229	446.114	193.313	484.837	288.896	673.819	24.915	61.287	84.947	250.524
176.130	451.385	196.226	490.083	290.691	673.403	26.250	65.529	88.258	259.730

Chapter 6. Molecular Antiferromagnet : [DMFc][TCNQ]

6.1 Introduction

The charge transfer salt between decamethylferrocene (DMFc) and 7,7,8,8-tetracyano-*p*-quinodimethane (TCNQ) has two polymorphs with 1:1 composition[13]. One is a 1D phase with mixed columns and the other is a dimeric phase, which shows paramagnetism but has a singlet ground state. Of these two polymorphs the 1D phase is of great interest because its crystalline structure is similar to that of [DMFc][TCNE]. Magnetically the $[TCNQ]^-$ radical behaves similarly to the $[TCNE]^-$ radical. A remarkable difference between these two radicals is their dimensions. The cyano group moieties, on which the unpaired electron is mainly distributed, are separated further in a $[TCNQ]^-$ radical by intervening quinone ring than in a $[TCNE]^-$ radical. Hence an overlap with the π-orbital of the cyclopentadienyl ring is expected to be small in comparison to [DMFc][TCNE] and thus strength of the magnetic interaction is also weak. In practice, magnetic susceptibility measurement[35] revealed the Curie-Weiss behavior of [DMFc][TCNQ] with a small Weiss temperature θ = +3 K, in contrast to the large Weiss temperature θ = +30 K for [DMFc][TCNE]. Miller *et al.*[13] described, about the metamagnetic behavior of the compound, that a dominant interaction is intrachain ferromagnetism with a weak interchain antiferromagnetism. This idea well explained the behavior of magnetic susceptibility under an applied field, that is, only 0.15 T ($\sim$0.2 K) of external field is sufficient to change the antiferromagnetic behavior to the ferromagnetic one[35].

By means of ^{57}Fe Mössbauer spectroscopy, Miller *et al.*[13] found that below the antiferromagnetic phase transition temperature 2.55 K, $[DMFc]^+$ cations occupy two non-equivalent sites with the ratio 2:1 in the 1D phase. This observation implies that the magnetic ordering is associated with a structural change. Miller *et al.* suggested that this magnetostructural phase transition has a spin Peierls nature[13] and they speculated a model structure, which can

provide an explanation for the 1:2 ratio of non-equivalent sites. It is an asymmetric trimerization in a mixed column : ···DADADADA··· → ···DAD ADA DAD···, where D and A denote a donor molecule $[DMFc]^+$ and an acceptor molecule $[TCNQ]^-$, respectively. Thus the calorimetric study of [DMFc][TCNQ] is of interest from a viewpoint of magnetostructural coupling. Comparison with the magnetic phase transition of the TCNE homologue is also interesting in the sense, how the magnetic behavior is modified by changing from a symmetrically alternating chain in the TCNE complex to an asymmetrically arrayed chain in the TCNQ complex.

6.2 Experimental

(1) Preparation of sample

Although the 1D phase of [DMFc][TCNQ] is thermodynamically metastable in comparison to the dimeric phase, it can be prepared under a suitable experimental condition. To obtain the 1D phase rapid crystallization from a solution is required. The preparation was carried out according to the method of Miller *et al.*[13]. A hot dichloroethane solution of TCNQ (3.76 g/ 400 ml) was added to a hot dichloroethane solution of DMFc (6.00 g/ 100 ml). Dark green precipitates were rapidly formed and filtered. Obtained tiny crystals of the 1D phase were washed with cold dichloroethane and desiccated in a vacuum. All the procedures were carried out in a glove box filled with argon gas to prevent decomposition of the compound. The yield was 67 %. *Anal.* Calcd for $C_{32}H_{34}FeN_4$: C, 72.45; H, 6.46; N, 10.56%. Found : C, 72.46; H, 6.46; N, 10.52%.

In order to identify the 1D phase, powder X-ray diffraction and infrared spectra were recorded. The powder pattern of this compound is compared with calculated lines for both the 1D phase and the dimeric phase using their lattice constants[13] in Fig. 6.1. Of 56 observed diffraction lines, 7 lines coincide with the 1D phase, while 15 lines coincide with the dimeric phase. This

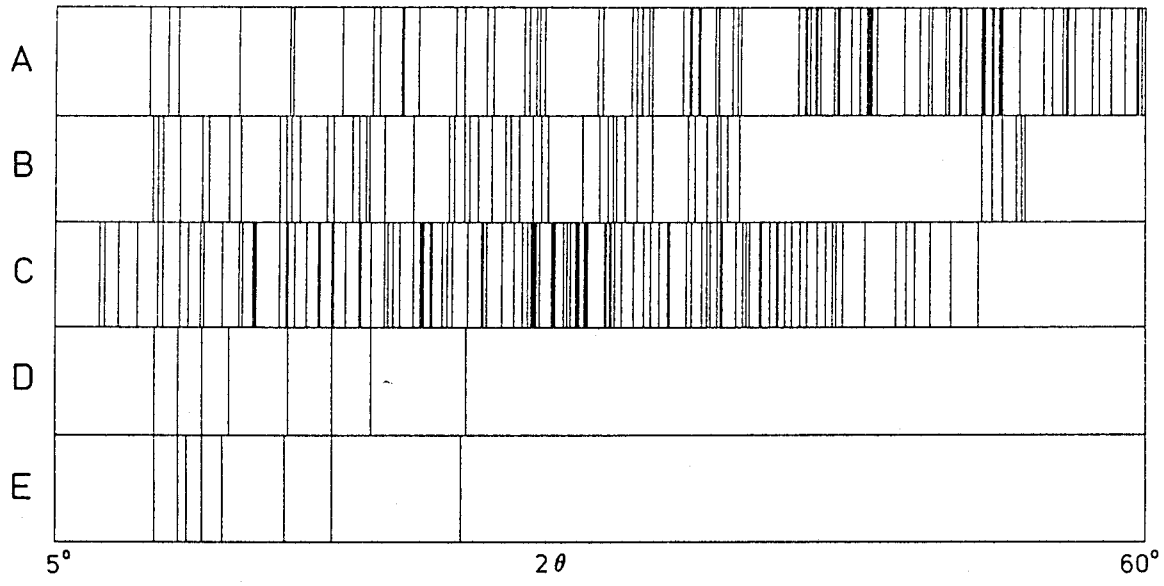

Fig. 6.1 X-ray powder diffraction patterns for decamethylferrocenium tetracyanoquinodimethanide. Patterns A and C are calculated by use of lattice parameters for the dimeric phase and for the 1D phase, respectively [13]. Pattern B represents the observed data. Patterns D and E are reported ones for fresh and air-exposed sample [36].

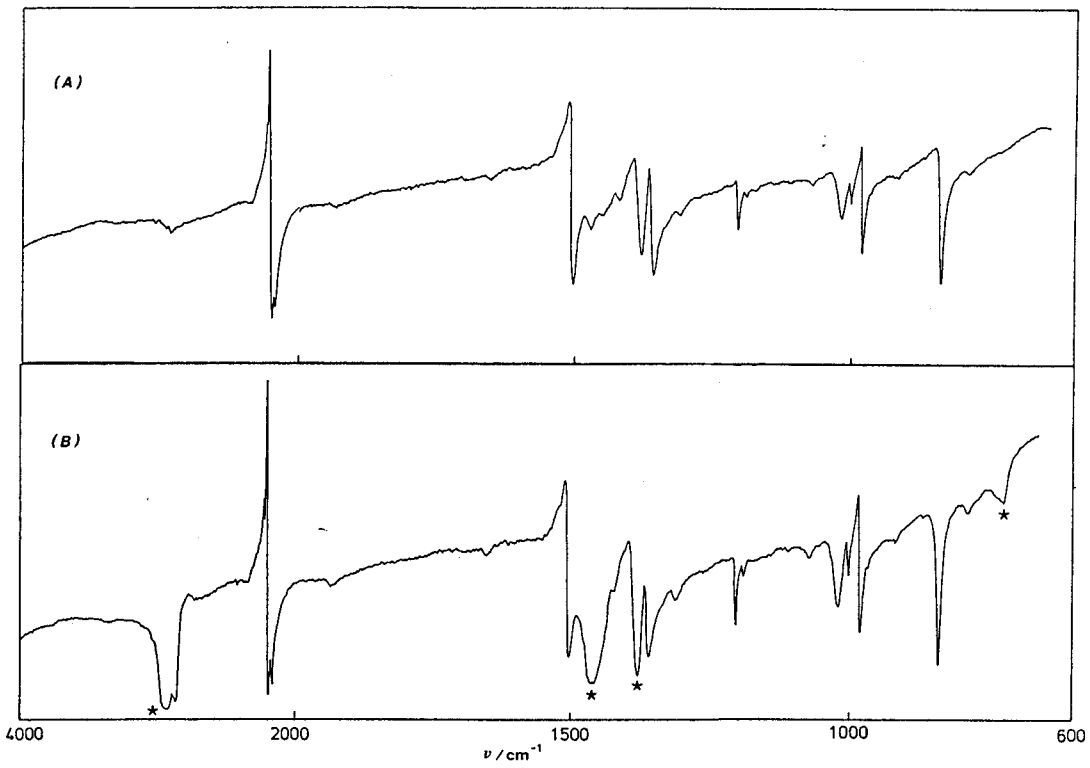

Fig. 6.2 IR spectra of decamethylferrocenium tetracyanoquinodimethanide recorded by means of (A) KBr disk method and (B) Nujol mull method. Absorption peaks with * are assigned to Nujol.

suggests that the sample is a mixture of two polymorphs of [DMFc][TCNQ]. A partial decomposition of the X-ray sample, however, cannot be denied because the powder diffraction was recorded in air without any protections against oxidation. For this reason, another fact may be understood, that is, more than half of the observed lines can be assigned to neither of the two polymorphs. The infrared spectra also revealed a curious behavior. As can be seen from Fig. 6.2, some of the absorption peaks are accompanied by weird negative peaks at higher wave-number side. This phenomenon was observed in both KBr disk and nujol mull, and can be explained by the Christiansen filter effect. This effect is associated with a rapid change of the refractivity of the crystals near some absorption bands. When the refractivity of the crystal becomes equal to the refractivity of surrounding KBr or nujol, the surface scattering of infrared light is suppressed and hence the transparency is enhanced. This effect is avoidable in principle by grinding a sample to the grain size smaller than wave lengths of the incident light. From the absence of a characteristic absorption band of carbonyl group, it is concluded that the sample contains no [*p*-$(NC)_2C=C_6H_4=C(O)CN]^-$ anions produced by an oxidation of $[TCNQ]^-$ anions.

(2) Calorimetry

In a sample container, 2.7373 g of the sample was loaded with 21 kPa of ^3He gas. Heat capacities were measured in the temperature region between 1-25 K by means of the very low temperature calorimeter. The adiabatic mode, where a AuFe(0.07 %)-Chromel thermocouples were attached to the calorimeter, was used for the temperature control of the thermal shield.

6.3 Results and Discussion

The calorimetric results were tabulated in Table 6.1 and shown in Figs. 6.3 and 6.4. In these figures the heat capacities of [DMFc][TCNE] are also shown for comparison. A sharp peak centered at 2.54 K was observed. This transition

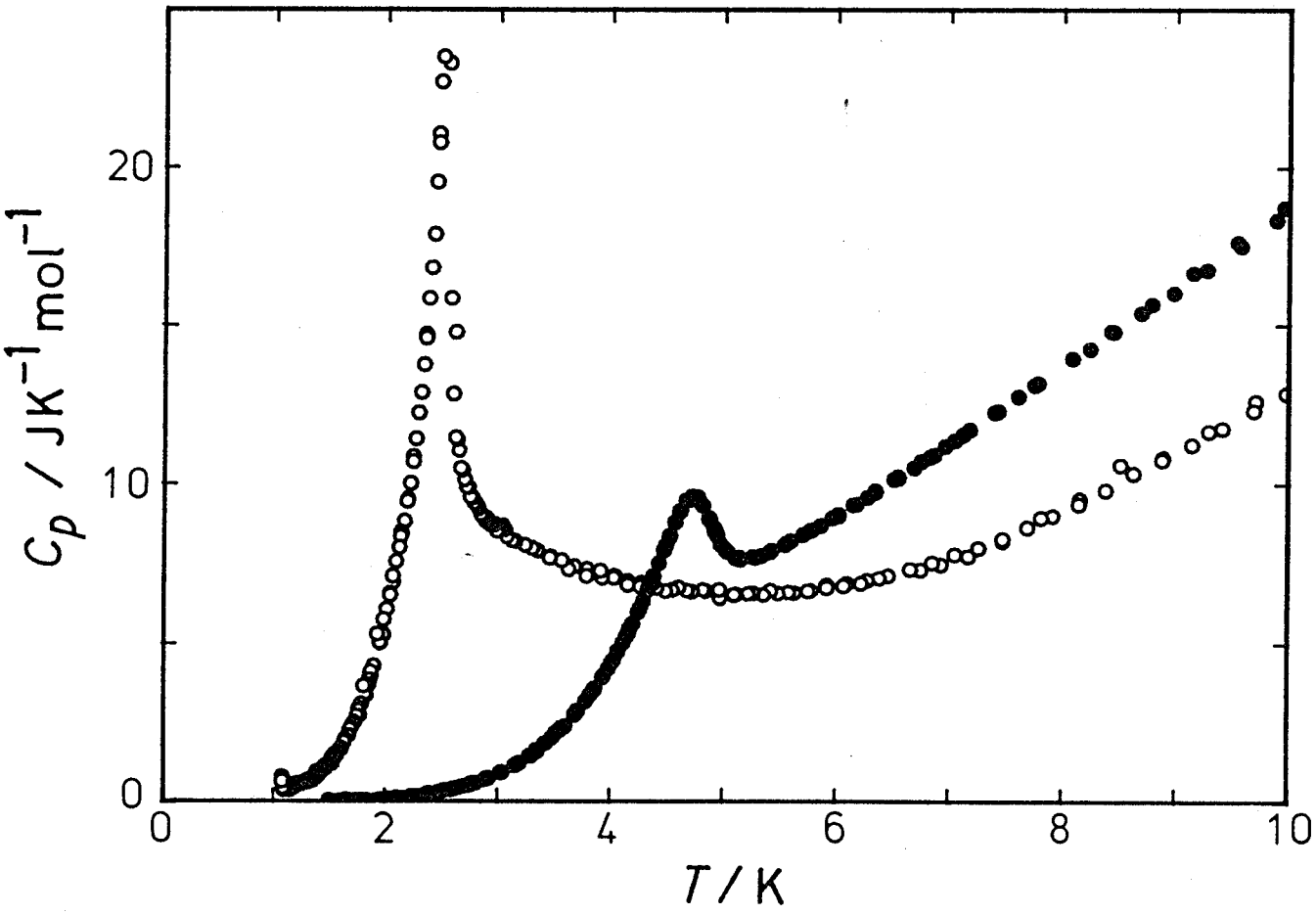

Fig. 6.3 Comparison of molar heat capacities between the two charge-transfer complexes. Open circles show the data of decamethylferrocenium TCNQ, while filled circles show the data of decamethylferrocenium TCNE.

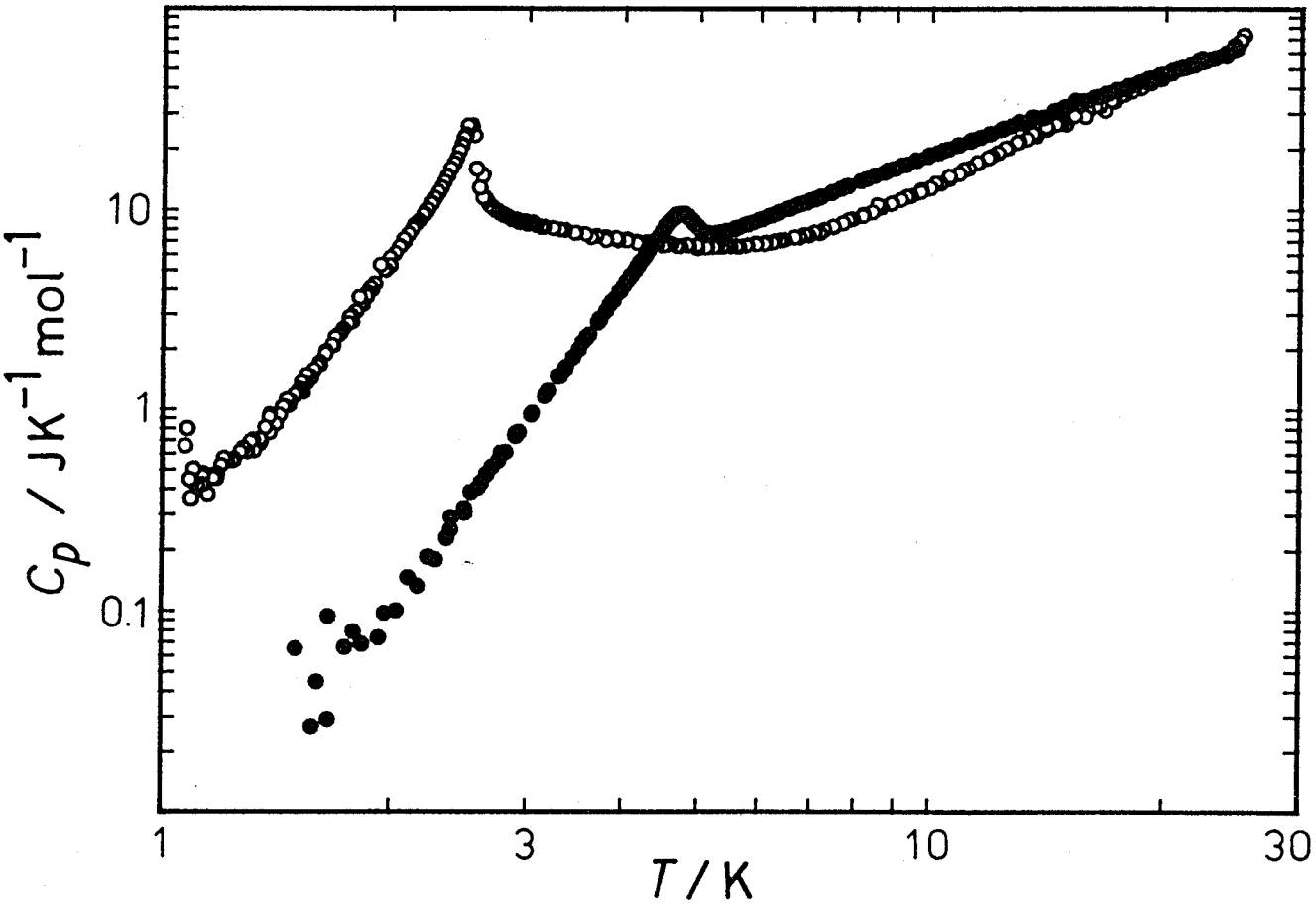

Fig. 6.4 Comparison of molar heat capacities between the two charge-transfer complexes. Open circles show the data of decamethylferrocenium TCNQ, while filled circles show the data of decamethylferrocenium TCNE.

temperature agreed well with the reported Neel temperature[13]. No latent heat was observed and the phase transition is considered to be of second order.

Based on the ^{57}Fe Mössbauer spectroscopy, which suggests some structural change associated with this phase transition, Miller *et al.*[13] pointed out that such a magnetostructural behavior is analogous to a spin Peierls transition. Thus we shall discuss the heat-capacity anomaly in relation to the spin Peierls transition. The shape of the phase-transition peak bears a resemblance to that derived from a mean field theory except that the heat-capacity gap remains about two thirds of the peak height and there is a large tail at high temperature side. In the spin Peierls transition, the heat capacity above the transition temperature has a linear dependence of temperature due to antiferromagnetic magnon in a 1D chain, and the heat-capacity gap amounts to 1.43 times of the linear term value at the transition temperature, *i.e.* $1.43 \cdot (k_B^2/3J) \cdot T_N$, where J stands for the antiferromagnetic exchange interaction[37]. If we use the Weiss temperature, +3 K, in place of J, this relation provides a heat-capacity gap of about 6.7 J K^{-1} mol^{-1}. The observed value is twice as large as the prediction. The spin Peierls transition occurs at the temperature where the increment of elastic energy by lattice distortion is compensated with the reduction of magnetic energy resulting from the induced energy gap, J, in magnetic excitation spectrum. In the present complex the expected energy gap $\sim$3 K is comparable to the transition temperature T_N = 2.54 K and the reduction of magnetic energy is expected to be not so large. Thus it is desirable to abandon the possibility of the spin Peierls nature in the present compound.

One of the remarkable features of this phase transition is similarity of the low temperature tail between the TCNQ and TCNE complexes as seen in Fig. 6.4. This behavior suggests an Ising character in the magnetic interaction for the TCNE compound. Hence we can consider that in [DMFc][TCNQ] the magnetic

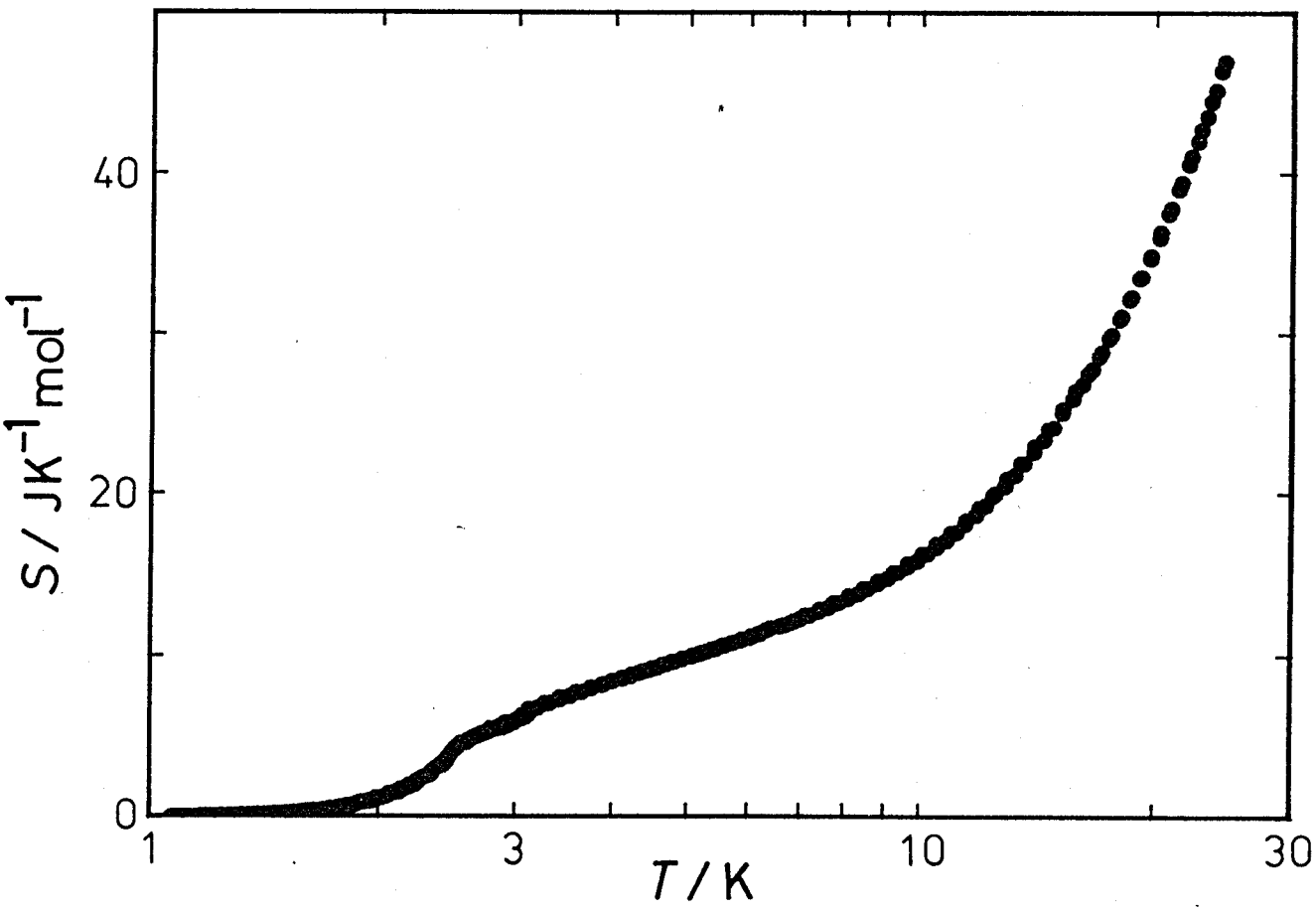

Fig. 6.5 Temperature dependence of molar entropy of decamethylferrocenium tetracyanoquinodimethanide.

interaction has a strong Ising anisotropy as in the TCNE compound. It is to be noted, however, that such a behavior of the low temperature tail is also found in the spin Peierls phase where magnetic excitation has an energy gap. The spin Peierls nature is exclusive to the Ising anisotropy which stabilizes the Neel ground state rather than the spin Peierls phase. Thus we must choose either the spin Peierls nature or the Ising anisotropy to interpret the observed exponential tail behavior.

The molar entropies are shown in Fig. 6.5. From the figure one can read 4.0 J K^{-1} mol^{-1} for the critical entropy, which is acquired up to the transition temperature. The difference between the true critical entropy and the molar entropy at T_N is negligible because T_N is as low as 2.54 K and the lattice contribution is small enough. This value of the critical entropy is, however, to be regarded as a lower bound because of doubt about possible admixing of the dimeric phase as discussed in the last section.

By adopting tentatively the normal heat capacity of [DMFc][TCNE] as that of [DMFc][TCNQ], a rough estimation of the total transition entropy was made. This procedure is admitted because the dominant contribution of the Debye heat capacity is similar between the two compounds possessing a homologous crystal structure and nearly the same crystal density. As a result, the transition entropy was obtained to be ΔS = 11.2 J K^{-1} mol^{-1}, which is very close to the magnetic entropy, 2 R ln 2. This value strongly suggests that the observed phase transition is dominated by magnetic ordering process and the structural transformation reported from the Mössbauer spectra is not essential.

If we regard the phase transition as a pure antiferromagnetic transition, it turns out that the transition behavior shows a remarkable short range ordering effect inherent in low dimensional magnets. The low dimensionality in the present compound is, however, weaker than that in the TCNE analogue. This may be attributable to the difference of the counter anion size, which directly

affects significant exchange paths.

Table 6.1 Molar heat capacities of decamethylferrocenium tetracyanoquinodimethanide.

$\frac{T}{K}$	$\frac{Cp}{JK^{-1}mol^{-1}}$	$\frac{T}{K}$	$\frac{Cp}{JK^{-1}mol^{-1}}$	$\frac{T}{K}$	$\frac{Cp}{JK^{-1}mol^{-1}}$	$\frac{T}{K}$	$\frac{Cp}{JK^{-1}mol^{-1}}$	$\frac{T}{K}$	$\frac{Cp}{JK^{-1}mol^{-1}}$	$\frac{T}{K}$	$\frac{Cp}{JK^{-1}mol^{-1}}$
1.0909	0.4453	1.8655	3.8490	11.9702	18.4942	1.7991	3.0971	2.8428	9.0632	9.1445	11.2311
1.1024	0.5011	1.9559	5.0292	12.4745	20.1570	1.8167	3.6548	2.8608	8.9837	9.4123	11.7526
1.1158	0.4213	2.0499	6.5750	12.9988	21.6530	1.8360	3.3542	2.8791	8.9779	9.6885	12.3053
1.1339	0.4613	2.1478	8.4942	13.5392	23.7351	1.8575	3.6931	2.8971	8.9552	9.9717	12.8471
1.1519	0.3790	2.2508	10.8590	14.1016	24.8751	1.8800	4.1050	2.9152	8.7835	10.2625	13.5496
1.1727	0.4525	2.3555	14.5988	14.6873	26.5657	1.9053	4.2990	2.9331	8.7237	10.5632	14.2601
1.1864	0.4765	2.4601	21.0503	15.2890	29.1231	1.9333	5.2896	2.9512	8.7346	10.8714	15.1056
1.1986	0.5233	2.6220	14.7986	15.9131	30.9184	1.9630	5.0179	2.9695	8.7415	11.1893	16.0084
1.2076	0.5676	2.7878	9.4229	16.5102	32.6829	1.9908	5.2784	2.9879	8.5567	11.5163	17.0407
1.2223	0.5507	2.8913	8.8579	17.0443	34.8387	2.0210	6.0646	3.0053	8.5541	11.8546	18.0420
1.2429	0.5511	3.0058	8.5631	17.5634	36.9154	2.0478	6.5158	3.0238	8.6498	12.2024	19.1227
1.2714	0.6148	3.1500	8.2329	18.0999	38.5811	2.0753	6.9366	3.0418	8.7071	12.5587	20.1704
1.2999	0.6129	3.3004	8.0040	18.6539	40.0427	2.1016	7.5791	3.0598	8.5852	12.9222	21.5156
1.3258	0.6219	3.4575	7.7421	19.2212	42.4012	2.1259	8.0005	3.0779	8.3775	13.2970	22.3190
1.3541	0.6795	3.6234	7.3476	19.8067	44.3769	2.1491	8.4382	3.1247	8.2502	13.6809	23.2162
1.3894	0.7615	3.7874	7.1428	20.4098	47.2221	2.1725	8.8311	3.2347	8.1192	14.0830	25.6448
1.4326	0.9316	3.9285	7.0803	21.0306	50.6002	2.1983	9.4593	3.3450	7.9399	14.5016	26.5123
1.4483	1.0282	4.0435	7.1558	21.6619	52.8682	2.2248	10.0009	3.4549	7.7170	14.9240	26.4985
1.4636	1.1312	4.1588	6.8762	22.3017	55.9706	2.2493	10.6833	3.5637	7.6339	15.3419	34.8021
1.4803	1.1026	4.2708	6.8092	22.9617	55.6923	2.2732	11.4123	3.6774	7.4582	15.7870	28.9583
1.4959	1.1912	4.3795	6.9048	23.6366	57.9587	2.2953	12.2314	3.7926	7.3617	16.2483	32.6244
1.5107	1.2124	4.4961	6.6695	24.3276	61.3413	2.3162	12.8706	3.9106	7.3002	16.7205	30.9194
1.5225	1.2793	4.6104	6.7932	25.0373	68.3673	2.3372	13.7463	4.0331	7.0962	17.1978	34.3002
1.5341	1.2188	4.7275	6.6428			2.3596	14.7176	4.1596	6.9914	17.6983	37.1565
1.5509	1.3562	4.8487	6.6626	1.0809	0.7967	2.3824	15.8492	4.2835	6.9559	18.2162	39.1679
1.5729	1.4491	4.9733	6.4531	1.1017	0.4370	2.4034	16.8372	4.4156	6.7694	18.7529	40.9737
1.6042	1.6489	5.0987	6.5455	1.1339	0.4218	2.4236	17.8950	4.5486	6.7129	19.3020	44.3585
1.6438	1.8915	5.2257	6.5809	1.1746	0.4692	2.4422	19.5269	4.6844	6.6878	19.8399	45.1435
1.6817	2.0803	5.3605	6.5489	1.2108	0.5662	2.4599	20.7618	4.8238	6.7105	20.3414	48.4701
1.7193	2.4067	5.4970	6.5985	1.2472	0.5666	2.4762	22.6632	4.9685	6.7163	20.8896	49.7893
1.7667	2.8907	5.6357	6.6177	1.2832	0.6399	2.4918	23.4445	5.1188	6.5672	21.5037	51.1015
1.8238	3.4084	5.7775	6.6950	1.3211	0.7026	2.5066	26.0510	5.2702	6.6174	22.1311	55.0592
1.8848	3.9794	5.9223	6.7618	1.3500	0.7102	2.5214	25.7451	5.4252	6.6879	22.7500	55.7774
1.9931	5.7590	6.0718	6.8398	1.3719	0.8086	2.5362	26.0975	5.5881	6.6275	23.3514	56.7460
2.0739	7.1110	6.2254	6.9166	1.3907	0.9418	2.5518	23.2502	5.7548	6.6626	23.9653	59.9548
2.1421	8.3564	6.3838	7.0691	1.4148	0.8408	2.5716	15.8706	5.9233	6.8543	24.5965	64.8555
2.2024	9.5235	6.7526	7.3234	1.4451	1.0267	2.5958	12.8460	6.0990	6.9065	25.2429	73.1001
		6.9338	7.4949	1.4732	1.0527	2.6172	11.4680	6.2802	7.0188		
1.0764	0.6563	7.1727	7.7488	1.4976	1.1669	2.6329	11.4117	6.4660	7.1467		
1.0939	0.3609	7.4763	8.2328	1.5154	1.2459	2.6493	11.0651	6.6577	7.3590		
1.1353	0.4770	7.8116	8.9593	1.5301	1.3801	2.6663	10.5077	6.8552	7.5548		
1.1837	0.4532	8.1597	9.5271	1.5519	1.4801	2.6837	10.4468	7.0563	7.8117		
1.2457	0.5573	8.5194	10.5954	1.5858	1.5750	2.7008	10.1478	7.2631	8.0037		
1.3104	0.6882	8.8954	10.8380	1.6184	1.6704	2.7181	9.9206	7.4747	8.2978		
1.3869	0.9102	9.2951	11.6542	1.6468	1.9697	2.7356	9.9169	7.6918	8.6404		
1.4569	1.0277	9.7034	12.6063	1.6767	2.0985	2.7533	9.6042	7.9160	9.0154		
1.5359	1.3420	10.1248	13.5335	1.7046	2.3376	2.7712	9.5837	8.1475	9.3603		
1.6156	1.7130	10.5610	14.6330	1.7316	2.5125	2.7891	9.4222	8.3851	9.8061		
1.6928	2.2886	11.0134	15.7996	1.7573	2.7003	2.8066	9.3439	8.6307	10.3238		
1.7769	2.9424	11.4834	17.1134	1.7799	2.7297	2.8248	9.2414	8.8837	10.7474		

REFERENCES TO PART II

[1] J. S. Miller, J. C. Calabrese, A. J. Epstein, R. W. Bigelow, J. H. Zhang, and W. M. Reiff, *J. Chem. Soc., Chem. Commun.* **1986**, 1026.

[2] C. G. Barraclough, R. L. Martin, S. Mitra, and R. C. Sherwood, *J. Chem. Phys.* **53**, 1638 (1970).

[3] S. Mitra, A. K. Gregson, W. E. Hatfield, and R. R. Weller, *Inorg. Chem.* **22**, 1729 (1983).

[4] H. H. Wickman, A. M. Trozzolo, H. J. Williams, G. W. Hull, and F. R. Merritt, *Phys. Rev.* **155**, 563 (1967).

[5] N. Arai, M. Sorai, H. Suga, and S. Seki, *J. Phys. Chem. Solids* **38**, 1341 (1977).

[6] J. S. Miller, J. C. Calabrese, H. Rommelmann, S. R. Chittipeddi, J. H. Zhang, W. M. Reiff and A. J. Epstein, *J. Am. Chem. Soc.* **109**, 769 (1987).

[7] S. Chittipeddi, K. R. Cromack, J. S. Miller, and A. J. Epstein, *Phys. Rev. Lett.* **58**, 2695 (1987).

[8] S. Chittipeddi, M. A. Selover, A. J. Epstein, D. M. O'Hare, J. Manriquez, and J. S. Miller, *Synth. Met.* **27**, B417 (1988).

[9] W. M. Reiff, *J. Appl. Phys.* **63**, 2957 (1988); J. H. Zhang, W. M. Reiff, and J. S. Miller, *Hyperfine Interact.* **42**, 1099 (1988).

[10] A. J. Epstein, S. Chittipeddi, A. Chakraborty, and J. S. Miller, *J. Appl. Phys.* **63**, 2952 (1988).

[11] J. S. Miller, A. J. Epstein, and W. M. Reiff, *Chem. Rev.* **88**, 201 (1988).

[12] G. A. Baker, Jr., G. S. Rushbrooke, and H. E. Gilbert, *Phys. Rev.* **135**, A1272 (1964).

[13] J. S. Miller, J. H. Zhang, W. M. Reiff, D. A. Dixon, L. D. Preston, A. H. Reis, Jr., E. Gebert, M. Extine, J. Troup, A. J. Epstein, and M. D. Ward, *J. Phys. Chem.* **91**, 4344 (1987).

[14] R. C. Thiel, H. de Graaf, and L. J. de Jongh,
Phys. Rev. Lett. **47**, 1415 (1981);
L. J. de Jongh, *J. Appl. Phys.* **53**, 8018 (1982);
L. J. de Jongh, R. C. Thiel, and J. Reedijk, *Phys. Rev.* **B30**, 4041 (1984).

[15] J. S. Miller and A. J. Epstein, *J. Am. Chem. Soc.* **109**, 3850 (1987).

[16] H. M. McConnell, *Proc. R. A. Welch Found. Chem. Res.* **11**, 144 (1967).

[17] R. S. Threlkel, J. E. Bercaw, P. E. Seidler, J. M. Stryker,
and R. G. Bergman, *Org. Synth.* **65**, 42 (1987).

[18] R. B. King and M. B. Bisnette, *J. Organomet. Chem.* **8**, 287 (1967).

[19] D. F. Shriver and M. A. Drezdson,
"*The Manipuration of Air-Sensitive Compounds, 2nd ed.*",
John Wiley and Sons, New York (1986).

[20] B. Bleaney, J. F. Gregg, R. W. Hill, M. Lazzouni, M. J. M. Leask,
and M. R. Wells, *J. Phys.* **C21**, 2721 (1988).

[21] H. W. J. Blöte, *Physica* **79B**, 427 (1975).

[22] M. Sorai and S. Seki, *J. Phys. Soc. Jpn.* **32**, 382 (1972).

[23] A. Abragam and B. Bleaney,
"*Electron Paramagnetic Resonance of Transition ions*",
Oxford University Press, Oxford (1970).

[24] M. J. Cohn, M. D. Timken, and D. N. Hendrickson,
J. Am. Chem. Soc. **106**, 6683 (1984).

[25] E. Middleton, E. L. Little, D. D. Coffman, and V. A. Englehardt,
J. Am. Chem. Soc. **80**, 2795 (1958).

[26] J. D. Johnson and J. C. Bonner, *Phys. Rev.* **B22**, 251 (1980).

[27] J. Villain, *Physica* **79B**, 1 (1975).

[28] K. A. Long and A. R. Bishop, *J. Phys.* **A12**, 1325 (1979).

[29] D. J. Scalapino, Y. Imry, and P. Pincus, *Phys. Rev.* **B11**, 2042 (1975).

[30] H. A. Kramers and G. H. Wannier, *Phys. Rev.* **60**, 252 (1941).

[31] M. E. Fisher, *Am. J. Phys.* **32**, 343 (1964).

[32] H. Tanaka, H. Dachs, K. Iio, and K. Nagata, *J. Phys.* **C19**, 4879 (1986).

[33] B. S. Lee, *J. Phys.* **C13**, 2651 (1980).

[34] J. B. Torrance, J. E. Vazquez, J. J. Mayerle, and V. Y. Lee, *Phys. Rev. Lett.* **46**, 253 (1981).

[35] G. A. Candela, L. J. Swartzendruber, J. S. Miller, and M. J. Rice, *J. Am. Chem. Soc.* **101**, 2755 (1979).

[36] J. S. Miller, A. H. Reis, Jr., E. Gebert, J. J. Ritsko, W. R. Salaneck, L. Kovnat, T. W. Cape, and R. P. Van Duyne, *J. Am. Chem. Soc.* **101**, 7111 (1979).

[37] A. I. Buzdin and L. N. Bulaevskii, *Sov. Phys. Usp.* **23**, 409 (1980).

PART III

SOME OTHER FERROCENIUM SALTS

Chapter 7. Biferrocenium Radical Salts

7.1 Introduction

Biferrocenium radical salts form an interesting family which belongs to mixed-valence compound[1]. Biferrocenium or substituted biferrocenium radical ions contain a common skeletal structure of the ferrocenylferrocene, which consists of two iron atoms, a bridging bidentate fulvalene ligand, and two terminating cyclopentadiene ligands (See Fig. 7.1). Formally the oxidation number of iron is II for one iron atom like in a neutral ferrocene molecule, and III for the other iron atom like in a ferrocenium cation. The coexistence of different oxidation numbers is characteristic of mixed-valence compounds. In biferrocenium salts, the mixed-valency manifests itself in a variety of manner and all three types of mixed-valency (class I , II , and III according to the classification by Robin and Day[2]) have been observed. In this paper two compounds belonging to class II are studied. One is biferrocenium triiodide, $[(C_5H_5)Fe(C_5H_4\text{-}C_5H_4)Fe(C_5H_5)]^+(I_3)^-$, and the other is $1',1'''$-diethylbiferrocenium triiodide, $[(C_5H_4Et)Fe(C_5H_4\text{-}C_5H_4)Fe(C_5H_4Et)]^+(I_3)^-$. They are abbreviated hereafter as $[BFc]I_3$ and $[DEBFc]I_3$, respectively.

Class II mixed valence compound contains plural (metal) atoms of one and the same kind, which have different valencies distinguishable by their coordination environment or electron density. Since the difference between these atoms is, however, very small, these atoms can sometimes exchange their valencies each other. Such an exchange is always associated with a distortion of coordination environment through electron-vibration coupling. Hence one can regard these molecules as a non-rigid molecule undergoing a large amplitude vibration between several stable molecular configurations. When a crystal is formed with such

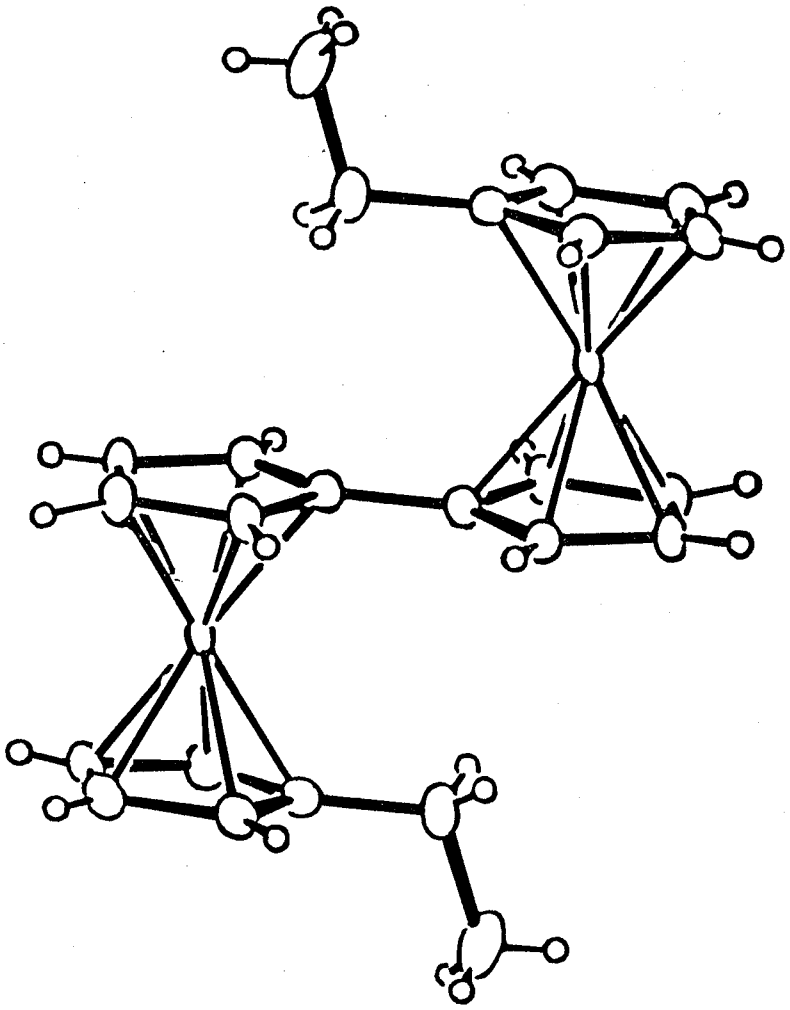

Fig. 7.1 Molecular structure of 1',1'''-diethylbiferrocenium cation radical [8].

non-rigid molecules, one can expect a structural phase transition characteristic of anharmonic oscillators. Actually this kind of phase transition is observed in $[BFc]I_3$ at 328 K. This phase transition was examined by means of calorimetry[3], X-ray structural analysis[4], and ^{57}Fe Mössbauer spectroscopy[3], and it was confirmed that the unpaired electron stays on one ferrocenyl moiety without traveling between two ferrocenyl groups in the low temperature phase named as a valence-trapped state. On the other hand, in $[DEBFc]I_3$ a phase transition was found at 66 K but the relationship between this phase transition and the mixed-valency has not been fully elucidated yet. The coexistence of two non-equivalent Fe sites was derived from ^{57}Fe Mössbauer spectroscopy up to $\sim$220 K. We tentatively assumed that the phase transition at 66 K is not concerned with the mixed-valency and the valence-trapping of $[DEBFc]^+$ on cooling proceeds without phase transitions because of its asymmetric crystalline environment. Therefore, at low temperatures we can treat both $[BFc]I_3$ and $[DEBFc]I_3$ as in a valence-trapped state, where the unpaired electron is fixed on one of the ferrocenyl groups.

As in the case of the $[DMFc]^+$ cation considered in part II, $[BFc]^+$ and $[DEBFc]^+$ cations are paramagnetic species with anisotropic *g*-factor. This is a reflection of the valence-trapped state in these compounds. The physical properties of the valence-trapped state is essentially considered as a simple superimposition of the properties of each valency, so that the magnetism of these biferrocenium compounds can be regarded as that of equimolar mixture of diamagnetic ferrocene and paramagnetic ferrocenium which is magnetically anisotropic. This situation makes contrast to the compound characterized by the valence-averaged state. For instance, diiodobiferrocenium triiodide has almost isotropic *g*-factor as distribution of the unpaired electron loses the cylindrical symmetry. The *g*-factor of $[BFc]I_3$ is $g_{\parallel} = 3.58$ and $g_{\perp} = 1.72$[5].

In comparison with the $[DMFc]^+$ cation, this is less anisotropic owing to more asymmetric molecular shape. Thus the comparison of solid state magnetic behavior between [DMFc][TCNE] and these two biferrocenium salts is interesting.

7.2 Experimental

(1) Calorimetry

The very low temperature calorimeter was used for the calorimetry of these compounds. For both the compounds the adiabatic mode was adopted between 1-20 K, while the isoperibol mode was used below 1 K. All procedures for sample mounting were carried out in a air without inert atmosphere.

In a sample container with inner volume of 14 cm^3, 3.4123 g of $[BFc]I_3$ was mixed with 5.7720 g of silicone oil. Calorimetry was made in the temperature region between 80 mK and 20 K. Below 200 mK the thermal relaxation time for the equilibration in the calorimeter was elongated to longer than $\sim$2 hours. Thus observed data below 200 mK involved somewhat large ambiguity.

For the calorimetry of $[DEBFc]I_3$, 8.5306 g of the sample was used together with 5.0968 g of silicone oil. Heat capacities were measured in the temperature range between 60 mK and 20 K. Below 200 mK, one to two hours were required for thermal equilibration of the calorimeter. An alternative method was attempted for 30-80 mK, in which the calorimeter was connected to the mixing chamber of the refrigerator with 20 cm of oxygen free copper (0.5 mmϕ) in order to cool down the sample as low as possible. In this measurement an a.c. resistance bridge Mk.III (Oxford Instruments) was used in place of the cryobridge model 103 ($A\Sigma A$) because the cryobridge sometimes exhibited unstable balance below 50 mK. At the same time a microcomputer PC-9801F (NEC) was unplugged to avoid the generation of high frequency electric noise. This method permitted relatively great heat leaks from the calorimeter, so that sufficient thermal equilibration could not be guaranteed in the measurement.

(2) Calorimetry using a pellet sample

For $[BFc]I_3$ the pellet sample was also utilized for the calorimetry. A pellet (2 cmϕ, 2.7 mmt, 1.7998 g) was formed by means of an oil press. The press condition was 300 MPa and 180 s under evacuation. Evacuation over long period was avoided as the elimination of iodine, $I_3^- \rightarrow I^- + I_2\uparrow$, is promoted under vacuum. The calorimetry was made by ordinary isoperibol mode.

(3) Magnetic susceptibility

For $[DEBFc]I_3$ the magnetic susceptibility measurement was done by means of a Hartshorn bridge working with a top-loading type $^3He/^4He$ dilution refrigerator. This measurement was carried out under direction of Dr. Mamoru Ishizuka and Prof. Kiichi Amaya at Faculty of Engineering Science, Osaka University. Silicone oil mull of $[DEBFc]I_3$ was enveloped with a piece of platinum foil to the size of about 2 mm × 5 mm × 5 mm. The bridge circuit consisted of a variable mutual inductor 4229 (H. Tinsley) and a lock-in amplifier Model 124A (PAR) equipped with a low pass transformer. The measurement frequency was selected at 102 Hz and the primary coil generated an external field with amplitude of 10 μT. The data was collected in the temperature region between 55 mK and 4.6 K.

7.3 Results and Discussion

Observed heat capacities are tabulated in Tables 7.1 and 7.2, and shown in Figs. 7.2 and 7.3 for $[BFc]I_3$ and $[DEBFc]I_3$, respectively. Heat capacities of both the compounds are remarkably enhanced below 1 K. Especially the anomalous heat capacity of $[BFc]I_3$ has an unique profile which provides a very slow decay with temperature. It is also noteworthy that these anomalies occur at very different temperatures despite of their similar chemical structures, *i.e.* $[BFc]I_3$ has its maximum of anomalous heat capacity around 120 mK, while

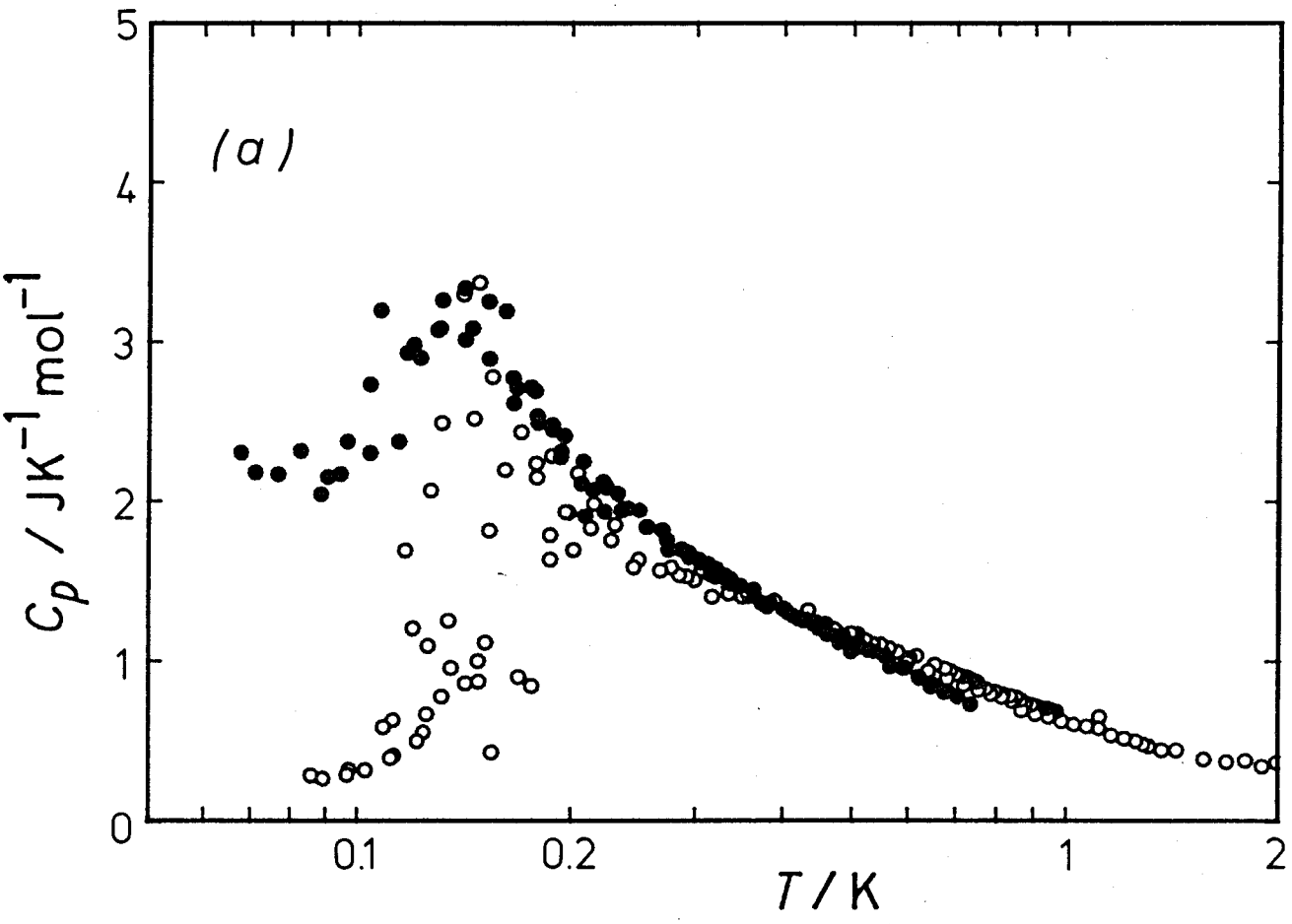

Fig. 7.2 Molar heat capacities of biferrocenium triiodide. (a), Low temperature region. Open circles are measured by silicone-oil method, while filled circles are measured by pellet-sample method.

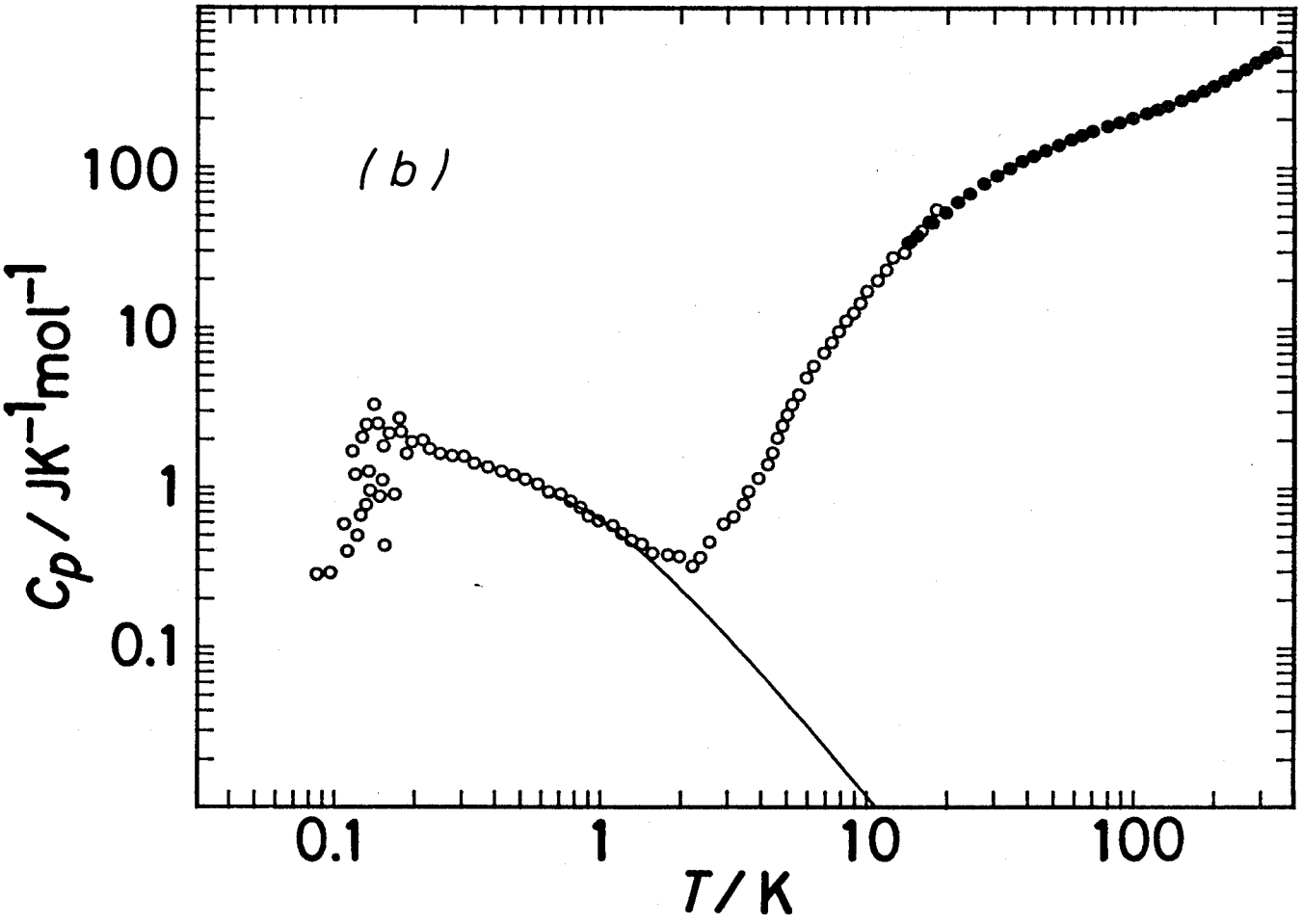

Fig. 7.2 Molar heat capacities of biferrocenium triiodide. (b), Comparison with high temperature data. Open circles show the present study. Filled circles are measured by Sorai *et al.* [3]. Solid curve is a high temperature expansion of ferromagnetic Heisenberg chain.

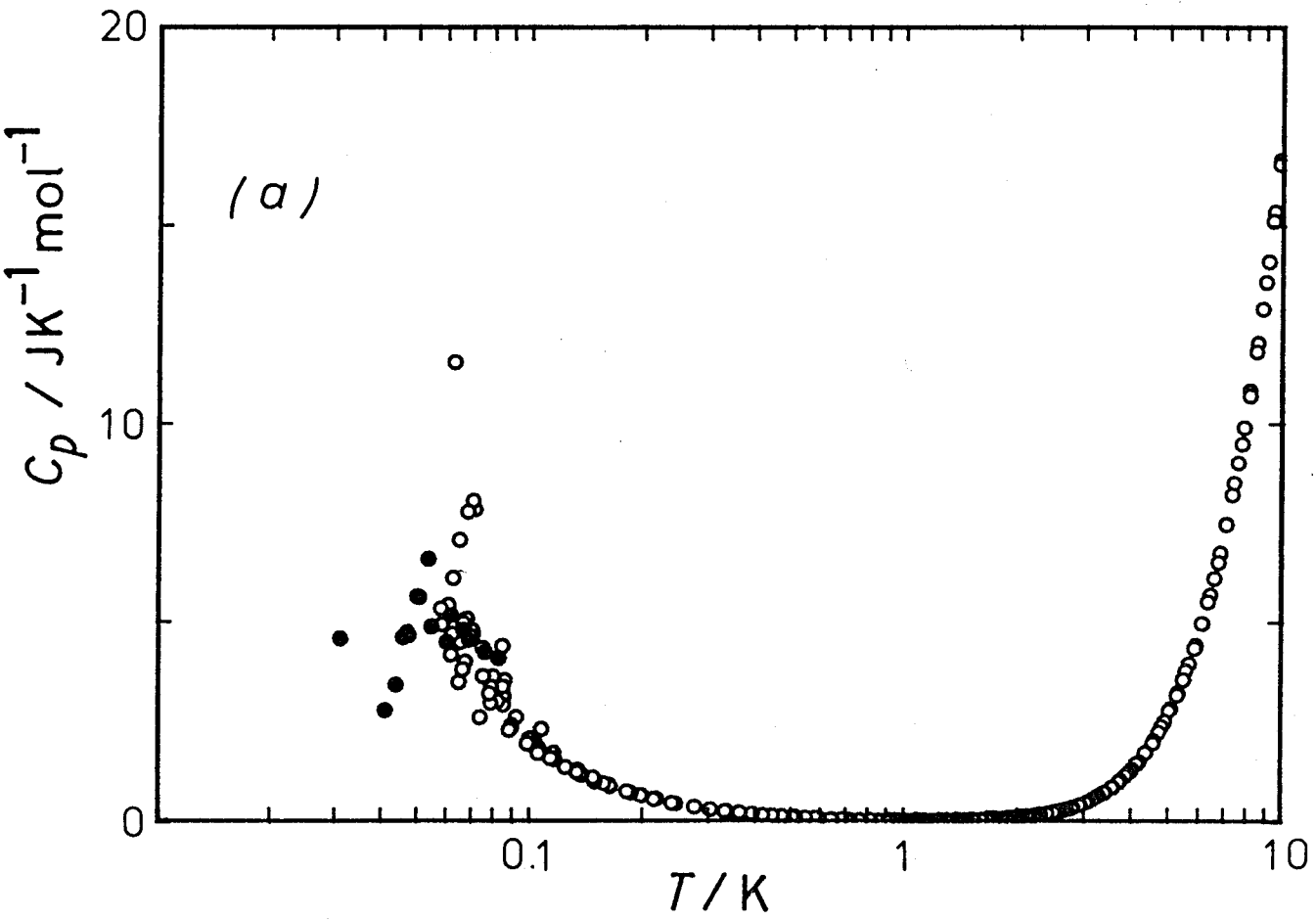

Fig. 7.3 Molar heat capacities of 1',1'''-diethylbiferrocenium triiodide.
(a), Low temperature region. Open circles are measured by silicone-oil method, while filled circles are measured by direct heat-connection method.

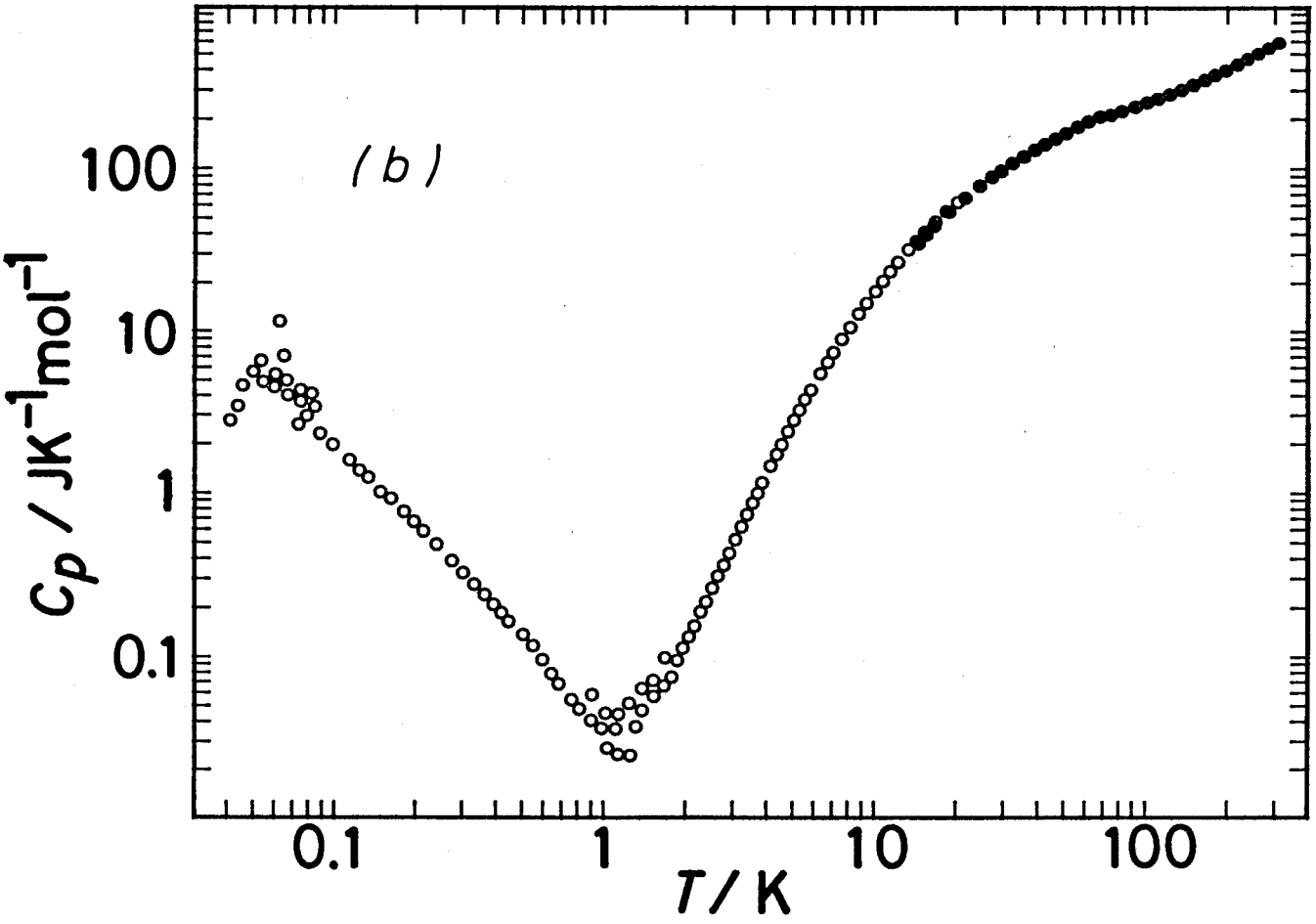

Fig. 7.3 Molar heat capacities of 1',1'''-diethylbiferrocenium triiodide.
(b), Comparison with high temperature data. Open circles show the present study. Filled circles are measured by Nakashima *et al.* (unpublished).

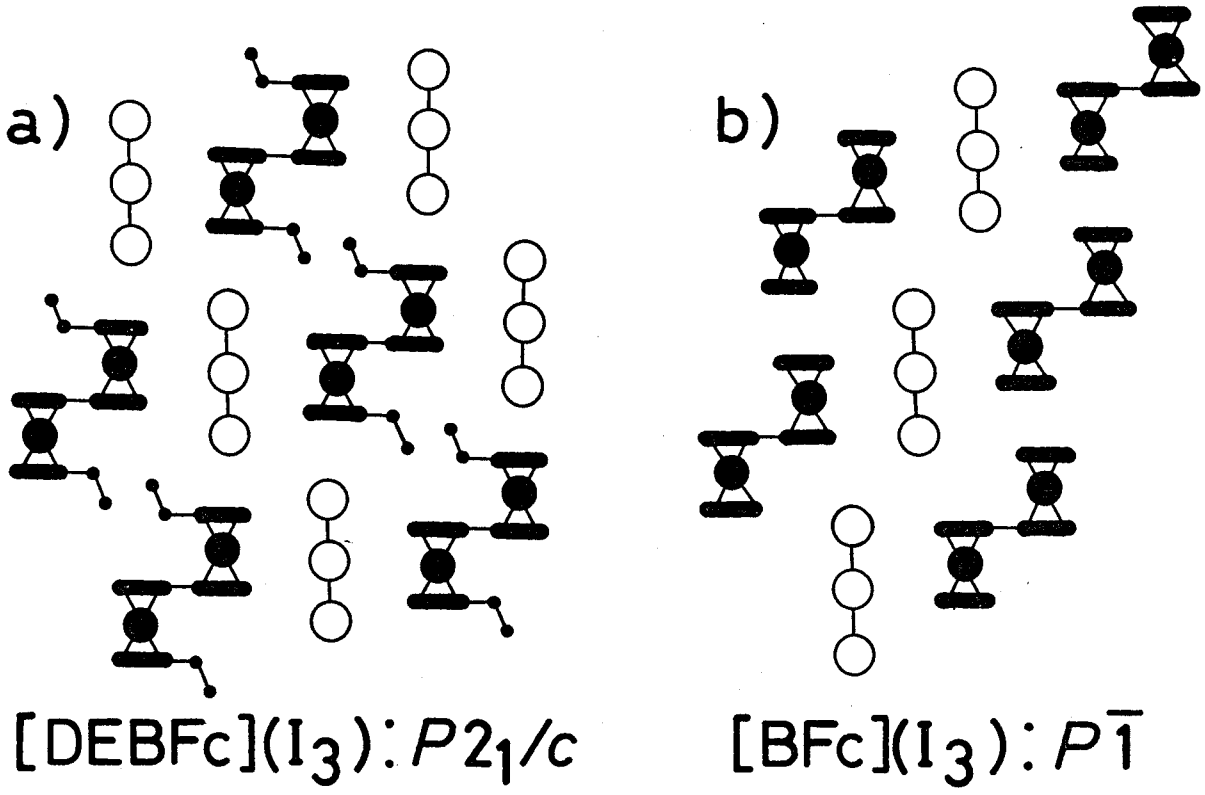

Fig. 7.4 Schematic drawing of molecular packing in a crystal [8].
a), 1',1'''-Diethylbiferrocenium triiodide;
b), biferrocenium triiodide.

[DEBFc]I_3 has a heat-capacity maximum at about 60 mK.

(1) [BFc]I_3

In Fig. 7.2(a) plotted are both the heat-capacity data measured by ordinary silicone oil method and the pellet method are plotted. In spite of long thermal relaxation time over 2 hours, these two kinds of data coincide well each other between 150-400 mK. Above 400mK the pellet data seem to be too small. This deviation would be explained by the lack of precise heat-capacity data of the addendum. On the other hand, the silicone-oil data below 400 mK exhibit a characteristic feature of non-equilibration. Thus we adopted the silicone-oil data above 400 mK and the pellet data below 400 mK as reliable ones. As shown in Fig. 7.2(b), the heat capacities above 13 K agrees well with those measured previously in the range 13-360 K by Sorai *et al.*[3].

The observed heat capacity anomaly is conceivably attributable to a magnetic phase transition. This speculation is based on the following two observations. One is the extremely gradual behavior of the high temperature tail. This behavior will be discussed in detail in chapter 9. The other is the excess entropy $\Delta S \sim 5$ J K^{-1} mol^{-1}, which was calculated by numerical integration of heat capacity. If the contribution from the low temperature tail below 80 mK, which has not been measured, is taken into accounts, the total excess entropy amounts to $\sim$ 5.7 J K^{-1} mol^{-1}. This value is very close to R ln 2 (= 5.76 J K^{-1} mol^{-1}) which is expected for a magnetic ordering process in a s = 1/2 system. Hence we can safely attribute the present anomaly to a magnetic origin.

If we tentatively regard the critical temperature as being T_C = 140 mK, the excess entropy acquired above T_C can be estimated to be $(S_\infty - S_C)/R \sim 0.4$ for the present compound. This quantity serves as a diagnostic measure of the short range order. The value obtained here is very large in comparison to ordinary 3D magnets, for example 0.1$\sim$0.2 for 3D Ising magnets and 0.2$\sim$0.26 for 3D Heisenberg magnets[6]. The present value is rather close to those of 2D Ising

magnets, 0.36~0.43[7]. Therefore, the gradual tail behavior of this compound can be regarded as arising from the manifestation of a short range order effect inherent in low dimensional magnets. However, more detailed analysis of this tail behavior will be done in chapter 9, where it will turn out that the gradual tail of this compound cannot be understood in terms of low dimensional Ising magnet but Heisenberg magnet.

The low dimensionality suggested from the anomalous heat capacity can be found in the actual crystal structure. Schematic drawing of the crystal structure is given in Fig. 7.4[4,8]. It is easily seen that close contact of cyclopentadienyl rings between neighboring molecules makes a columnar structure and each column is isolated by surrounding triiodide anions. This 1D nature of the lattice structure may reflect in preferred direction of the magnetic interaction. Although we described in chapter 1 that in a molecular magnet it is generally difficult to correlate the exchange path with its crystal structure, the 1D exchange path is clearly recognized along the columnar direction in the present compound. Consequently we can conclude that [BFc]I_3 exhibits the feature of 1D Heisenberg magnet and, in addition, the lattice dimensional crossover from 1D to 3D.

(2) [DEBFc]I_3

In Fig. 7.3(a) several data points measured by the direct heat-connection method are plotted together with the heat capacities measured by usual method. The former apparently exhibits monotonous increasing tendency below 50 mK. This behavior is, however, not fully confident because of large heat leaks and short temperature-drift observation times. It is better to treat them as reference data.

Temperature dependence of the magnetic susceptibilities between 55 mK and 4.6 K is plotted in Fig. 7.5. From this plot the Weiss temperature was estimated to

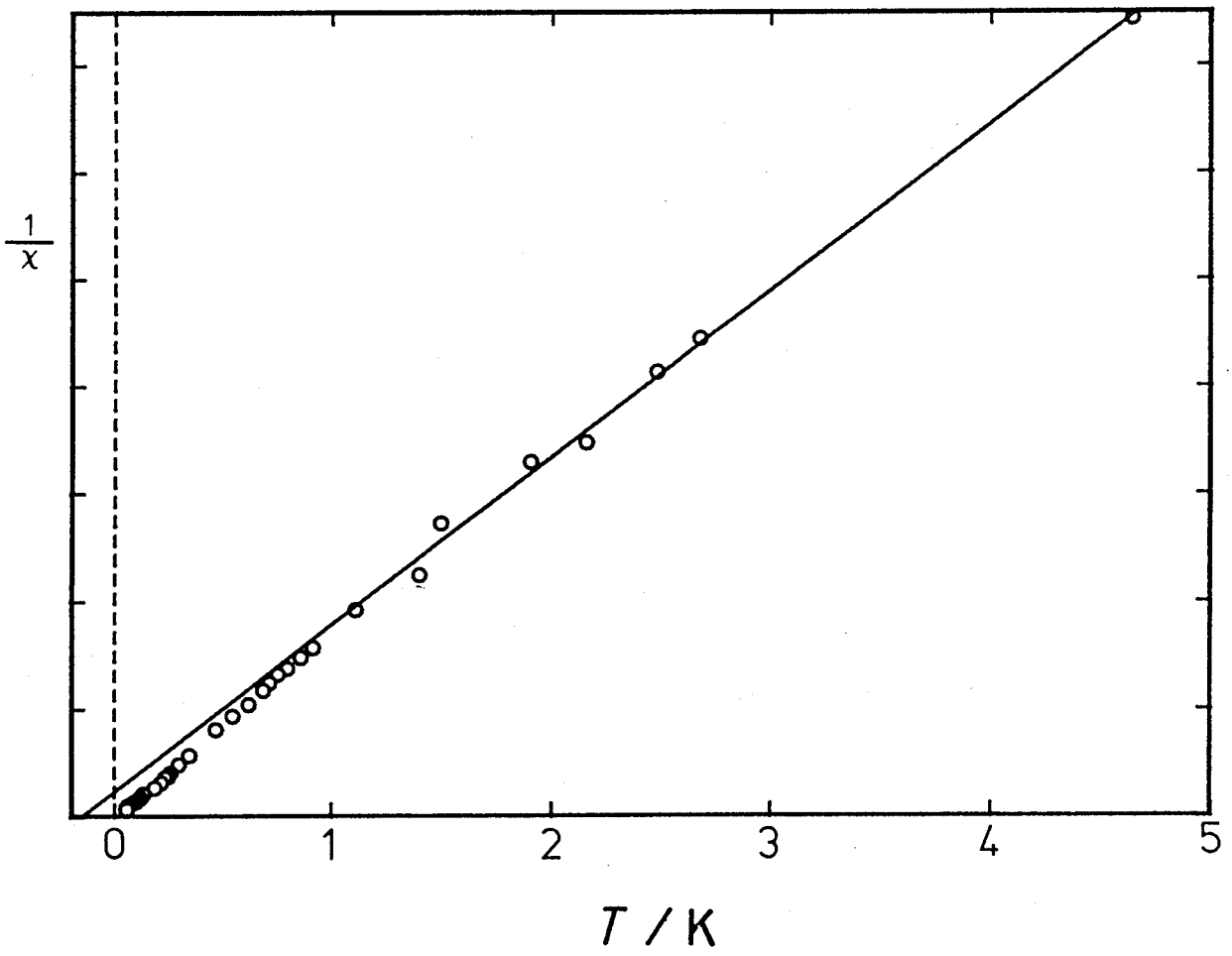

Fig. 7.5 Curie plot of magnetic susceptibility of 1',1'''-diethylbiferrocenium triiodide. The straight line represents results of linear regression between 1-5 K.

be the order of -0.1 K, *i.e.* the antiferromagnetism. This result does not coincide with the magnetic susceptibility measured with a Faraday balance by Mori[9]. Mori's data exhibit a crossover between different Curie-Weiss behaviors, *i.e.* above 7.5 K the Weiss temperature is about -1∼-1.5 K, whereas below 7.5 K this behavior changes to the one with a Weiss temperature of +1∼+1.5 K. Presently there are no explanations for the discrepancy between the two sets of magnetic susceptibility measurement. It is noted, however, that elimination of iodine may easily occur by slight evacuation and a small difference in the chemical composition can affect the strength of magnetic interaction. Anyway, the estimated Weiss temperature -0.1 K is consistent with the heat capacity anomaly observed below 0.1 K.

Based on the discussion in chapter 9 and the existence of antiferromagnetic exchange interaction, we can identify the observed anomalous heat capacity as an antiferromagnetic phase transition. From the gross profile of the heat-capacity anomaly, the critical temperature is tentatively estimated to be 60 mK. By use of this T_N, the short range order entropy, $(S_\infty - S_c)/R$, can be likewise calculated as in the case of $[BFc]I_3$. The short range order entropy was $(S_\infty - S_c)/R \sim 0.39$. This is a very similar value to $[BFc]I_3$, indicating a remarkable short range order effect.

The crystal structure of $[DEBFc]I_3$ is schematically shown in Fig. 7.4[4,8]. In this structure no evidences of low dimensional lattice can be found immediately. Each $[DEBFc]^+$ radical cation is rather isolated by its ethyl groups and surrounding triiodide anions. If one notes only the positions of iron atoms, however, weak 2D nature can be traced in the plane perpendicular to the crystallographic *a*-axis. This may introduce 2D nature to the magnetic interaction. Another possibility of low dimensional magnet is a random magnet. As stated in section 7.1, the absence of mixed-valence phase transition can introduce disorder with respect to the location of unpaired electron in a

molecule. If we assume all iron sites are equivalent, the crystal is regarded as an equimolar mixture of magnetic atoms and nonmagnetic atoms with a random configuration, *i.e.* a diluted magnet with an occupancy of 50 per cent. In a dilute magnet the effective dimension is known to be diminished when the occupancy approaches a percolation threshold, so that a similar effect is expected to be introduced into the magnetic aspect of the present compound by the randomness of the mixed valency. The reliability of this random magnet is to be checked by means of structural analysis at very low temperatures. From the crystalline structure available at present, the weak 2D property is more plausible explanation of the remarkable short range order effect.

Table 7.1 Molar heat capacities of biferrocenium triiodide.

$\frac{T}{K}$	$\frac{Cp}{JK^{-1}mol^{-1}}$	$\frac{T}{K}$	$\frac{Cp}{JK^{-1}mol^{-1}}$	$\frac{T}{K}$	$\frac{Cp}{JK^{-1}mol^{-1}}$	$\frac{T}{K}$	$\frac{Cp}{JK^{-1}mol^{-1}}$	$\frac{T}{K}$	$\frac{Cp}{JK^{-1}mol^{-1}}$	$\frac{T}{K}$	$\frac{Cp}{JK^{-1}mol^{-1}}$
0.1517	1.1207	0.1965	1.9382	0.7322	0.8947	13.7513	26.9491	10.5028	17.0795	0.1301	3.0762
0.1787	2.2420	0.2045	2.1812	0.7380	0.8861	14.2005	32.4480	10.8330	17.8290	0.1421	3.0164
0.1885	2.4530			0.7431	0.8790	14.6619	34.9143	11.1734	18.8211	0.1537	2.8960
0.2016	1.7003	0.0969	0.2915	0.7473	0.8795	15.1401	35.9504	11.5212	21.3510	0.1662	2.6210
0.2136	1.8380	0.1092	0.5861	0.7510	0.8748	15.6326	38.7668	11.8841	23.2243	0.1794	2.4985
0.2283	1.7637	0.1170	1.6932	0.7577	0.8519	16.1437	39.5497	12.2608	24.7442	0.1936	2.3230
0.2459	1.5921	0.1274	2.0719	0.7736	0.8301	16.6149	41.9994	12.6475	26.8847	0.2092	1.9125
		0.1484	1.0058	0.7983	0.8159	17.0266	44.7830	13.0466	27.4892	0.2252	2.0910
0.1549	0.4335			0.8196	0.7992	17.5009	48.7831	13.4586	29.7435	0.2412	1.9623
0.1760	0.8482	0.1028	0.3172	0.8379	0.7866	18.0629	51.4132	13.8827	29.6016	0.2574	1.8445
0.1868	1.7960	0.1219	0.5006	0.8538	0.7768	18.6371	54.9023	14.8018	35.4011	0.2736	1.7624
0.1986	1.9350	0.1321	2.4921	0.8676	0.7583	19.2264	55.9412	15.5250	37.9146	0.2899	1.6940
0.2155	1.9899	0.1462	2.5200	0.8794	0.7399			16.1231	40.7161	0.3060	1.6211
0.2314	1.8577	0.1551	2.7806	0.8959	0.7307	1.1185	0.6543	16.6744	43.6275	0.3206	1.5856
0.2498	1.6410	0.1688	0.9059	0.9102	0.7204	1.2886	0.4801	17.2153	46.1428	0.3372	1.5163
0.2680	1.5748	0.1759	2.7161	0.9224	0.7123	1.4357	0.4441	17.7698	50.2201	0.3554	1.4403
0.2851	1.5445	0.1868	1.6403	0.9330	0.7071	1.5689	0.3904	18.3391	54.6023	0.3735	1.3719
0.2999	1.5146			0.9420	0.7067	1.6895	0.3739	18.9250	55.8824		
0.3175	1.4117	0.0894	0.2657	0.9500	0.6991	1.7953	0.3827			0.0678	2.3072
0.3351	1.4300	0.1130	0.4109	0.9566	0.6981	1.8948	0.3465	pellet sample		0.0826	2.3163
0.3564	1.4237	0.1244	0.5567	0.9626	0.6918	1.9858	0.3717			0.0966	2.3781
0.3818	1.3642	0.1320	0.7817	0.9676	0.6876	2.0683	0.3533	0.0712	2.1819	0.1078	3.2038
0.4069	1.3097	0.1359	0.9606	0.9718	0.6854	2.1435	0.3917	0.0884	2.0471	0.1203	2.9841
0.4317	1.2656	0.1423	0.8647			2.2182	0.3258	0.1041	2.3046	0.1312	3.0920
0.4567	1.2194	0.1485	0.8784	0.0975	0.3209	2.2856	0.3666	0.1143	2.3819	0.1418	3.3435
0.4814	1.1709	0.1486	3.3755	0.1128	0.6291	2.3743	0.3677	0.1229	2.9019	0.1532	3.2571
0.5058	1.1574			0.1200	1.2043	2.4741	0.4078	0.1319	3.2668	0.1658	2.7773
0.5072	1.1092	0.2776	1.5954	0.1263	1.0997	2.5760	0.4596	0.1456	3.0917	0.1793	2.5435
0.5539	1.0619	0.2921	1.5363			2.6862	0.4646	0.1678	2.7127	0.1933	2.2859
0.5989	0.9988	0.3066	1.5786	5.2198	3.1247	2.7986	0.4655	0.1880	2.4845	0.2079	2.2564
0.6418	0.9407	0.3211	1.5342	5.3957	3.6301	2.9154	0.5972	0.2068	2.1200	0.2223	2.1308
0.6823	0.8956	0.3355	1.4760	5.5811	3.8195	3.0396	0.6484	0.2232	1.9402	0.2363	1.9506
0.7202	0.8528	0.3506	1.4090	5.7680	4.2867	3.1722	0.6654	0.2383	1.9594	0.2943	1.6835
0.7549	0.8234	0.3640	1.4521	5.9558	4.8815	3.3089	0.7467	0.2562	1.8453	0.3131	1.6126
0.7867	0.7999	0.3773	1.3576	6.1500	5.2611	3.4517	0.7888	0.2748	1.7026	0.3309	1.5406
0.8157	0.7778	0.3896	1.3872	6.3501	5.7564	3.6003	0.9544	0.2940	1.6553	0.3480	1.4768
0.8424	0.7559	0.4022	1.3360	6.5552	6.0355	3.7562	1.0784	0.3155	1.5453	0.3641	1.4255
0.8687	0.6939	0.4140	1.2901	6.7642	6.4106	3.9203	1.1558	0.3371	1.4902	0.3836	1.3715
0.9073	0.6706	0.4254	1.2712	6.9786	6.9571	4.0898	1.2722	0.3586	1.4133	0.4059	1.3187
0.9464	0.6521	0.4348	1.3255	7.1993	7.5348	4.2635	1.4113	0.3802	1.3479	0.4283	1.2597
0.9876	0.6247	0.4465	1.2469	7.4268	8.1860	4.4456	1.6642	0.4011	1.3305	0.4497	1.2112
1.0294	0.6071	0.4594	1.2381	7.6614	8.9033	4.6351	2.0721	0.4220	1.2718	0.4745	1.1634
1.0717	0.5942	0.4734	1.2065	7.9023	9.5752	4.8342	2.4727	0.4419	1.2391	0.5014	1.1130
1.1157	0.5802	0.4866	1.1628	8.1478	10.3564	5.0428	2.8802	0.4618	1.1751	0.5278	1.0721
1.1634	0.5367	0.4987	1.1794	8.4009	11.1490	5.2622	3.3152	0.4808	1.1229	0.5579	1.0307
1.2111	0.5170	0.5098	1.1724	8.6621	11.7925	5.4936	3.7466	0.4989	1.0675	0.5906	0.9628
1.2604	0.5005	0.5224	1.1381	8.9294	12.4237	5.7367	4.2402	0.5156	1.0930	0.6222	0.8975
1.3138	0.4712	0.5360	1.1101	9.2015	13.4824	5.9907	4.7355	0.5384	1.0679	0.6526	0.8547
1.3694	0.4460	0.5499	1.1089	9.4824	14.4257	6.2543	5.3552	0.5663	0.9696	0.6816	0.8130
		0.5651	1.0874	9.7721	15.4682	6.5306	5.9147	0.5942	0.9639		
0.0858	0.2860	0.5812	1.0615	10.0688	17.0748	6.9354	6.9940	0.6215	0.9055	0.0943	2.1746
0.1118	0.3955	0.6029	1.0200	10.3771	17.9488	7.4626	8.4257	0.6473	0.8445	0.1620	3.1991
0.1257	0.6705	0.6181	1.0362	10.6904	18.5749	7.9098	9.7651	0.6757	0.8120	0.1782	2.6989
0.1349	1.2589	0.6546	0.9836	11.0069	19.8788	8.3017	10.8315	0.7055	0.7793	0.1959	2.4195
0.1413	3.3029	0.6777	0.9585	11.3342	20.7563	8.6530	11.8024	0.7343	0.7358	0.2150	2.0776
0.1535	1.8219	0.6896	0.9413	11.6704	21.9535	8.9727	12.5829			0.2331	2.0522
0.1615	2.2029	0.7004	0.9209	12.0169	22.1774	9.2701	13.4493	0.0768	2.1705	0.2507	1.9508
0.1702	2.4386	0.7100	0.9151	12.5691	27.7309	9.5644	14.3427	0.0906	2.1546	0.2695	1.8257
0.1792	2.1536	0.7184	0.9058	12.9031	27.9252	9.8678	15.2794	0.1043	2.7344	0.2868	1.7075
0.1880	2.2885	0.7257	0.9000	13.3185	28.4436	10.1804	16.1649	0.1176	2.9353	0.3035	1.6405

Table 7.2 Molar heat capacities of 1',1''' -diethylbiferrocenium triiodide.

$\frac{T}{K}$	$\frac{Cp}{JK^{-1}mol^{-1}}$	$\frac{T}{K}$	$\frac{Cp}{JK^{-1}mol^{-1}}$	$\frac{T}{K}$	$\frac{Cp}{JK^{-1}mol^{-1}}$	$\frac{T}{K}$	$\frac{Cp}{JK^{-1}mol^{-1}}$	$\frac{T}{K}$	$\frac{Cp}{JK^{-1}mol^{-1}}$	$\frac{T}{K}$	$\frac{Cp}{JK^{-1}mol^{-1}}$
0.9111	0.0585	5.7067	3.9570	1.6999	0.0744	17.3978	49.9316	0.2153	0.5891	0.1817	0.7736
0.9628	0.0570	5.9195	4.4245	1.7871	0.0748	17.9613	52.4323	0.2457	0.4744		
1.0204	0.0451	6.1404	4.9682	1.8758	0.0954	18.5434	54.9928	0.2755	0.3912	0.0579	5.3319
1.0798	0.0505	6.3707	5.5142	1.9693	0.1118	19.1447	57.6143	0.3028	0.3306	0.0628	11.5544
1.1371	0.0444	6.6090	6.1063	2.0687	0.1333	19.7653	60.2338	0.3324	0.2818	0.0667	4.9772
1.1971	0.0455	6.8538	6.7449	2.1738	0.1552	20.4056	62.9477	0.3636	0.2426	0.0753	3.6617
1.2595	0.0246	7.1057	7.4533	2.2838	0.1905	21.0663	65.6135	0.3933	0.2112	0.0854	2.9288
1.3134	0.0523	7.3674	8.1932	2.4011	0.2239	21.7476	68.1854	0.4204	0.1881	0.1004	1.9627
1.3895	0.0640	7.6379	9.0165	2.5252	0.2634	22.4500	70.6830	0.4468	0.1669	0.1166	1.5695
1.4538	0.0467	7.9180	9.9080	2.6551	0.3117	23.1689	73.4138	0.4737	0.1524	0.1361	1.2061
1.5239	0.0714	8.2077	10.8407	2.7919	0.3658	23.9035	76.7875	0.5040	0.1381		
1.6887	0.0988	8.5075	11.8305	2.9352	0.4417	24.6561	82.7283	0.5491	0.1182	0.0622	4.6972
1.7517	0.1087	8.8180	12.9273	3.0867	0.5227			0.5969	0.0967	0.0683	5.0955
1.8314	0.0954	9.1386	14.0985	3.2461	0.6242	0.0649	3.5180	0.6420	0.0788	0.0750	4.3613
1.9177	0.1089	9.4699	15.3469	3.4126	0.7368	0.0685	7.7691	0.6833	0.0683	0.0858	3.1493
2.0014	0.1220	9.8136	16.6431	3.5861	0.8752	0.0717	7.8331	0.7202	0.0615	0.0989	1.9819
		10.1695	17.9921	3.7682	1.0496	0.0848	4.4127	0.7627	0.0547	0.1140	1.6066
1.3172	0.0372	10.5355	19.5471	3.9601	1.2470	0.1079	2.3458	0.8157	0.0482	0.1342	1.2566
1.3660	0.0406	10.9143	21.0535	4.1626	1.4713	0.1478	1.1272	0.8610	0.0453		
1.4184	0.0413	11.3058	22.7359	4.3739	1.7285	0.2187	0.5927	0.9007	0.0408	0.0608	5.4368
1.4769	0.0490	11.7123	24.5793	4.5952	2.0364	0.3367	0.2878	0.9330	0.0380	0.0656	4.5115
1.5380	0.0541	12.1349	26.2512	4.8271	2.3916	0.4459	0.1676	0.9629	0.0378	0.0708	4.6938
1.6029	0.0581	12.5615	28.2806	5.0706	2.7977	0.5140	0.1290	0.9887	0.0364	0.0791	2.9844
1.6688	0.0662	12.9763	30.0539	5.3267	3.2370	0.5820	0.1016	1.0110	0.0345	0.0886	2.3156
1.7385	0.0745	13.4487	32.3463	5.5915	3.7830	0.6464	0.0735	1.0357	0.0275	0.1005	2.1000
1.8106	0.0893	13.9862	34.1549	5.8699	4.3445	0.7105	0.0570	1.0876	0.0268	0.1165	1.6125
1.8853	0.0973	14.4817	36.7942	6.1611	4.9601	0.7697	0.0456	1.1334	0.0250	0.1376	1.1905
1.9631	0.1136	14.9582	38.9552	6.4653	5.6849	0.8214	0.0370	1.1809	0.0220	0.1642	0.8969
2.0442	0.1286	15.4419	41.1370	6.7844	6.5057	0.8664	0.0297	1.2302	0.0248	0.1984	0.6721
2.1283	0.1495	15.9416	43.0182	7.1155	7.4665	0.9090	0.0266	1.2666	0.0230	0.2403	0.4907
2.2155	0.1641	16.4556	45.9954	7.4596	8.5025	0.9471	0.0226	1.2997	0.0225		
2.3053	0.1938	16.9897	48.0668	7.8215	9.5002	0.9807	0.0188	1.3326	0.0262	wire	connected
2.3984	0.2187	17.5388	50.4380	8.1977	10.7133	1.0107	0.0163	1.3565	0.0256		
2.4956	0.2497	18.1050	52.8757	8.5911	12.0616	1.0374	0.0158	1.3743	0.0249	0.0311	4.5831
2.5961	0.2860	18.6887	55.4552	9.0052	13.5966	1.0612	0.0152			0.0460	4.6097
2.7006	0.3278	19.2914	58.4391	9.4175	15.1118	1.0828	0.0130	0.0669	4.8993	0.0476	4.6709
2.8093	0.3781	19.9154	61.1474	9.7909	16.5311	1.1021	0.0085	0.0739	2.6360	0.0502	5.6454
2.9226	0.4305	20.5598	63.6970	10.1333	17.8842			0.0803	3.6506	0.0536	6.5853
3.0400	0.4924	21.2241	66.3291	10.4637	19.2285	0.0663	3.8355	0.0895	2.3653	0.0601	4.5099
3.1620	0.5602	21.9092	68.9010	10.8012	20.6465	0.0707	8.0621	0.1007	2.1112	0.0668	4.8117
3.2884	0.6619	22.6119	71.1618	11.1496	22.1189	0.0860	3.5581	0.1161	1.6153		
3.4255	0.7427	23.3311	74.1279	11.5095	23.6965			0.1367	1.2176	0.0411	2.7914
3.5712	0.8678	24.0712	77.6874	11.8808	25.3243	0.0617	4.1863	0.1634	0.9321	0.0440	3.4309
3.7225	0.9937	24.8287	84.2878	12.2641	27.0375	0.0675	4.0248	0.1993	0.6796	0.0473	4.7439
3.8802	1.1593			12.6600	28.8453	0.0705	4.8080			0.0507	5.6303
4.0451	1.3235	1.1098	0.0361	13.0686	30.1491	0.0782	3.2255	0.0585	4.9368	0.0546	4.8959
4.2165	1.5063	1.1486	0.0316	13.4894	32.4125	0.0823	3.0273	0.0625	6.1091	0.0619	5.1750
4.3941	1.7542	1.1967	0.0343	13.9233	33.5739	0.0851	3.3952	0.0651	7.0580	0.0690	4.5456
4.5772	1.9830	1.2476	0.0521	14.3734	36.3072	0.0925	2.6273	0.0701	4.6464	0.0761	4.2555
4.7532	2.2487	1.3186	0.0364	14.8371	38.3386	0.1031	2.0843	0.0792	3.3780	0.0828	4.1087
4.9272	2.5253	1.3906	0.0469	15.3152	40.5503	0.1164	1.7464	0.0901	2.4442		
5.1116	2.8426	1.4621	0.0482	15.8113	42.6402	0.1347	1.3179	0.1059	1.8825		
5.3029	3.1831	1.5378	0.0575	16.3239	45.0275	0.1576	0.9865	0.1246	1.3852		
5.5011	3.5604	1.6174	0.0591	16.8521	47.5173	0.1868	0.7408	0.1491	1.0207		

Chapter 8. Ferrocenium Hexafluorophosphate

8.1 Introduction

Ferrocenium hexafluorophosphate ($[Fc]PF_6$) and similar metallocenium salts demonstrate a variety of phase transition sequences unexpected from their relatively simple crystal structures. Three phases are known in $[Fc]PF_6$, which are divided by two phase transitions at 213 K and 347 K[10]. These phase transitions are considered to arise from orientational order-disorder phenomena concerning both the $[Fc]^+$ cation and $(PF_6)^-$ anion. The highest temperature phase belongs to a cubic space group, $Pm\bar{3}$, where both the cations and anions are disordered in twelve and four orientations, respectively, and construct a pseudo body-centered CsCl type cubic lattice. In the intermediate phase (a monoclinic structure, $P2_1/c$), $(PF_6)^-$ anion is fully ordered, while $[Fc]^+$ cation reorients between four directions three of which are slightly tipped off from an axis. This reorientational motion is suppressed in the lowest temperature phase and $[Fc]^+$ cation is completely ordered[11]. The present calorimetric study is concerned with this lowest temperature phase where $[Fc]^+$ cations are aligned so as to make their molecular axes staggered each other.

In $[Fc]PF_6$, only $[Fc]^+$ cation has a magnetic moment due to an unpaired electron with spin $s = 1/2$. For this species an anisotropic g-factor is expected as in the case of $[DMFc]^+$ or $[BFc]^+$ cations. Actually $[Fc]^+$ has $g_{\parallel} = 4.35$ and $g_{\perp} = 1.26$[12]. Since the neighboring $[Fc]^+$ cations are arranged with their molecular axes crossed, the Ising nature cannot be simply expected for the magnetic interaction even if the g-value has a strong anisotropy. Hence the character of magnetic interaction provides an interesting problem in addition to the exchange-path problem.

8.2 Experimental

(1) Calorimetry

For heat-capacity measurements, 6.7277 g of [Fc]PF_6 and 3.2225 g of silicone oil was used. Prior to mixing, the silicone oil was evacuated to remove air and water, and then saturated with nitrogen gas. Sample mounting procedures were carried out under inert atmosphere of nitrogen. Heat capacities were measured in the temperature region between 95 mK and 20 K.

(2) Calorimetry using a pellet sample

A pellet sample was attempted for the calorimetry to obtain more reliable data at lowest temperatures. 0.64 g of the sample (density d = 1.5 gcm^{-3}) was mixed with 3.5 g of copper powder (d = 8.92 gcm^{-3}). The copper powder (Wolstenholme, MD60) was washed twice with ethylether and desiccated in a vacuum before use. The mixture was shaped into a pellet with its weight of 3.9392 g. The pellet was mounted in a pellet holder without vacuum seal because the present compound is stable under vacuum. The weight of the sample and the copper powder involved in the pellet were estimated to be 0.60896 g and 3.33024 g respectively under an assumption of uniform mixture.

8.3 Results and Discussion

Molar heat capacities of [Fc]PF_6 are given in Table 8.1 and Fig. 8.1. A very small anomaly well separated from the lattice contribution was observed bellow 1 K. The excess entropy of this anomaly was evaluated to be merely $\sim$1.2 J K^{-1} mol^{-1} from the silicone-oil data. The pellet data below 0.2 K showed remarkable deviation from the silicone-oil data which exhibited rather a rapid diminution. In the temperature region below 0.2 K the silicone-oil-mull sample is considered to be not fully thermally relaxed and to exhibit non-equilibrium behavior owing to a long thermal relaxation time exceeding 1 hour. Thus the larger heat capacities comparable to the pellet data should be observed below 0.2 K if the thermal equilibration would be completely attained. On the other hand the

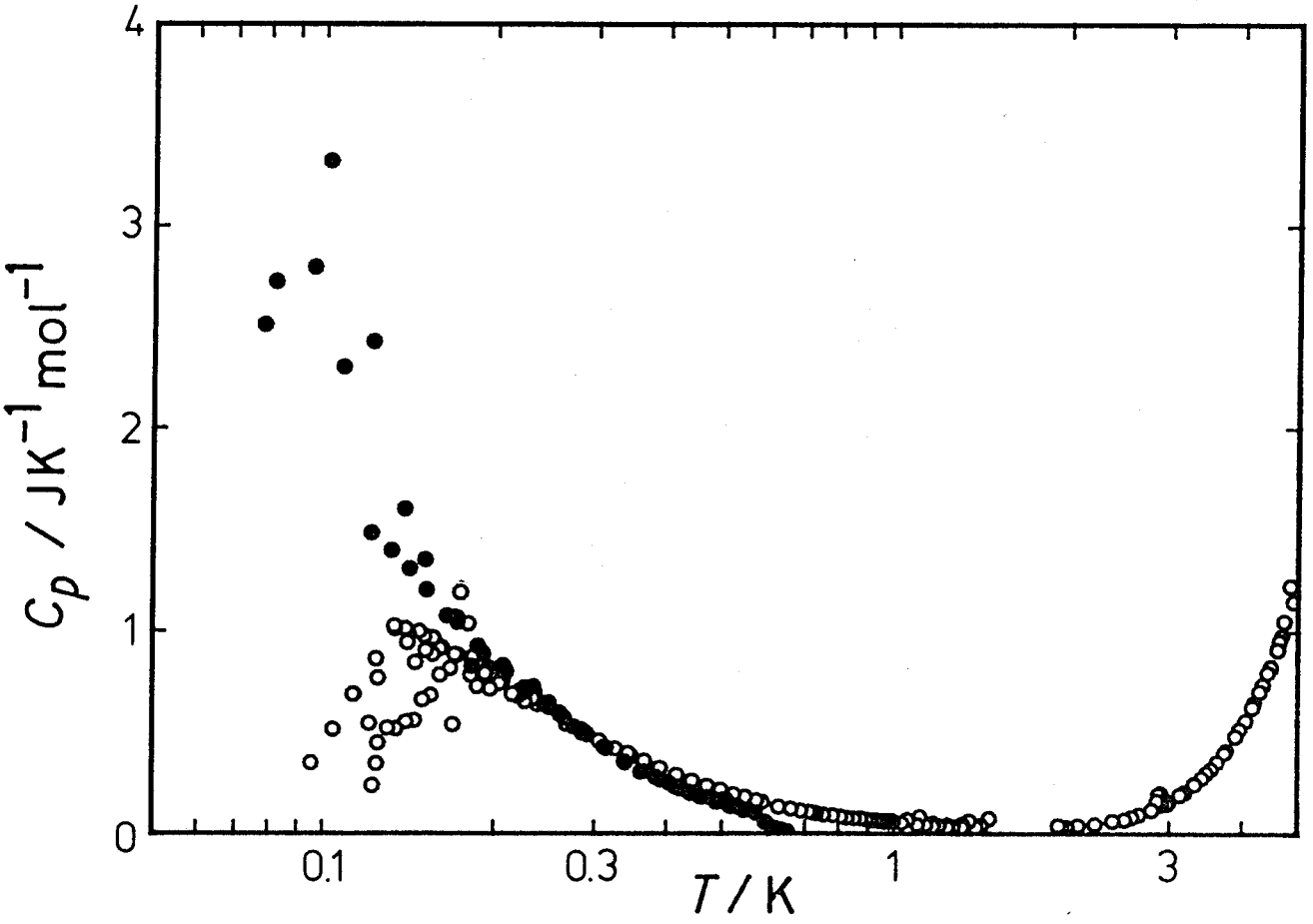

Fig. 8.1 Molar heat capacities of ferrocenium hexafluorophosphate. Open circles show silicone-oil data, whereas filled circles show pellet-sample data.

pellet data are not completely reliable because of the uncertainty involved in the sample weight.

Since any degrees of freedom except for electron spin cannot be considered to contribute below 1 K, the observed anomaly should be attributable to a magnetic origin. And the very small excess entropy is considered to be a part of the total magnetic entropy, R ln 2 (= 5.76 J K^{-1} mol^{-1}). The profile of this anomaly will be examined in chapter 9, in which it will be concluded that this anomaly is not a Schottky type arising from the singlet-triplet energy scheme of a dimer formation. In addition, some short range order effect will be concluded. In order to explain this short range effect, two hypotheses are considered : one is a 1D Ising model and the other is a 2D Heisenberg model. Although the strong single ion anisotropy of $[Fc]^+$ cation supports the Ising character, it is difficult to obtain a clear conclusion for the delicate question as to which model is more appropriate for the present compound.

Table 8.1 Molar heat capacities of ferrocenium hexafluorophosphate.

$\frac{T}{K}$	$\frac{Cp}{JK^{-1}mol^{-1}}$	$\frac{T}{K}$	$\frac{Cp}{JK^{-1}mol^{-1}}$	$\frac{T}{K}$	$\frac{Cp}{JK^{-1}mol^{-1}}$	$\frac{T}{K}$	$\frac{Cp}{JK^{-1}mol^{-1}}$	$\frac{T}{K}$	$\frac{Cp}{JK^{-1}mol^{-1}}$	$\frac{T}{K}$	$\frac{Cp}{JK^{-1}mol^{-1}}$
0.1229	0.2423	0.9798	0.0675			11.2304	11.8271	5.3081	1.4945	0.6172	0.0376
0.1304	0.5253	0.9863	0.0667	2.8599	0.1692	11.6606	12.8835	5.5900	1.7723	0.6356	0.0273
0.1352	0.5241	0.9917	0.0674	2.8708	0.2006	12.1889	14.2320	5.8349	2.0351	0.6515	0.0175
0.1406	0.5577	0.9967	0.0650	2.8836	0.1590	12.8497	16.1831	6.0567	2.2898		
0.1454	0.5632			2.8962	0.2074	13.4170	17.6282	6.2828	2.5563	0.1222	2.4331
0.1499	0.6678	0.0955	0.3551	2.9095	0.1489	13.8794	18.1470	6.5700	2.9525	0.1520	1.2089
0.1554	0.6894	0.1141	0.6930	2.9730	0.1535	14.5199	20.2418	6.9383	3.4975	0.1870	0.9338
0.1610	0.7887	0.1256	0.7728	3.1335	0.1955	15.2164	22.1305	7.3343	4.1518	0.2259	0.7294
0.1697	0.5444	0.1343	1.0130	3.3227	0.2508	15.8154	23.8651	7.6834	4.7725	0.2654	0.5793
0.1746	1.1929	0.1421	0.9851	3.4855	0.3065	16.4471	25.7525	7.9899	5.3387	0.2899	0.5067
0.1871	0.7337	0.1511	0.9770	3.6310	0.3598	17.1450	27.7564	8.3211	5.9248	0.3144	0.4310
0.1970	0.7225	0.1609	0.9174	3.7683	0.4180	17.8244	29.6394	8.7406	6.7219	0.3383	0.3632
0.2075	0.7587	0.1712	0.8882	3.9137	0.4895	18.4848	31.3030	9.2428	7.6350	0.3615	0.3119
0.2200	0.6851	0.1823	0.7891	4.0617	0.5647	19.2749	33.5024	9.7371	8.4700	0.3838	0.2870
0.2340	0.6747	0.1936	0.8049	4.2102	0.6532	20.3245	36.3673	10.1719	9.3661	0.4045	0.2562
0.2506	0.6296	0.2045	0.7465	4.3579	0.7431	21.1964	38.1191	10.5849	10.2742	0.4235	0.2296
0.2686	0.5495	0.2154	0.6975	4.4924	0.8314	21.7297	39.4455	11.0578	11.2927	0.4410	0.2061
0.2868	0.5027	0.2265	0.6613	4.6161	0.9122	22.4873	41.5383	11.6376	12.6207	0.4570	0.1894
0.3059	0.4653	0.2385	0.6439	4.7329	1.0506			12.2338	13.9758	0.4714	0.1880
0.3263	0.4269	0.1047	0.5207	4.8476	1.2230	1.0584	0.0757	12.7619	15.6692	0.4847	0.1786
0.3483	0.3884	0.1134	0.6942			1.1115	0.0919	13.2283	16.7923	0.4965	0.1638
0.3432	0.4047	0.1211	0.5503	4.7035	0.9799	1.1758	0.0575	13.6426	17.9789	0.5069	0.1772
0.3667	0.3659	0.1243	0.8670	4.9150	1.1468	1.2430	0.0483	14.0296	18.5948	0.5160	0.1565
0.3913	0.3315	0.1341	1.0252	5.1157	1.3180	1.3199	0.0544	14.4634	20.0313	0.5346	0.1392
0.4171	0.2975	0.1401	1.0113	5.2962	1.4894	1.4182	0.0465	15.1468	22.1435		
0.4438	0.2665	0.1481	1.0013	5.4752	1.6637			16.1358	24.7699	0.0959	2.7979
0.4709	0.2427	0.1569	0.9690	5.6795	1.8619	1.1393	0.0500	17.1294	27.5445	0.1830	0.8327
0.4981	0.2212	0.1247	0.3507	5.8903	2.0979	1.2037	0.0463	17.8913	29.7594	0.2342	0.7330
0.5249	0.2011	0.1458	0.8494	6.0820	2.3177	1.2710	0.0406	18.5068	31.3197	0.2597	0.6063
0.5505	0.1867	0.1566	0.8875	6.2584	2.5149	1.3528	0.0685	19.2243	33.3399	0.2859	0.5101
0.5751	0.1716	0.1679	0.8206	6.4214	2.7316			19.9784	35.0909		
0.5897	0.1609	0.1803	1.0380	6.5743	2.9392	1.9249	0.0461	20.6928	36.5891	0.0783	2.5173
0.6287	0.1407	0.1932	0.7942	6.7175	3.1236	1.9953	0.0404			0.0869	6.8568
0.6620	0.1281	0.1256	0.4533	6.8527	3.3384	2.0838	0.0475	pellet	sample	0.1084	2.3100
0.6884	0.1196	0.1414	0.9446	6.9812	3.5297	2.2309	0.0543			0.1319	1.4001
0.7122	0.1131	0.1519	0.9060	7.1035	3.6817	2.3938	0.0685	0.1391	1.6034	0.1511	1.3557
0.7338	0.1073	0.1625	0.9221	7.2203	3.8514	2.5097	0.0749	0.1719	1.0732	0.1725	1.0491
		0.1733	0.8849	7.3321	4.0202	2.5852	0.0891	0.2071	0.8365	0.1917	0.8958
0.7224	0.1098	0.1841	0.8769	7.4394	4.2174	2.6649	0.1001	0.2462	0.6465	0.2103	0.8068
0.7550	0.1010	0.1960	0.8238	7.5428	4.4075	2.7990	0.1227	0.2834	0.5233	0.2274	0.7053
0.7837	0.0961	0.2087	0.7847	7.6427	4.5314	2.9968	0.1620	0.3116	0.4371	0.2445	0.6508
0.8089	0.0905	0.2224	0.7127	7.7390	4.6264	3.1884	0.2083	0.3392	0.3564	0.2607	0.5953
0.8305	0.0846	0.2362	0.7044	7.8321	4.7819	3.3195	0.2492	0.3658	0.3151	0.2765	0.5351
0.8538	0.0829	0.2501	0.6558	7.9223	5.0120	3.4193	0.2803	0.3912	0.2727	0.2916	0.4934
0.8769	0.0820			8.0101	5.1070	3.5437	0.3250	0.4148	0.2376		
0.8979	0.0760	1.0317	0.0601	8.2186	5.5145	3.7379	0.4063	0.4367	0.2114	0.0820	2.7267
0.9158	0.0735	1.1005	0.0504	8.5384	6.0970	3.9755	0.5244	0.4611	0.1857	0.1019	3.3190
0.9322	0.0733	1.1713	0.0435	8.8443	6.6663	4.1720	0.6319	0.4874	0.1640	0.1214	1.4862
0.9445	0.0677	1.2414	0.0415	9.2071	7.3653	4.3017	0.7093	0.5162	0.1427	0.1419	1.3107
0.9554	0.0685	1.3140	0.0371	9.6984	8.3961	4.4362	0.8018	0.5463	0.1242	0.1653	1.0793
0.9646	0.0671	1.3884	0.0359	10.2694	9.6388	4.6555	0.9544	0.5726	0.1109		
0.9726	0.0670	1.4632	0.0814	10.7922	10.8429	4.9771	1.2017	0.5964	0.0655		

Chapter 9. A Morphological Analysis of Excess Heat Capacity Curves

9.1 Introduction of the Exponent *n*

Excess heat capacity provides useful information about physicochemical properties of materials. Of course, the excess enthalpy and entropy as integrated quantities are useful measures for the thermodynamic stability of matter, degrees of freedom concerning thermal excitation, and so on. In contrast to this, the excess heat capacity as a derivative quantity involves more detailed informations in its profile. Heat-capacity measurement is essentially a kind of spectroscopy which is exempted from any kind of selection rules. In fact, heat capacity is related to a Laplace transformation of an energy spectrum, hence it contains complete information about the density of states of a matter in principle. As a spectroscopy, heat-capacity measurement suffers from broadness of absorption lines due to Boltzmann's factor. Nevertheless it serves as a powerful tool to elucidate the energy level structure near the ground state.

Morphological discussion of heat-capacity anomalies has been so far done by many thermodynamicists[13-15]. In those studies the Schottky heat-capacity anomaly was a main subject. The Schottky anomaly, which corresponds to the absorption line stated above, is caused by thermal excitation between a finite number of discrete energy levels. For example, a two-level system, in which a g_0-fold degenerate ground level is separated by an energy gap ε from a g_1-fold excited level, brings about a Schottky anomaly given by the following equation,

$$C/R = (g_1/g_0)(\varepsilon/k_B T)^2 \exp[-\varepsilon/k_B T] \cdot \{1 + (g_1/g_0)\exp[-\varepsilon/k_B T]\}^{-2}.$$

This equation provides a single maximum when plotted against logarithmic temperature, whose shape, *i.e.* the maximum height and width, is uniquely determined by the ratio g_1/g_0. The peak temperature depends on both the g_1/g_0 and the energy gap ε (see Fig. 9.1).

On the other hand, alternative heat-capacity anomaly is phase transitions,

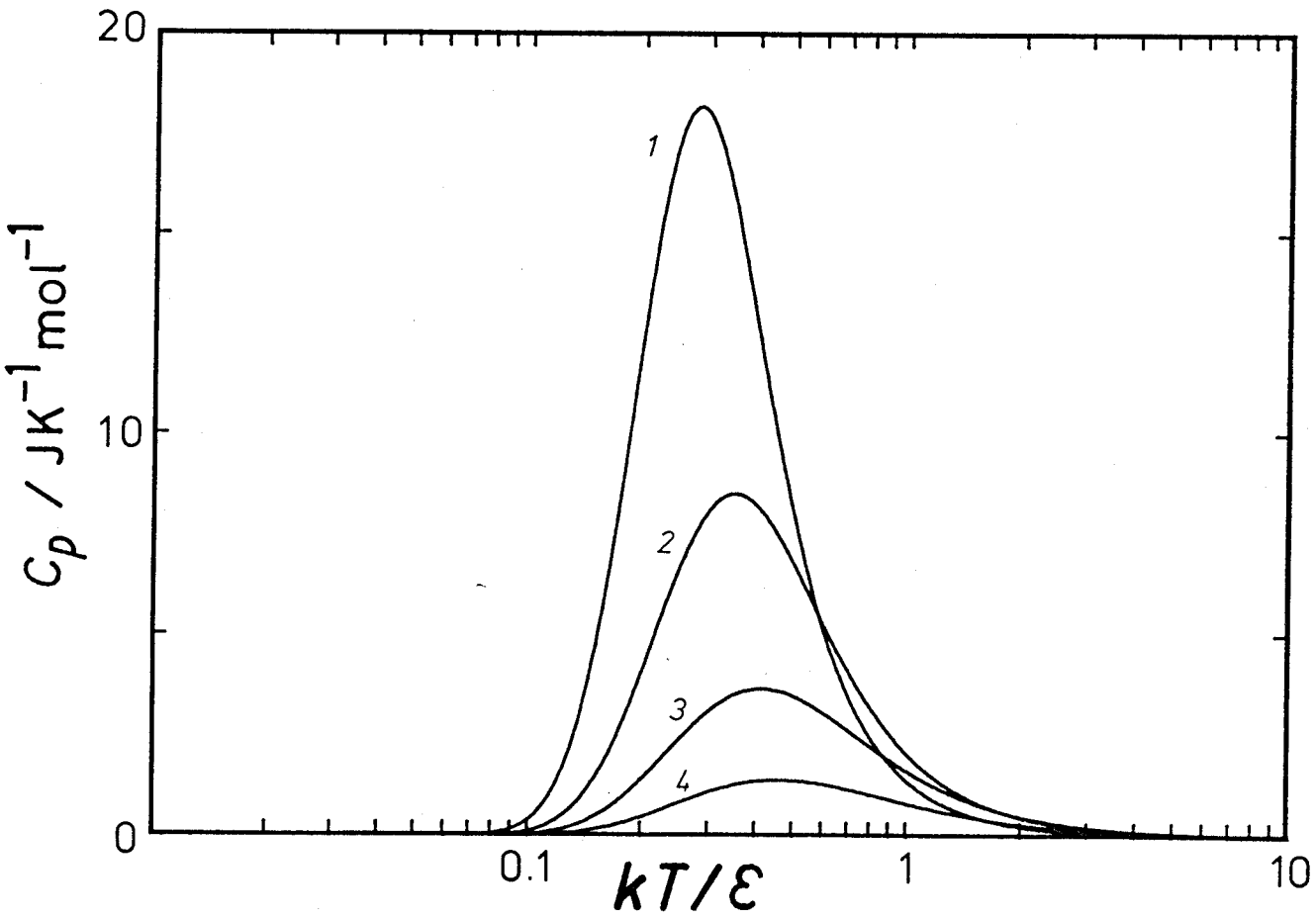

Fig. 9.1 Schottky heat-capacity anomaly of a system with two energy levels, ε apart. Curves 1,2,3, and 4 correspond to anomalies with degeneracy ratio, g_1/g_0 = 10, 3, 1, and 1/3.

which exhibit a variety of morphologies. A phase transition is observed in heat capacity as a singular point such as discontinuity, divergence, and cusp, and is usually associated with enhanced heat capacities around the transition temperature. Such an enhancement of heat capacity is called high temperature or low temperature tail of the phase transition. An unified approach to treat anomalous heat capacities caused by phase transitions is not known. Only available are solutions obtained for the respective model systems. Especially for the first kind of phase transition, which shows a discontinuity in the entropy at the transition temperature, morphological treatment from the viewpoint of energy spectrum is difficult because complete reconstruction of energy spectrum is required at the phase transition. Contrary to this, the situation is largely altered for the second kind of phase transitions where the anomalous heat capacity can be, in principle, interpreted on the basis of the density of states associated with a singularity[14].

The heat-capacity anomalies described in the last two chapters were observed below 1 K. Since the maxima of these anomalies are expected to appear below the lowest observable temperature of our calorimeter, we could not obtain the whole anomalies whereas only high temperature tails were observed. Such anomaly-tails are often observed when some kind of order is generated and reduces gradually the entropy of a system. Because the gradual reduction of entropy on cooling leads to disproportionation of an energy distribution in the energy spectrum, these tails can be attributed to either the Schottky anomaly, where the ordering remains local, or a growth of the correlation length of an order parameter throughout the crystal, which may give rise to a phase transition of the second kind. However, identification of the origin is a difficult problem solely by use of the heat-capacity data concerning the anomaly-tails. In order to solve the problem we shall propose a new method which provides an useful criterion to

judge whether an anomalous heat capacity originates in a phase transition or in a Schottky anomaly.

Since the absolute value of heat capacities varies gradually in the tail region, it provides only limited knowledge as to discrimination between a Schottky anomaly and a phase transition. Taking this situation into account, we introduce a temperature exponent n defined by $C \propto T^{-n}$ or $n = -(\partial \ln C/\partial \ln T)$. By this treatment, one can reveal more characteristic feature of the anomaly and can easily assign the anomaly to either of origins. Although the exponent n is a differential quantity independent of the absolute value of heat capacity, comparison of n between the observed and theoretical values provides a clue to check the applicability of a given theoretical model. This comparison is valid because the absolute value of heat capacity in the tail region is easily adjustable by scaling of temperature with interaction strength.

9.2 Properties of the Exponent n

(1) High temperature limit

When an energy spectrum possesses an upper bound, the internal energy shows saturation at high temperatures and the heat capacity decays according to T^{-2}. This is easily understood as follows. At high temperature limit ($\beta = 1/k_B T \rightarrow 0$), the internal energy can be expressed by

$$\langle E \rangle \sim \int g(E) E \mathrm{d}E - \beta \int g(E) E^2 \mathrm{d}E,$$

where $g(E)$ denotes the density of states associated with the energy spectrum. If the energy spectrum has an upper bound, that is, the density of states $g(E)$ has a cut-off energy, the integrals involved in the expression of $\langle E \rangle$ converge to provide finite values. From the definition of heat capacity, $C = -(1/k_B T^2)(\partial \langle E \rangle/\partial \beta)$, one can obtain the T^{-2} decay behavior of the heat capacity. Hence in this case the exponent n tends to 2 at high temperatures.

The Schottky anomaly is known to behave as T^{-2} at high temperatures. The

expression for the two-level Schottky heat capacity given in section 9.1 clearly demonstrates such a behavior by replacing the Boltzmann factor $\exp[-\varepsilon / k_B T]$ with unity. However, this behavior is not restricted in the case of Schottky anomalies. One can also find this tendency ($n \to 2$) in many phase transitions. Generally the heat-capacity anomaly, except for first order phase transitions, must decay as T^{-2} at high temperatures.

(2) Low temperature limit

At low temperature limit the heat-capacity anomaly is dominated by the nature of elementary excitations. If the elementary excitation has a gapless spectrum, the exponent n takes a finite value characteristic of a given density of states, which is determined by dispersion relation of the excitation and the dimension of crystalline lattice, d. Goldstone bosons are typical examples, which exist in the ordered phase resulting from a spontaneous breakdown of symmetry : $n = -d$ for phonon, $n = -d$ for antiferromagnetic magnon, and $n = -d/2$ for ferromagnetic magnon[6]. Alternative example is conduction electrons in metal, whose heat capacity has linear dependence on temperature and thus $n = -1$. Such behaviors with finite n are characteristic of continuum energy spectra.

When there exists an energy gap between the ground and the first excited states, n shows negative divergence behavior. Thermal excitation over an energy gap is governed by the Boltzmann factor, so that we can obtain the internal energy as $\langle E \rangle \sim \varepsilon \exp[-\varepsilon / k_B T]$, where ε is the energy gap. By differentiating $\langle E \rangle$ with respect to T, one can derive $n = 2 - \varepsilon / k_B T \to -\infty$ at low temperature limit. Such a divergence is a common behavior of the energy spectrum with an energy gap, for example the Ising magnet, the Einstein oscillator, and the Schottky anomaly.

(3) Coexistence of plural contributions

In real substances the heat capacity is composed of several contributions.

When the heat capacity consists of two components C_1 and C_2, the exponent n for the total heat capacity, $C = C_1 + C_2$, becomes $n = (C_1/C)n_1 + (C_2/C)n_2$, where $n_1 = -(\partial \ln C_1/\partial \ln T)$ and $n_2 = -(\partial \ln C_2/\partial \ln T)$. This expression can be reduced to $n \sim (1 - C_2/C_1)n_1 + (C_2/C_1)n_2$ on the assumption of $C_1 \gg C_2$. This result indicates that even if "noise" component C_2 has relatively large contribution, the exponent n is not seriously affected by the existence of C_2 as far as the C_2 is varied slowly with temperature or actually temperature independent.

This relation, however, exhibits a curious effect at low temperature limit, if the total heat capacity consists of a Schottky contribution C_1 and a weakly temperature dependent contribution C_2 (*e.g.* a noise component or magnon contribution). It is apparently expected that the negative divergence of n described above is caused by the leading term n_1, but this divergence is virtual in practice. A competition occurs between the exponential decay of C_1 and the T^{-1} divergence of n_1 so that the term $(C_1/C)n_1$ vanishes as a result of superior exponential decay at low temperature limit. Consequently at extremely low temperatures the identification of a Schottky contribution by means of the exponent n would be difficult because of the temperature independent noise contribution.

(4) Comparison between heat capacities arising from a phase transition and from a Schottky anomaly

As already described, the main motif to introduce this exponent n is the discrimination between a Schottky heat-capacity anomaly and a phase transition only by use of partial data concerning the high temperature tail of the anomaly. We present here the characteristic behavior of each anomaly and the criterion for discriminating these two anomalies. Although both a Schottky anomaly and a phase transition take $n \sim 2$ at high temperature limit, deviation from this extreme value on going from high to low temperatures exhibits different behavior in each case.

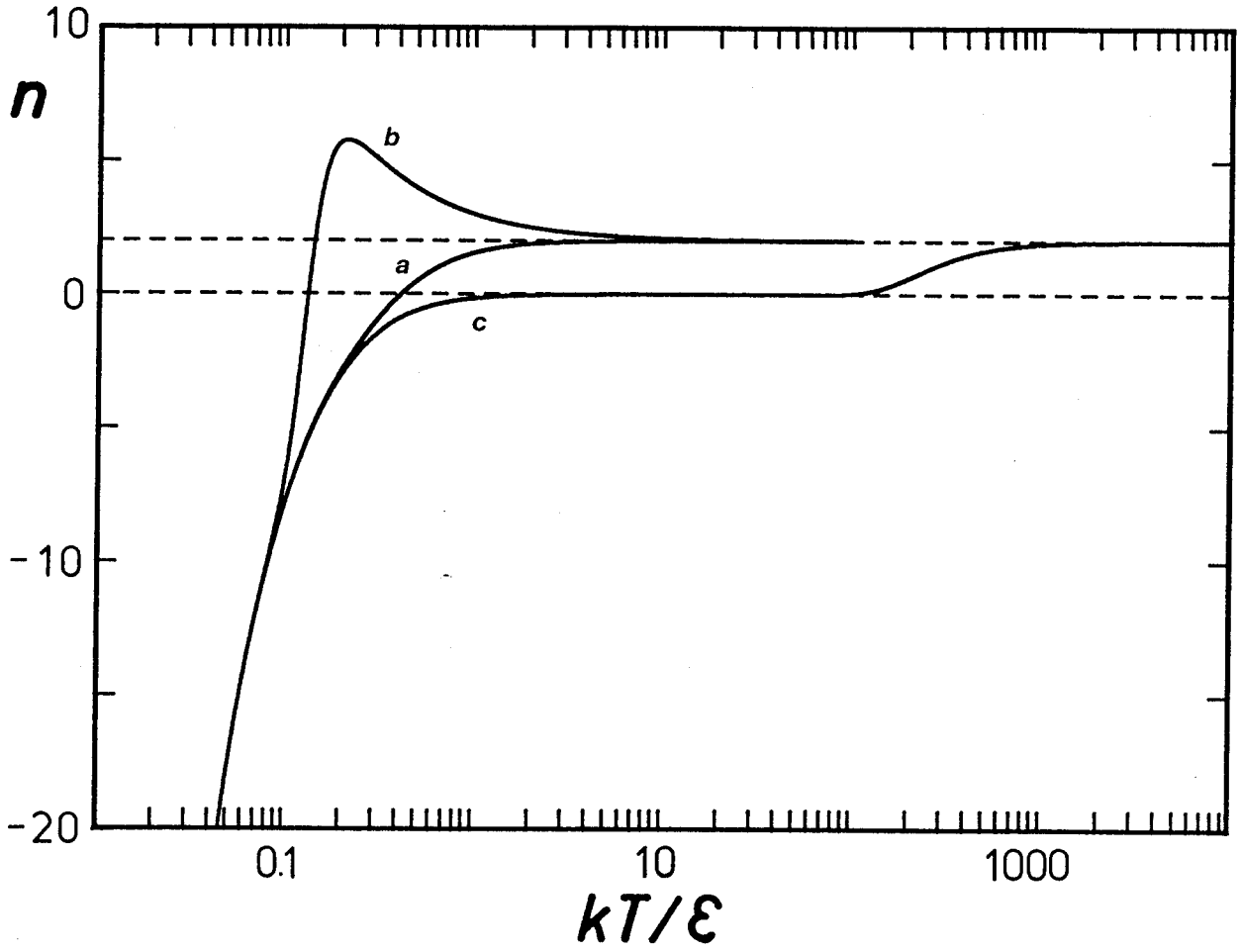

Fig. 9.2 Temperature exponents, n, for three Schottky anomalies.
a, 2-level Schottky anomaly with g_1/g_0 = 1;
b, 2-level Schottky anomaly with g_1/g_0 = 1000;
c, Schottky anomaly arising from equispaced 1000 levels.

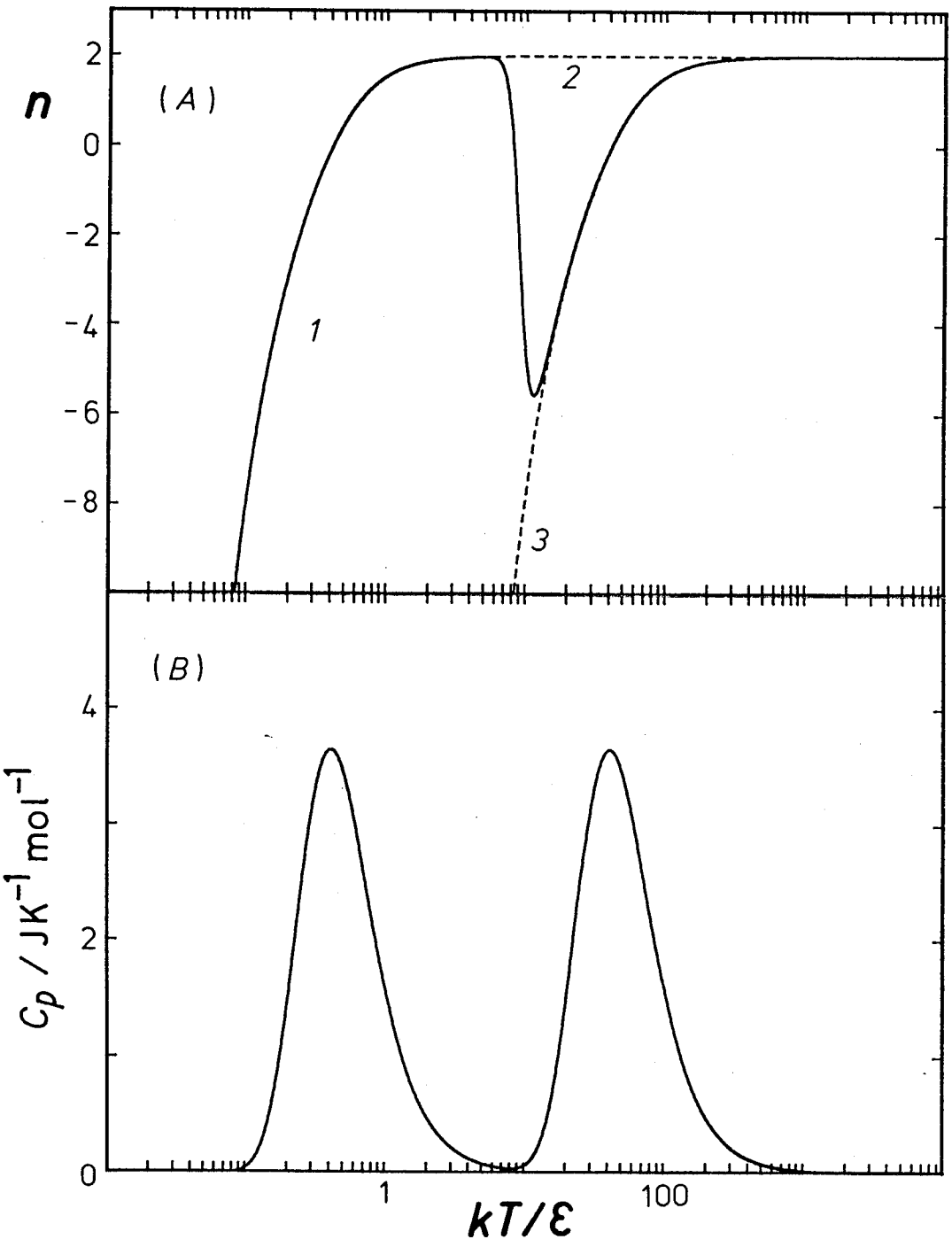

Fig. 9.3 Schottky anomaly with two maxima and its temperature exponent, n.
(A), Temperature exponents for three systems.
1, Three-level system which corresponds to (B);
2, two-level system with an energy gap ε;
3, two-level system with an energy gap 100ε.
(B), Schottky anomaly arising from a three-level system, which is comprised of a non-degenerate ground level, a non-degenerate first excited level at ε, and a doubly degenerate second excited level at 100ε.

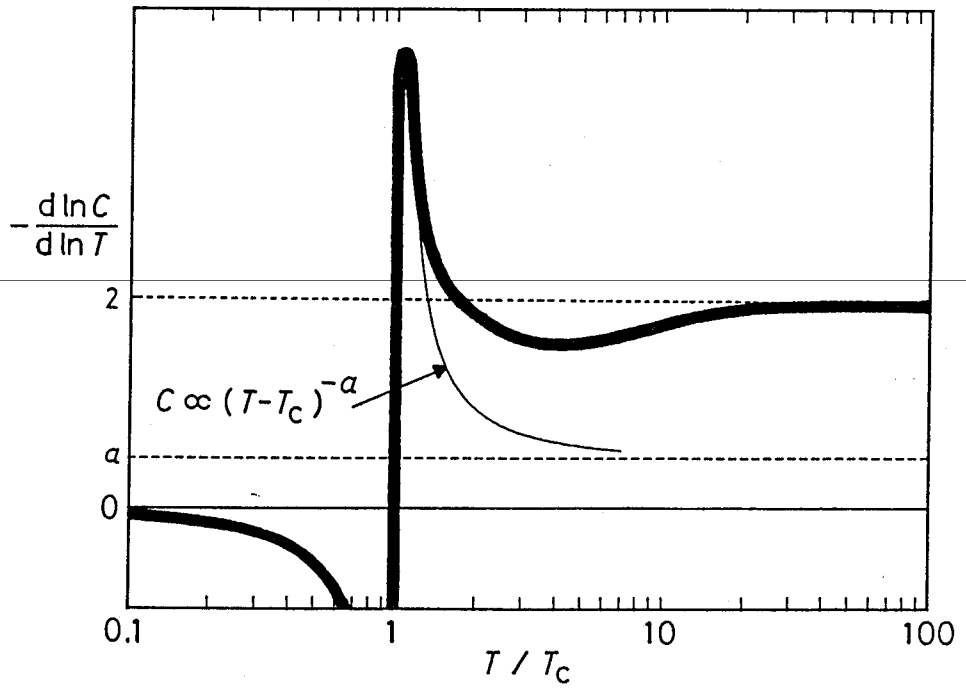

Fig. 9.4 Schematic diagram of temperature exponent accompanying a critical phenomenon. The thick curve represents an interpolation between critical region and asymptotic limit, $n = 2$.

A Schottky heat capacity has a rather simple behavior of deviation. For example the Schottky anomaly due to a two-level system is again considered. By differentiation of the Schottky heat capacity given in section 9.1, the exponent n is derived as

$$n = 2 - (\varepsilon / k_B T) \cdot [1 - (g_1/g_0)\exp(-\varepsilon / k_B T)]/[1 + (g_1/g_0)\exp(-\varepsilon / k_B T)].$$

This expression implies that n has one or two stationary values (including extremum) according to g_1/g_0. One of these stationary values is obviously the asymptotic limit $n = 2$ at $T \to \infty$. Another stationary value, which can present when $g_1/g_0 > 1$, corresponds to a maximum (see Fig. 9.2). This behavior remains unchanged when the excited level is replaced with an assembly of energy levels bundled within much smaller width than the energy gap. Contrary to this, when such a replacement is done for the ground level, it makes more stationary-values possible and somewhat complicated behavior in the intermediate temperature region is obtained. If plural peaks are clearly resolved in the Schottky anomaly generated by the energy scheme with a finite width in its ground state, we can apply the relation, $n \sim (1 - C_2/C_1)n_1 + (C_2/C_1)n_2$, to predict the behavior of n (see Fig. 9.3). Anyway, as far as the deviative behavior from the asymptotic limit $n = 2$ is concerned, we can conclude that on cooling the exponent n shows a monotonous decrease or a broad maximum followed by a monotonous decrease for the Schottky anomaly derived from a quasi-2-level system.

Even if the energy spectrum is much more dispersive and far from 2-level system, the monotonously decreasing behavior stated above still holds in many cases. For example, when the density of states is assumed to obey the Gaussian distribution, the monotonously decreasing behavior is also reproduced because the Gaussian distribution is the limiting case of binomial distribution which can be reduced exactly to the 2-level system. Another example is the uniform

distribution of the density of states. Such an equispaced multilevel system shows the Einstein oscillator-like behavior at low temperature limit, whereas the monotonously decreasing behavior at high temperature limit similar to the quasi-2-level system with $g_1/g_0 \ll 1$ possessing a finite ground state width (see Fig. 9.2(c)).

For phase transitions, the deviation behavior of n from the high temperature limit shows diversity of the character of interactions, crystalline structures and so on. Thus one cannot treat phase transitions by means of an unified approach. However, since critical phenomena are applicable to relatively wide range of second order phase transitions near the critical temperature, one can interpolate between the critical behavior and the asymptotic behavior of high temperature limit. The critical behavior of heat capacity can be described with a critical exponent α as $C \propto (T-T_C)^{-\alpha}$, where T_C denotes the critical temperature. By differentiation one can obtain $n = \alpha \cdot [1 + T_C/(T-T_C)]$. Reliable temperature region, where this expression is applicable, depends on matter or theoretical model but $|T-T_C|/T_C < 0.1$ is reasonably expected[16]. The critical exponent α has relatively small value $\alpha \sim 0.1$. For example, $\alpha = 1/8$ is suggested for the 3D Ising magnet. Hence one can estimate $n \sim 1$ at $T = 1.1T_C$. After interpolating between $n \sim 1$ and $n = 2$ at high temperature limit smoothly, the downward convex region should exist in the intermediate temperature region (see Fig. 9.4). More detailed discussion is possible by use of several parameters inherent in each substance[15] but the general tendency of the behavior is conserved. Therefore we can regard the existence of this downward convex region as the criterion by which one can identify the anomalous heat capacity as arising from a second order phase transition or, at least, no Schottky anomaly in its origin.

9.3 Applications

(1) Biferrocenium radical salts

To convert heat-capacity data to the temperature exponent n, a simple procedure utilizing a linear regression was adopted. In our experiments heat-capacity data were collected with temperature increments of 3-10 per cent (typically 5 per cent) of the absolute temperature. Thus data points are located almost equidistantly with respect to temperature axis when the temperature axis is scaled logarithmically. Average slopes in log-log plot, $-n$, were determined by a linear regression of a group of consecutive data points. In Fig. 9.5 the temperature exponents n obtained by 20-point linear regression are shown for $[BFc]I_3$ and $[DEBFc]I_3$.

In the case of $[DEBFc]I_3$, the characteristic feature of a phase transition, *i.e.* downward convex region, is easily found around 0.2 K. Although the decrease of n is seen above 0.5 K, which might be due to the contribution of lattice heat capacity, the whole shape of the curve suggests that this heat-capacity anomaly is attributable to a phase transition. To compare this n-curve was with several theoretical models, the temperature exponents n of some Heisenberg magnets were calculated from high temperature expansions of theoretical heat capacities and shown in Fig. 9.6. The same plots were made for Ising magnets in Fig. 9.7. In these theoretical models, Heisenberg ferromagnet with simple cubic lattice seems to provide an excellent agreement with $[DEBFc]I_3$. This agreement, however, does not necessarily mean that $[DEBFc]I_3$ belongs to a Heisenberg magnet because converses are not always true. Other candidates are easily found, for example dimensional crossover of Heisenberg chains to 3D ordering. It should be rather concluded that the heat-capacity anomaly of $[DEBFc]I_3$ is a phase transition which possesses little Ising character since the observed n shows evidently disagreement with the monotonous

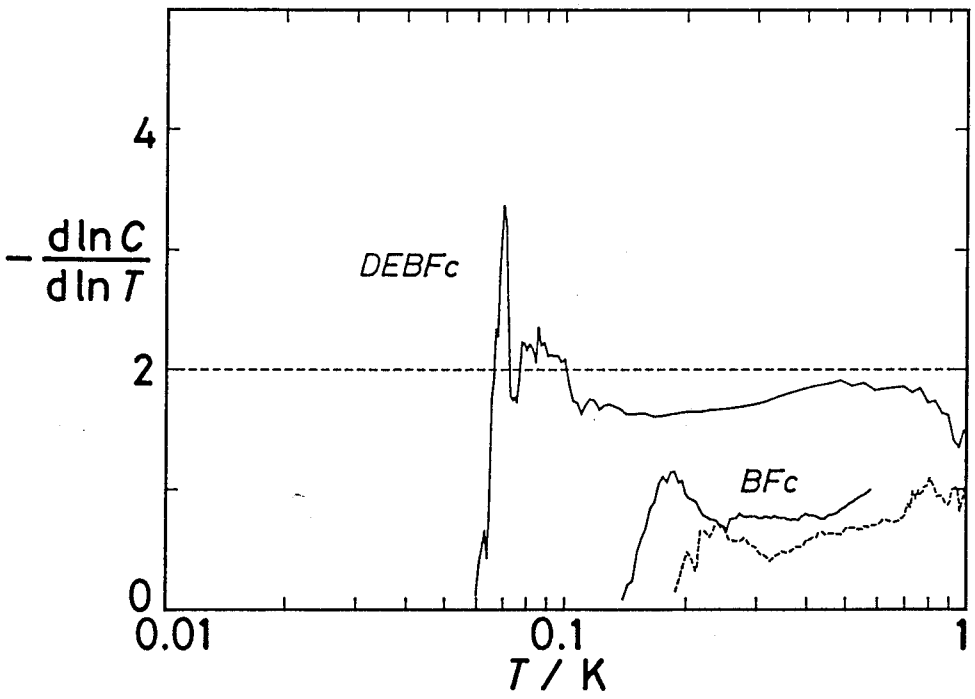

Fig. 9.5 Temperature exponents of 1',1'''-diethylbiferrocenium triiodide (DEBFc) and biferrocenium triiodide (BFc). For BFc, two curves are provided : the broken curve shows silicone-oil data, whereas the full curve shows pellet-sample data.

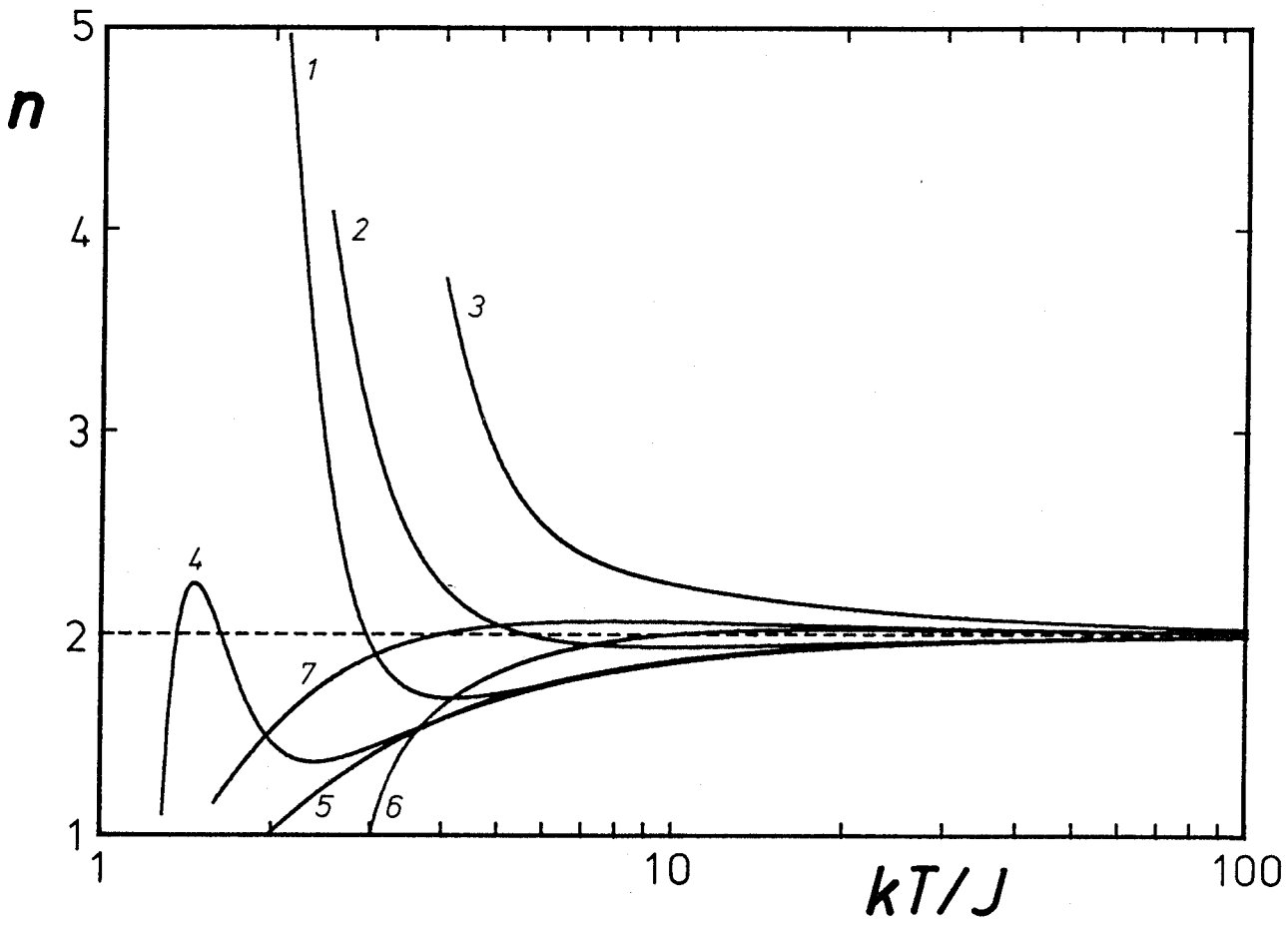

Fig. 9.6 Temperature exponents for some Heisenberg models [18-19]. Theoretical curves are calculated by using the results of high temperature expansions for
1, simple cubic lattice (3D);
2, bcc lattice (3D);
3, fcc lattice (3D);
4, square lattice (2D);
5, ferromagnetic chain (1D);
6, triangular lattice (2D);
7, antiferromagnetic chain (1D).

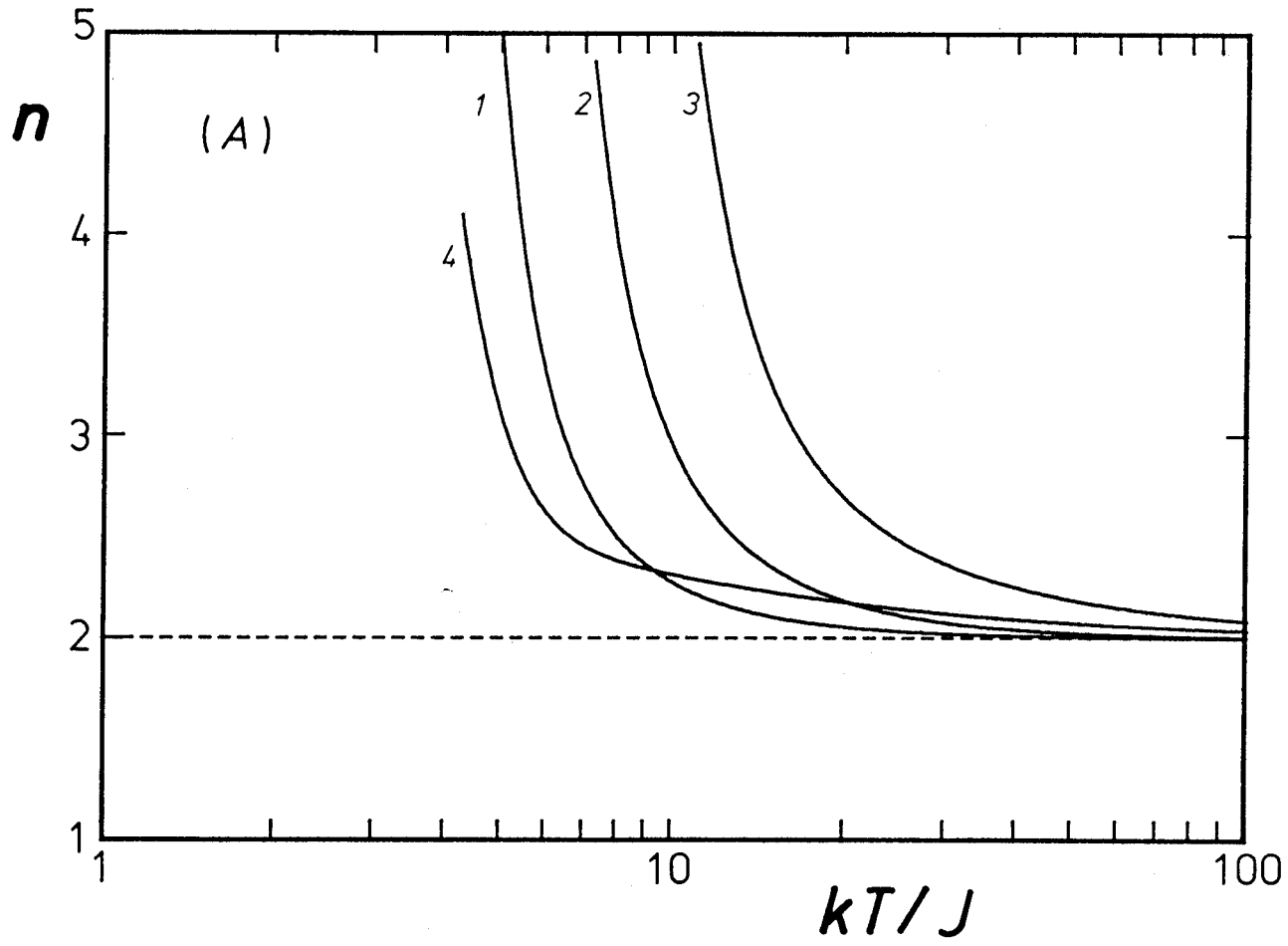

Fig. 9.7 Temperature exponents for some Ising models [17].
(A), 3D systems.
1, Simple cubic lattice;
2, bcc lattice;
3, fcc lattice;
4, cristobalite lattice.

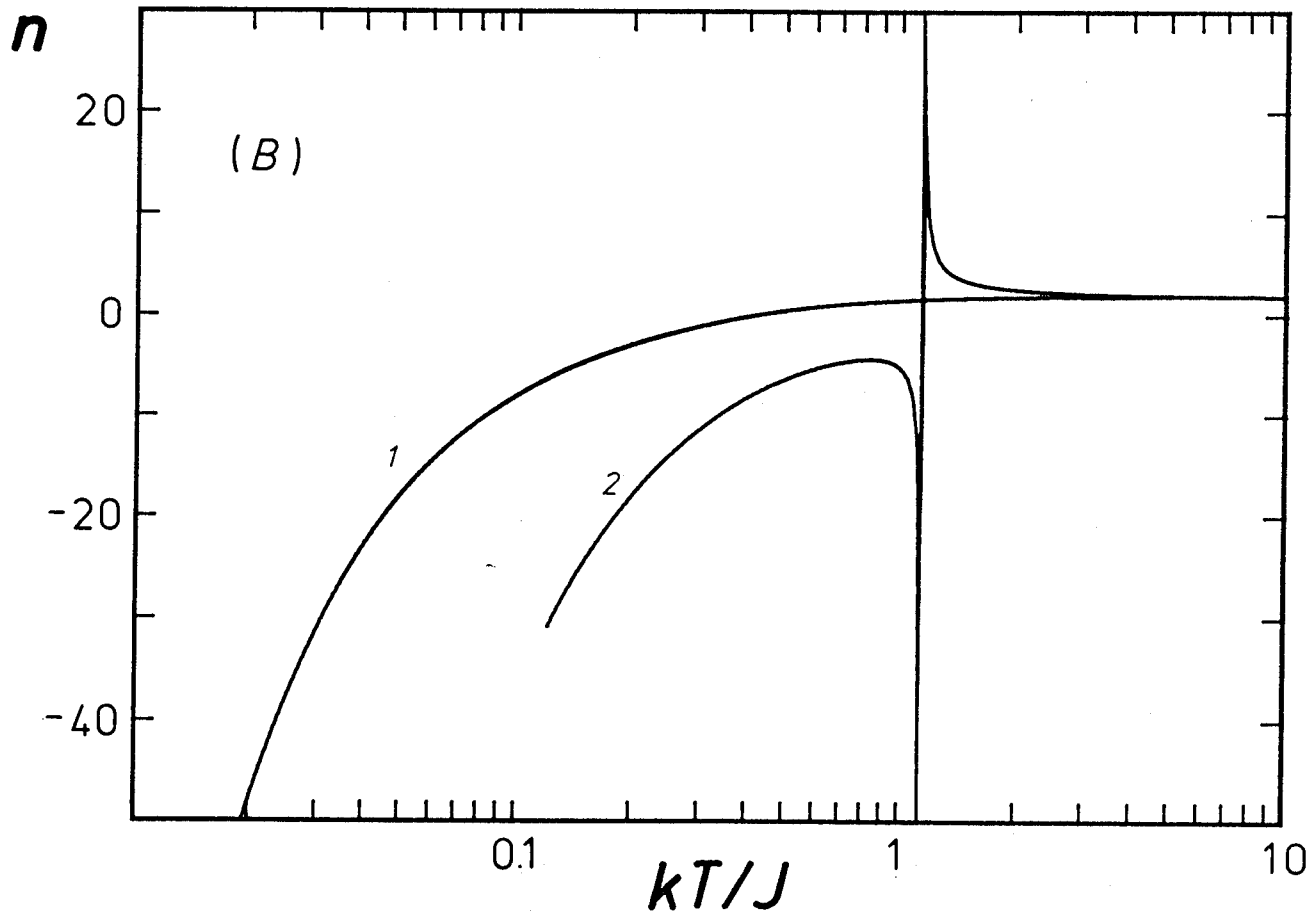

Fig. 9.7 Temperature exponents for some Ising models [17].
(B), 1 or 2D systems.
1, Ferro- or antiferromagnetic chain (1D);
2, Onsager's exact solution of square lattice (2D).

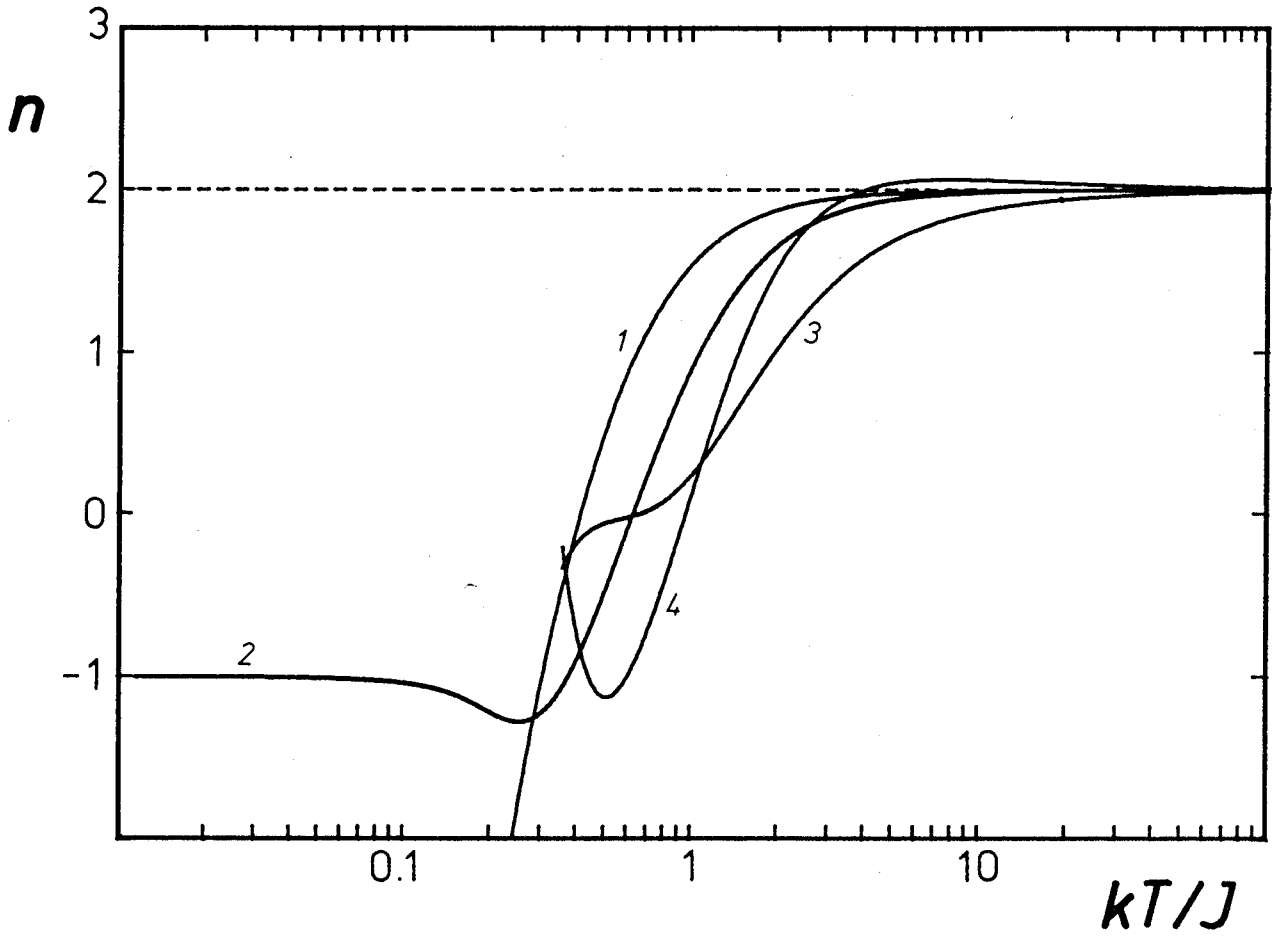

Fig. 9.8 Temperature exponents for some 1D systems [19-20].
1, Ferro- or antiferromagnetic Ising chain;
2, ferro- or antiferromagnetic XY chain;
3, ferromagnetic Heisenberg chain;
4, antiferromagnetic Heisenberg chain.

variation of Ising magnets.

For [BFc]I_3, two *n*-curves are shown in Fig. 9.5. The full curve was calculated using the data collected by the silicone-oil method, while the broken curve was calculated from the data of the pellet sample. Though these two curves show some discrepancy in their absolute values, the whole profiles are similar to each other. Obvious convex regions are again found and the origin of the heat-capacity anomaly is concluded to be of no Schottky type. These *n*-curves of [BFc]I_3 exhibit another characteristic feature, that is, relatively small absolute values. The absolute values of *n* in the downward convex region are less than unity. Such a behavior is not found in any theoretical models treated here. In this case, therefore, it may be considered that this magnetic system exhibits a lattice dimensional crossover from 1D to 3D. The persistent low value of *n* is the manifestation of very long high temperature tail characteristic of low dimensional magnets where remarkable short range fluctuation dominates the thermodynamic properties. Magnetic systems with high lattice dimensions such as 2D or 3D, which exhibit phase transitions, do not take values lower than $n = 1$, whereas only the systems possessing no phase transitions can take such values. Among them, however, the ones showing persistent low *n* values are hardly found. Even in most fluctuating 1D systems, Ising and XY models show the rapid change from 0 to 1 during 1/5 decades of temperature (See Fig. 9.8). Thus the 1D Heisenberg magnet is the last candidate for [BFc]I_3. Since the 1D Heisenberg magnet cannot undergo a phase transition, the lattice dimensionality-crossover to 3D must be introduced to explain the downward convexity in *n*. This interpretation is consistent with the crystal structure. As shown in Fig. 7.4, the structure of [BFc]I_3 is dominated by segregated columns of $[BFc]^+$ cations and I_3^- anions. The $[BFc]^+$ cations are stacked side to side in the columns. Each column of the cations is isolated by four columns of triiodide anions. This situation is in contrast to [DEBFc]I_3,

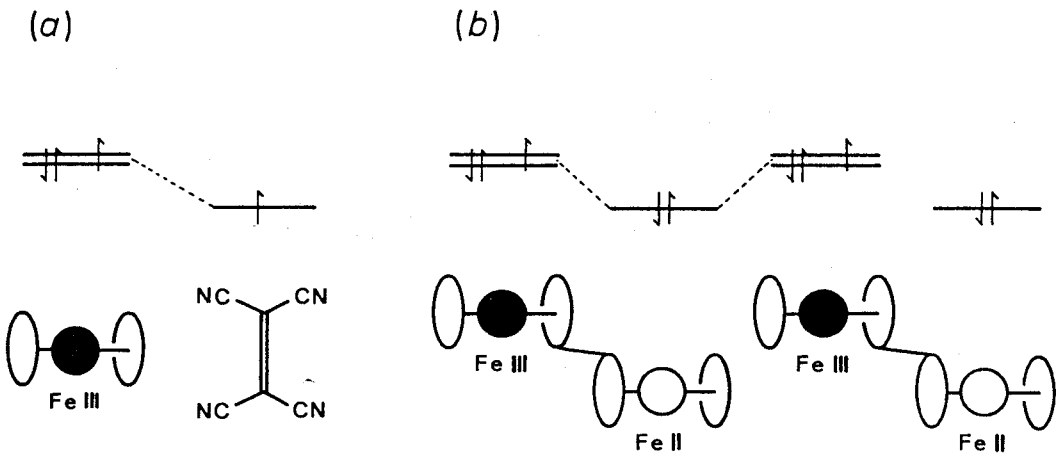

Fig. 9.9 Speculation on overlapping of magnetic orbitals. (a), Decamethylferrocenium tetracyanoethenide; (b), biferrocenium salts.

where the close contact between the magnetic cation radicals necessary for a column formation are prevented by ethyl group moieties and triiodide anions. These structural aspects are really reflected in the magnitude and the lattice dimensionality of magnetic interaction.

The most interesting conclusion in this section is that in these two biferrocenium radical salts the spins seem to behave as no Ising type but rather as Heisenberg type. This is a striking consequence in comparison with the case of [DMFc][TCNE] which has strong Ising character arising from its large anisotropy of g-factor. In the biferrocenium radicals the anisotropy of g-factor is smaller than that of $[DMFc]^+$ radicals but still significant (for example, $g_{\parallel} = 3.58$, $g_{\perp} = 1.72$ in $[BFc]I_3$ [5]) because the orbital angular momentum is more strongly quenched by their asymmetric coordination environments. Hence the Heisenberg tendency is plausibly attributed to the superexchange path. In the case of [DMFc][TCNE], the magnetic interaction occurs through "direct exchange" between the POMO (partially occupied molecular orbitals) of $[DMFc]^+$ and the SOMO (singly occupied molecular orbital) of $[TCNE]^-$ as shown in Fig. 9.9(a), so that Ising anisotropy is introduced after a straight fashion of Abragam and Bleaney described in section 5.2. On the other hand, in the biferrocenium radical salts the spin carriers, Fe(III), are separated by intervening Fe(II) constituents and the magnetic interaction must be dominated by "indirect exchange" (Fig. 9.9(b)). Thus the symmetry of the intermediate orbital is expected to affect the nature of magnetic interaction.

(2) Ferrocenium hexafluorophosphate

For $[Fc]PF_6$, two n-curves are shown in Fig. 9.10. The full curve was calculated on the basis of the data collected by the silicone-oil method, while the broken curve was calculated from the data of the pellet sample. As noted in section 8.3, pellet data are more reliable below 0.2 K, while above 0.2 K the

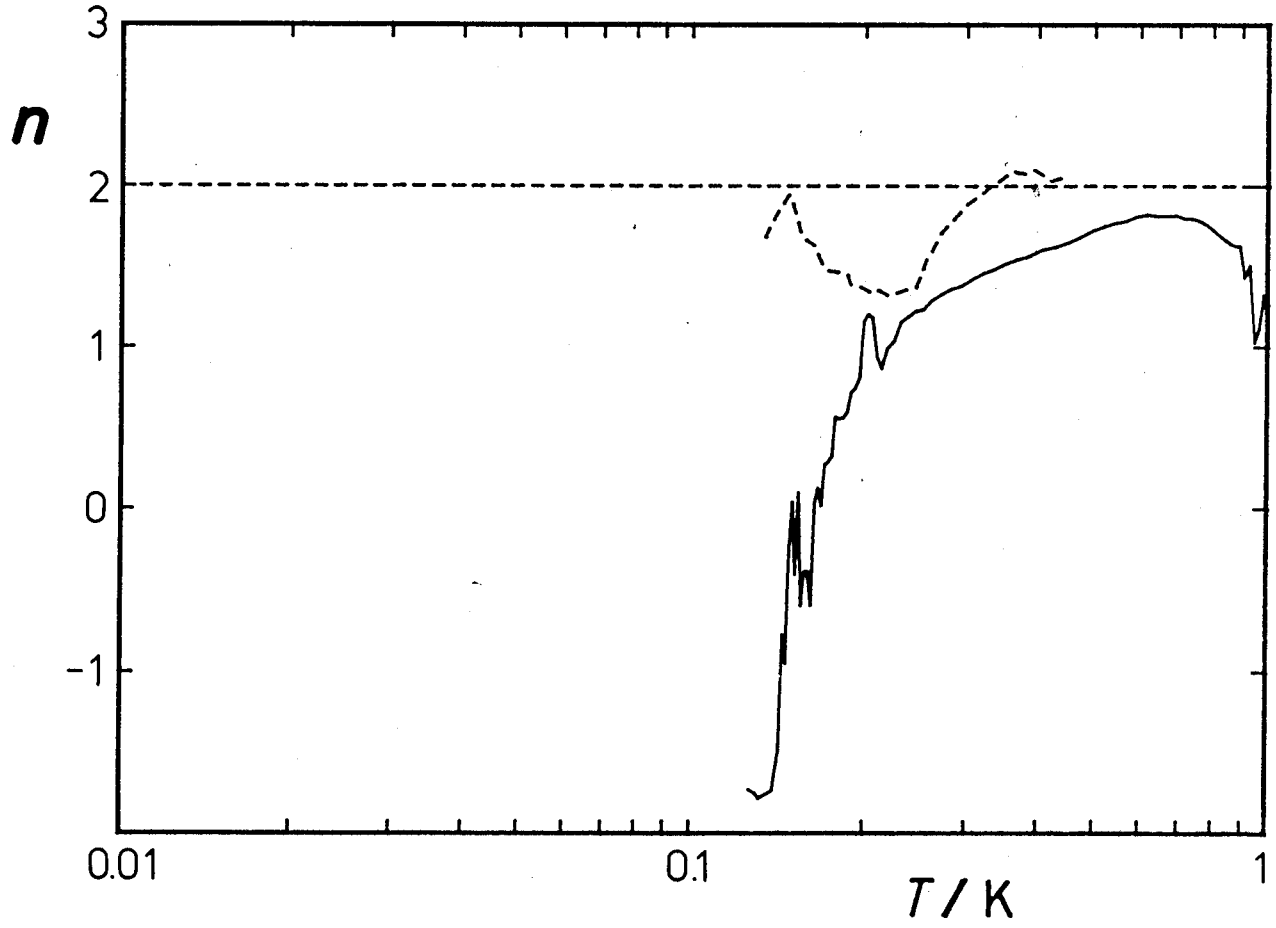

Fig. 9.10 Temperature exponents of ferrocenium hexafluorophosphate. The broken curve shows pellet-sample data, while the full curve shows silicone-oil data.

silicone-oil data should be adopted. When these two sets of reliable data are combined, one can recognize the downward convex profile around 0.2 K. This profile, however, allows two distinct interpretations. One is based on the agreement between the silicone-oil curve and a Schottky anomaly. Since a Schottky anomaly can be provided from 1D Ising magnet, a lattice dimensional crossover from 1D Ising magnet to 3D is considered to occur at 0.2 K. The other is suggested from the agreement between the whole convex profile and the behavior of Heisenberg ferromagnet in a square lattice. Since Heisenberg square ferromagnet has no phase transition, a dimensional crossover from 2D to 3D is expected to occur at lower temperatures, if any. These two interpretations provide an information that the short range order effect is relatively large but not extremely large in the present compound. When one assumes Heisenberg nature for the magnetic interaction, the magnetic lattice must have a dimension lower than or equal to 2, but larger than 1. The 1D Heisenberg magnet shows too strong short range order effect. On the other hand, if one assumes an Ising character, which places more restriction on spins and suppresses the short range order effect, 1D lattice with very strong fluctuation should be required.

In order to find which candidate is more plausible between them, knowledge about its crystal structure is helpful. At high temperatures, $[Fc]PF_6$ takes a cubic phase with pseudo CsCl structure, where the orientation of $[Fc]^+$ is disordered. Through two phase transitions at 347 K and 213 K, $[Fc]PF_6$ is orientationally ordered to a monoclinic phase, probably $P2_1/c$[11]. In this phase, arrangement of the $[Fc]^+$ cations is slightly complicated. If one notices only the position of the iron atoms, it turns out that the unit cell is not remarkably distorted apart from the high temperature cubic cell. Therefore, unique direction of molecular packing, which is closely related to exchange paths, is hard to find. If one also notices the molecular axes, however, two kinds of *bc*-planes are distinguished. In one plane, the molecular axes of $[Fc]^+$

cations are almost laid in plane, while in the other the molecular axes are normal to the plane. Hence one can obtain a 2D structure extending in the *bc*-plane. Both kinds of *bc*-plane involve two nonequivalent $[Fc]^+$ cations, whose axes are crossed each other. This structural aspect suggests that an Ising character simply expected from anisotropic *g*-factor is invalid for the present compound. Therefore it is very likely that the 2D Heisenberg model is more acceptable than the 1D Ising model.

REFERENCES TO PART III

[1] P. Day, *Int. Rev. Phys. Chem.* **1**, 149 (1981);
C. Creutz, *Prog. Inorg. Chem.* **30**, 1 (1983).

[2] M. B. Robin and P. Day, *Adv. Inorg. Chem. Radiochem.* **10**, 247 (1967).

[3] M. Sorai, A. Nishimori, D. N. Hendrickson, T.-Y. Dong, and M. J. Cohn, *J. Am. Chem. Soc.* **109**, 4266 (1987).

[4] T.-Y. Dong, D. N. Hendrickson, K. Iwai, M. J. Cohn, S. J. Geib, A. L. Rheingold, H. Sano, I. Motoyama, and S. Nakashima, *J. Am. Chem. Soc.* **107**, 7996 (1985).

[5] W. H. Morrison, Jr. and D. N. Hendrickson, *Inorg. Chem.* **14**, 2331 (1975).

[6] L. J. de Jongh and A. R. Miedema, *Adv. Phys.* **23**, 1 (1974).

[7] C. Domb, *Adv. Phys.* **9**, 149 (1960);
M. E. Fisher, *Rep. Prog. Phys.* **30**, 615 (1967).

[8] M. Konno and H. Sano, *Bull. Chem. Soc. Jpn.* **61**, 1455 (1988).

[9] W. Mori, Private communication.

[10] M. Sorai and Y. Shiomi, *Thermochim. Acta* **109**, 29 (1986).

[11] R. J. Webb, M. D. Lowery, Y. Shiomi, S. R. Wilson, M. Sorai, R. J. Wittebort, and D. N. Hendrickson, *J. Am. Chem. Soc.* (in press).

[12] R. Prins, *Mol. Phys.* **19**, 603 (1970).

[13] E. F. Westrum, Jr., *Pure Appl. Chem.* **55**, 539 (1983).

[14] P. H. E. Meijer, *Natl. Bur. Std. U. S., Spec. Publ.* **323**, 381 (1971);
P. H. E. Meijer, J. H. Colwell, and B. P. Shah, *Am. J. Phys.* **41**, 332 (1973).

[15] K. Ema, *J. Phys. Soc. Jpn.* **52**, 2798 (1983);
K. Ema, *Kotai Butsuri* **19**, 71 (1984).

[16] H. E. Stanley, "*Introduction to Phase Transitions and Critical Phenomena*", Oxford University Press, Oxford (1971).

[17] D. D. Betts and R. V. Ditzian, *Can. J. Phys.* **46**, 971 (1968);
M. F. Sykes, D. L. Hunter, D. S. McKenzie, and B. R. Heap,
J. Phys. **A5**, 667 (1972).

[18] G. A. Baker, Jr., H. E. Gilbert, J. Eve, and G. S. Rushbrooke,
Phys. Lett. **25A**, 207 (1967);
G. A. Baker, Jr., H. E. Gilbert, J. Eve, and G. S. Rushbrooke,
Phys. Rev. **164**, 800 (1967).

[19] G. A. Baker, Jr., G. S. Rushbrooke, and H. E. Gilbert,
Phys. Rev. **135**, A1272 (1964).

[20] S. Katsura, *Phys. Rev.* **127**, 1508 (1962).